Engineering Functional Capillary Networks

by

Stephanie Jo Grainger

A dissertation submitted in partial fulfillment
of the requirements for the degree of
Doctor of Philosophy
(Biomedical Engineering)
in The University of Michigan
2012

Doctoral Committee:

Associate Professor Andrew J. Putnam, Chair
Professor Jacques E. Nor
Professor Shuichi Takayama
Associate Professor Jan P. Stegemann

ACKNOWLEDGEMENTS

Now is the chance to thank everyone who has helped me along the way, and gotten me to where I am now. Most deserving of this appreciation is my thesis advisor, Dr. Andrew Putnam. Having welcomed me into the group when I was at a crossroads in my graduate education, I owe you innumerable kudos. You listened to my crazy ideas, toned me down when my statements were a bit too bold or I was too much of a perfectionist, and encouraged me to lead my own project. You were the sounding board for all of my scientific direction.

Next, I'd like to thank my thesis committee, Dr. Jacques Nor, Dr. Jan Stegemann, and Dr. Suichi Takayama. Each of you pushed me to know more and more about my project, and to produce a thorough, scientific conclusion at the end of the day. Your guidance kept me focused throughout the whole process, and for this, I thank you.

I would like to acknowledge my funding sources as well. Fellowship support from both the NIH Cellular Biotechnology Training Grant (T32-GM-008353), and a Rackham Merit Fellowship from the University of Michigan both allowed continuous support of my graduate education and advancement. This work was also partially funded by an award from the National Heart, Lung, and Blood Institute (R01-HL085339) and an American Recovery and Reinvestment Act supplement to that grant (R01-HL-085339-03S1), as well as a CAREER

award from the National Science Foundation (CBET-0968216). Several of these chapters have been published elsewhere previously. Chapter 2 has been published by Springer, while portions of chapters 3 and 4 have been published by the Public Library of Science. Chapter 5 will soon be published elsewhere.

To the members of the lab group: thank you a million times over for helping me out when I couldn't figure out my own logisitics, and for filling in the blanks when I needed you. Jake Ceccarelli and Bita Carrion, you have both led the way for me at the beginning, and I wouldn't have gotten to where I am now without your help and patience! Marina Vigen, for our morning chats and coffee trips – thanks! You let me vent when I was frustrated, and I have thoroughly enjoyed our science discussions, in trying to figure out what was happening when an unexpected result appeared. To the others in the lab: Dr. Yen Peng Kong, Isaac Janson, and Rahul Singh, thanks for being my labmates, and making the time more enjoyable. To the undergrads who have rotated through the lab: I hope that you are able to take away something valuable from your time here. I look forward to seeing you all in your shining moments to come.

All of my Ann Arbor friends, you are the ones that kept me sane! You made the weeks go by faster with fun plans in place for the weekend. The endless nights of hanging out, group dinners, and eating all of the desserts that I made – these things all made you my Ann Arbor family. The rides to the airport have always been appreciated too!

Mom and Dad, thanks for your constant encouragement, and the endless amounts of help that you've provided along the way. The countless trips to Ann

Arbor (even in the middle of winter), the “you can do it” that I needed every time I got stressed or frustrated, and the care packages all got me here. Grammy and Grampy, we lost you along the way, but without you, I wouldn’t have gotten here at all. Thanks for believing in me, supporting me, and always making me feel special. Amy, thanks for listening to all of my freak-out moments, for stepping up with everything at home when I came to Michigan, and for always making time for me when I could take a trip home to visit. I know it wasn’t easy!

Finally, I would like to thank my fiancé, Troy, for your endless love, support, and patience over the last few years. You never complained when I had to take a late night trip to the lab, or when I said I couldn’t hang out and have fun because I had to do work. You knew where I was coming from, and your understanding has been invaluable in finishing this work. The last year of being back-and-forth, in separate states – it hasn’t been easy, but we made it!

TABLE OF CONTENTS

LIST OF FIGURES

CHAPTER 2

CHAPTER 3

CHAPTER 4

CHAPTER 5

LIST OF ABBREVIATIONS

α-SMA	alpha smooth muscle actin
AdSC	adipose-derived stem cell
EC	endothelial cell
FGF	fibroblast growth factor
HGF	hepatocyte growth factor
MMP	matrix metalloproteinase
MSC	mesenchymal stem cell
MT	membrane type
NHLF	normal human lung fibroblast
PDGF	platelet-derived growth factor
TGF-β	transforming growth factor-beta
VE-cadherin	vascular endothelial cadherin
VEGF	vascular endothelial growth factor

ABSTRACT

A major translational challenge in the fields of therapeutic angiogenesis and tissue engineering is the ability to form functional networks of blood vessels. Cell-based strategies to promote neovascularization have led to the consensus that co-delivery of endothelial cells (ECs) with a supporting stromal cell type is the most effective approach. However, the choice of stromal cells has varied across studies, and their impact on the functional qualities of the capillaries produced has not been examined.

Our lab has developed methods to form interconnected networks of pericyte-invested capillaries both in vitro in a 3D cell culture model and in vivo. However, if the engineered vessels contain ECs that are misaligned or contain wide junctional gaps, they may function improperly and behave more like the pathologic vessels that nourish tumors. The purpose of this thesis was to determine if stromal cells of different origins yield capillaries with different functional properties, in complementary *in vitro* and *in vivo* models.

In vitro, a fluorescent dextran tracer was used to visualize and quantify transport across the endothelium. In EC-fibroblast co-cultures, the dextran tracer penetrated through the vessel wall and permeability was high through the first 5 days of culture, indicative of vessel immaturity. Beyond day 5, tracer accumulated at the vessel periphery, with very little transported across the

endothelium. When ECs were co-cultured with bone marrow-derived mesenchymal stem cells (MSCs) or adipose-derived stem cells (AdSCs), tighter control of permeability was achieved.

In vivo, all conditions yielded new vessels that inosculated with mouse dorsal vasculature and perfused the implant, but there were significant functional differences, depending on the identity of the co-delivered stromal cells. EC alone and EC-fibroblast implants yielded immature capillary beds characterized by high levels of erythrocyte pooling in the surrounding matrix, while EC-MSC and EC-AdSC implants produced more mature capillaries characterized by less extravascular leakage and expression of mature pericyte markers. Injection of dextran tracer into the circulation also showed that EC-MSC and EC-AdSC implants formed vasculature with more tightly regulated permeability. These results suggest that the identity of the stromal cells is key to controlling the functional properties of engineered capillary networks.

CHAPTER 1

Introduction

1.1 Motivation and Background of the Thesis

Cardiovascular diseases are the leading cause of death in the Western world, often requiring vascular reconstruction or other therapeutic intervention.(1) Because autologous donor vessels are not always a viable option for the treatment of these ischemic diseases, particularly for small diameter vessels such as capillaries, tissue engineered blood vessels are a highly studied area.(2) The process of engineering new vessels has been approached in two ways. New blood vessels can be engineered outside of the body and then implanted and ultimately anastamose with existing host vasculature.(3) Alternatively, treatment to encourage blood vessel growth can be administered (either as implanted cells(4, 5), or soluble factors(6)), resulting in the sprouting and growth of new vessels *in situ*.

The process of new capillaries sprouting and growing out of existing blood vessels, known as angiogenesis, is a complex process that is difficult to control.(7) Several pro-angiogenic regulators, including vascular endothelial growth factor (VEGF), fibroblast growth factor (FGF), platelet-derived growth

factor (PDGF), hepatocyte growth factor (HGF), and transforming growth factor-β (TGF-β), have previously been used to encourage capillary growth, both directly in the body, as well as *in vitro*.(8, 9) However, stimulating vessel formation with these proangiogenic molecules has caused uncontrolled growth and led to an abnormal cellular structure and function, as well as edema, hypertension, and septic shock *in vivo*.(10)

As an alternative to the direct administration of exogenous soluble factors, our lab has successfully developed a robust method for growing interconnected networks of pericyte-invested capillary blood vessels by distributing endothelial cells and supporting stromal cells in a 3D fibrin matrix.(11) These vessels are able to anastamose with host vasculature following implantation in order to restore blood flow, deliver nutrients, and remove metabolic waste products in previously ischemic tissues. However, these blood vessels have not been tested to determine their functionality as physiologically healthy vessel networks. If these new capillaries have grown too quickly, or with an imbalance of the previously described growth factors, they may contain endothelial cells that are misaligned, stacked, or contain wide junctional gaps.(12) Other differences in functionality or appearance may also exist which could hinder proper function in the body as well.

Multiple cell types have previously been shown to function as pericytes and promote capillary morphogenesis, specifically mesenchymal bone marrow-derived stem cells (MSCs)(11), fibroblasts(13), adipose-derived stem cells (AdSCs) (14), and vascular smooth muscle cells(15). Capillaries grown with each

cell type have been shown to grow into mature sprouts with stalks, tip cells, and hollow lumens.(11, 16) While each of these cell types promotes capillary sprout formation, it is still unknown whether each is capable of regulating vessel permeability in the same manner as healthy, mature vessels.(13) Previous work shows that these different cell types instruct endothelial cells to use different proteolytic mechanisms to remodel and promote capillary sprouting via different proteolytic enzymes, although the ultimate morphological outcomes appear to be similar.(17) More specifically, fibroblast-mediated capillary morphogenesis was only shown to be knocked down by the inhibition of both soluble MMPs and plasmin, thus allowing our lab to conclude that multiple proteases mediate this sprouting phenomenon.(14, 17) When MSCs were used in the place of fibroblasts, inhibition of soluble MMPs resulted in total knockdown of sprouting. Plasmin inhibition had no effect on sprouting in this system, thus allowing us to conclude that EC-MSC co-cultures utilize only soluble MMPs for sprouting. Specifically, MT1-MMP was found to mediate capillary morphogenesis. Adipose-derived stem cells promote angiogenesis via the plasminogen activator-plasmin axis. Based on these cues from previous work, the purpose of the experiments conducted in the scope of this dissertation was to evaluate the functional differences of engineered blood vessels formed in the presence of various stromal cell types.

1.2 Description of Engineered Blood Vessels

Engineered tissues require vascularization in order to overcome diffusional barriers and induce healthy tissue growth and maintenance.(18, 19) Blood vessels bring nutrients, other molecules such as growth factors and cytokines, as well as erythrocytes and various types of immune cells to tissues in different areas throughout the body. A healthy vascular network branches in a hierarchy of blood vessels, starting with arteries and veins to act as pipelines to transport large volumes of blood, and working downward in size to arterioles, venules, and finally, capillaries.(20) Capillaries maintain a large surface area within a tissue, allowing for oxygen diffusion and transport from the vessel into the surrounding tissue. These are the most numerous vessel type in the human body.(21, 22)

In order to grow engineered tissues in a laboratory setting, multiple cell types must work in tandem with extracellular matrix molecules to create a specific tissue.(23) Blood vessels must vascularize the new tissue at its outset in order to produce a three-dimensional product. The limits of diffusion, known to be approximately 200 microns in tissues such as muscle, have previously put a limit on the achievable thickness of engineered tissues.(24) Early successes in the field of tissue engineering have been with thin tissues (e.g., skin), relatively avascular tissues (e.g., cartilage), and hollow organs (e.g., bladder), where a dense vasculature is not necessary for tissue function and maintenance.(25-27)

All blood vessels are comprised of endothelial cells and some type of mural cells.(28) Endothelial cells line the inner side of a blood vessel, coming into

contact with the flowing blood and preventing clot formation.(29) Mural cells reside on the outer face of a blood vessel, embedded in the extracellular matrix. These cells work together with the endothelial cells to provide stabilization cues to the endothelial tubules.(29) Various different stromal cells work in concert with the endothelial cells to promote different types of blood vessels in different parts of the body. Capillary endothelial tubules are sparsely covered with pericytes, mural cells that provide stabilization cues to the endothelial cells to allow for proper nutrient and gas exchange to the surrounding tissue.(30) Capillaries can have endothelial layers that are continuous, fenestrated, or discontinuous in various places such as muscle, kidney, and liver.(31) Capillaries that comprise the blood-brain barrier are further specialized to include tight junctions that limit molecule permeability to protect the brain. In all capillaries, a layer of basement membrane (a specialized ECM) lies underneath the endothelial cells and provides a substrate for pericyte attachment.(32, 33) Pericytes are also a mechanism to prevent healthy blood vessels in properly nourished tissues from further sprouting. (34)

Arterioles, which have a much lower permeability than capillaries, are surrounded by a circumferentially arranged layer of smooth muscle cells, whose contractile properties allow for alteration of diameter for blood pressure control.(35) Postcapillary venules are the main area of macromolecular and cellular exchange into the blood.(36) Larger blood vessels contain additional layers of extracellular matrix and elastic lamina, due to their main function as tubes to carry blood, rather than allowing exchange of materials with the

surrounding tissue. An internal elastic lamina surrounds the endothelial cell tube, and an additional external elastic lamina provides a barrier to the outer extracellular matrix and connective tissue.(10)

Several methods can be employed to solve the challenge of creating tissue engineered blood vessels. One option is to create a vascular network *in vitro* that can then be implanted and anastamose with the host network. An alternative to this is to deliver a precise cocktail of pro-angiogenic factors to spatially and temporally control host vasculature recruitment. One limitation of this approach is the fact that the half-life of most pro-angiogenic protein factors is often extremely short, which can result in limited bioactivity.(37, 38) Also, the physiologic system is very complex and constantly changing, which is difficult to recapitulate. An alternative to this approach is to deliver a combination of appropriate cell types that can produce a physiologically relevant cocktail of these pro-angiogenic factors.(39) This approach is strengthened by the fact that the cells can respond to local changes in the environment and consequently alter the cues produced to induce vasculature sprouting.(40) Our lab has explored the utility of this second approach by delivering ECs with a variety of different stromal cell types to induce capillary sprouting, both *in vitro* and *in vivo*.

1.3 Introduction to Capillary Functionality

Capillary functionality in physiologically healthy tissues is phenotypically different than that seen in tumor physiology or in other pathological cases. Tumor physiology induces abnormal blood vessel growth due in part to the speed of

vessel formation and abnormal variations of pro-angiogenic cues released by the tumor itself.(41) Tumor vasculature has many phenotypic hallmarks, including irregular vessel diameters, abnormal branching patterns, and a disruption of the hierarchical differentiation structure into arteries, arterioles, capillaries, post-capillary venules, and veins.(42) These blood vessels are also known to have defective wall structures, and may contain wide junctional gaps between endothelial cells.(43) Levels of VE-cadherin are downregulated in cancer vasculature, indicating a lack of proper EC-EC cadherins junctions that control permeability between neighboring cells.(44) There is also often an incomplete basement membrane, which can encourage further angiogenic sprouting by failing to block the interstitial collagens that stimulate sprouting.(45) Tumor vasculature is also characterized by an abnormal pericyte coat, which implies a lack of stabilization within the vascular network, and can result in constant remodeling and continuous growth of the network to nourish the growing tumor structure.(46, 47) Previous work in other labs has also shown a faster than normal rate of endothelial cell turnover, as well as higher luminal resistance, and overexpression of integrins such as $\alpha_5\beta_1$. (48)

In most previous studies, the sole assessment of blood vessel functionality in engineered tissue applications has been the histological observation of vessel-like structures that contain lumens filled with host red blood cells.(49) However, there are many additional features of a blood vessel that are necessary for proper function. The vessel must respond to vasoactive stimuli in order to maintain proper blood pressure throughout the body.(50) Surrounding tissue

must be sufficiently oxygenated in order to avoid the development of a hypoxic environment.(24, 51) Newly sprouting blood vessels must lay down a basement membrane to provide a separation barrier between the endothelial cells and their collagenous extracellular environment (to produce stabilized vessels and discourage further sprouting) and to produce extracellular matrix proteins that provide mechanical support and stability to the area.(52, 53) Vascular permeability must be able to be tightly controlled as well. In arteries and arterioles, as well as veins and venules, permeability levels should be extremely low, as these types of vessels primarily function as conduits for convective blood transport throughout the body.(54) At the capillary level, the permeability capabilities are drastically different. Red blood cells should not be able to escape between neighboring ECs, but many growth factors, small gas molecules, and other small molecules should be able to reach the external tissue.(55)

1.4 Overarching Hypothesis

We hypothesize that the use of different stromal cell types will produce capillary networks with varying levels of functionality and rates of maturity.

1.5 Specific Aims

1. **Quantitatively determine the kinetics of capillary functionality by developing an *in vitro* model of inverse permeability.** Our hypothesis is that the engineered capillaries will be initially leaky as they are developing into

interconnected networks, but will mature into healthy networks of aligned, pericyte-stabilized endothelial cells with selective permeability that mimics that of physiologically healthy capillaries.

2. **Compare the performances of 3 different cell types (fibroblasts, MSCs, and AdSCs) as a functional pericyte coat for mature development and stabilization of a capillary network *in vitro*.** Our hypothesis is that the use of varying stromal cell types will enable capillary networks to mature at varying rates and with different functionalities due to the formation of stabilizing cell-cell junctions and pericytic associations.

3. **Quantitatively determine the kinetics of capillary function with an *in vivo* mouse model of subcutaneous wound healing.** We hypothesize that the kinetics of capillary morphogenesis and the achievement of functional, healthy vessels *in vivo* will mimic those of our *in vitro* model.

1.6 Translational Potential

Treatment of ischemic diseases in the clinic is a rising medical concern. Many patients are unable to withstand the highly invasive surgical treatments that are the current standard of care. Thus, new treatments are needed.(56) Ischemic diseases represent the leading cause of death in the western world, with heart disease, as well as other circulatory and peripheral vascular diseases as the leading players.(1) Commonly, bypass grafts are needed to circumvent blockages and restore blood flow to areas with high metabolic demands, such as the heart. The biggest challenge here is to find a suitable graft site where no

blockage currently exists. Often, patients who present with blockages in the vessels surrounding the heart also have blockages in vessels throughout the body, thus making it difficult to find a suitable graft.(57, 58)

Other peripheral ischemic diseases could also benefit from therapeutic angiogenesis or treatment with engineered capillary networks. Peripheral vascular diseases, such as diabetic retinopathy or ischemic neuropathy, could also potentially be treated by promoting increased angiogenic sprouting in areas of ischemia.(59, 60) Injection to the site of ischemia with pro-angiogenic growth factors, cytokines, or cells that are able to secrete these factors could be effective methods to induce vascularization where it is lacking.(61)

For effective translation of tissue engineered capillary networks to the clinic, physiological parameters of these new vessels need to be evaluated. Delivery of a cocktail containing a variety of pro-angiogenics (or specific cell types which are able to produce these pro-angiogenic signaling molecules) can result in broad variations in the phenotypes of the resulting blood vessels.(62) Evaluation of these differences is key to developing physiologically healthy blood vessels for effective treatment.

1.7 Preview of the Thesis

An in-depth review of the role that the extracellular matrix plays in the angiogenic process is given in Chapter 2. The development of the matrix is a complex interplay with the sprouting of new blood vessels during angiogenesis. If the matrix is incomplete or lacking one or more key components, the resulting

blood vessel sprouts may also lack stabilization cues and not function properly. Chapter 3 presents the *in vitro* assay design and development process, and the completion of the first specific aim. Following is Chapter 4, where the fully developed assay is used to address the second experimental aim that compares *in vitro* functional permeability differences for networks of capillary blood vessels formed in the presence of different stromal cell types. *In vitro* mechanistic cues and phenotypic differences in capillary growth with varying stromal cell types are also explored here. Chapter 5 brings the experimental plan full circle to an *in vivo* setting. Ultimate differences in functionality across the different treatment groups are compared, and stromal cell differentiation is investigated. Finally, the key findings and results are summarized in Chapter 6, and the ultimate translational applications of this work for the field of therapeutic angiogenesis are discussed.

1.8 References

1. Xu J, Kochanek K, Murphy S, and Tejada-Vera B. Leading Causes of Death. edited by Deaths: Final Data for 2007 TB. Atlanta, GA: Centers for Disease Control and Prevention, 2007.
2. Heyligers J, Arts C, Verhagen H, Groot Pd, and Moll F. Improving small-diameter vascular grafts: from the application of an endothelial cell lining to the construction of a tissue-engineered blood vessel. *Annals of Vascular Surgery* **19**, 448-456 (2005).
3. Chen X, Aledia A, Ghajar C, Griffith C, Putnam A, Hughes C, and George S. Prevascularization of a fibrin-based tissue construct accelerates the

formation of functional anastomosis with host vasculature. *Tissue Engineering Part A* **15**, 1363-1371 (2009).

4. Kniazeva E, Kachgal S, and Putnam A. Effects of extracellular matrix density and mesenchymal stem cells on neovascularization in vivo. *Tissue Engineering Part A* **17**, 905-914 (2011).
5. Melero-Martin J, Khan Z, Picard A, Wu X, Paruchuri S, and Bischoff J. In vivo vasculogenic potential of human blood-derived endothelial progenitor cells. *Blood* **109**, 4761-4768 (2007).
6. Saik J, Gould D, Watkins E, Dickinson M, and West J. Covalently immobilized platelet-derived growth factor-BB promotes angiogenesis in biomemetic poly(ethylene glycol) hydrogels. *Acta Biomaterials* **7**, 133-143 (2011).
7. Carmeliet P. Mechanisms of angiogenesis and arteriogenesis. *Nature Medicine* **6**, 389-395 (2000).
8. Richardson T, Peters M, Ennett A, and Mooney D. Polymeric system for dual growth factor delivery. *Nature Biotechnology* **19**, 1029-1034 (2001).
9. Zisch A, Schenk U, Schense J, Sakiyama-Elbert S, and Hubbell J. Covalently conjugated VEGF-fibrin matrices for endothelialization *Journal of Controlled Release* **72**, 101-113 (2001).
10. Jain R. Molecular regulation of vessel maturation. *Nature Medicine* **9**, 685-693 (2003).
11. Ghajar C, Blevins K, Hughes C, George S, and Putnam A. Mesenchymal stem cells enhance angiogenesis in mechanically viable prevascularized

tissues via early MMP upregulation. *Tissue Engineering* **12**, 2875-2888 (2006).

12. Hashizume H, Baluk P, Morikawa S, McLean J, Thurston G, Roberge S, Jain R, and McDonald D. Openings between defective endothelial cells explain tumor vessel leakiness. *Am J Path* **156**, 1363-1380 (2000).
13. Ghajar C, Chen X, Harris J, Suresh V, Hughes C, Jeon N, and George APS. The effect of matrix density on the regulation of 3-D capillary morphogenesis. *Biophysical Journal* **94**, 1930-1941 (2008).
14. Kachgal S, and Putnam A. Mesenchymal stem cells from adipose and bone marrow promote angiogenesis via distinct cytokine and protease expression mechanisms. *Angiogenesis* (2010).
15. Shepherd B, Jay S, Saltzman W, Tellides G, and Pober J. Human aortic smooth muscle cells promote arteriole formation by coengrafted endothelial cells. *Tissue Engineering Part A* **15**, 165-173 (2009).
16. Nakatsu M, Sainson R, Aoto J, Taylor K, Aitkenhead M, Perez-del-Pulgar S, Carpenter P, and Hughes C. Angiogenic sprouting and capillary lumen formation modeled by human umbilical vein endothelial cells (HUVEC) in fibrin gels: the role of fibroblasts and Angiopoietin-1. *Microvascular Research* **66**, 102-112 (2003).
17. Ghajar C, Kachgal S, Kniazeva E, Mori H, Costes S, George S, and Putnam A. Mesenchymal cells stimulate capillary morphogenesis via distinct proteolytic mechanisms. *Experimental Cell Research* **316**, 813-825 (2010).

18. Langer R, and Vacanti J. Tissue engineering. *Science* **260**, 920-926 (1993).

19. Jain R, Au P, Tam J, Duda D, and Fukumura D. Engineering vascularized tissue. *Nature Biotechnology* **23**, 821-823 (2005).

20. Maton A, Hopkins J, McLaughlin C, Johnson S, Warner M, LaHart D, and Wright J. *Human biology and health*. Englewood Cliffs, NJ: Prentice Hall, 1993.

21. Dawes J, and Prichard M. Studies of the vascular arrangements of the nose. *Journal of Anatomy* **87**, 311-322 (1953).

22. Wiedeman M. Dimensions of blood vessels from distributing artery to collecting vein. *Circulation Research* **12**, 375-378 (1963).

23. Levenberg S, Rouwkema J, Macdonald M, Garfein E, Kohane D, Darland D, Marini R, Blitterswijk Cv, Mulligan R, D'Amore P, and Langer R. Engineering vascularized skeletal muscle tissue. *Nature Biotechnology* **23**, 879-884 (2005).

24. Bottaro D, and Liotta L. Cancer: out of air is not out of action. *Nature* **423**, 593-595 (2003).

25. Bello Y, Falabella A, and Eaglstein W. Tissue-engineered skin: current status in wound healing. *American Journal of Clinical Dermatology* **2**, 306-313 (2001).

26. Cao Y, Vacanti J, Paige K, Upton J, and Vacanti C. Transplantation of chondrocytes utilizing a polymer-cell construct to produce tissue-

engineered cartilage in the shape of a human ear. *Plastic and Reconstructive Surgery* **100**, 297-302 (1997).

27. Oberpenning F, Meng J, Yoo J, and Atala A. De novo reconstitution of a functional mammalian urinary bladder by tissue engineering. *Nature Biotechnology* **17**, 149-155 (1999).
28. L'Heureux N, Germain L, Labbe R, and Auger F. In vitro construction of a human blood vessel from cultured vascular cells: a morphologic study. *Journal of Vascular Surgery* **17**, 499-509 (1993).
29. Pober J, and Sessa W. Evolving functions of endothelial cells in inflammation. *Nature Reviews: Immunology* **7**, 803-815 (2007).
30. Gerhardt H, and Betsholtz C. Endothelial-pericyte interactions in angiogenesis. *Cell and Tissue Research* **314**, 15-23 (2003).
31. Egginton S, and Gaffney E. Tissue capillary supply - it's quality not quantity that counts! *Experimental Physiology* **95**, 971-979 (2010).
32. Armulik A, Abramsson A, and Betsholtz C. Endothelial/Pericyte Interactions. *Circulation Research* **97**, 512-523 (2005).
33. Hughes C. Endothelial-stromal interactions in angiogenesis. *Current Opinion in Hematology* **15**, 204-209 (2008).
34. Bergers G, and Song S. The role of pericytes in blood-vessel formation and maintenance. *Neuro-Oncology* **7**, 452-464 (2005).
35. Baluk P, Hashizume H, and McDonald D. Cellular abnormalities of blood vessels as targets in cancer. *Current Opinion in Genetics & Development* **15**, 102-111 (2005).

36. Doherty N, Griffiths R, Hakkinen J, Scampoli D, and Milici A. Post-capillary venules in the "milky spots" of the greater omentum are the major site of plasma protein and leukocyte extravasation in rodent models of peritonitis. *Inflammation Research* **44**, 169-177 (1995).

37. Ramanujan S, Koenig G, Padera T, Stoll B, and Jain R. Local imbalance of proangiogenic and antiangiogenic factors: a potential mechanism of focal necrosis and dormancy in tumors. *Cancer Research* **60**, 1442-1448 (2000).

38. Lazarous D, Shou M, Stiber J, Dadhania D, Thirumurti V, Hodge E, and Unger E. Pharmacodynamics of basic fibroblast growth factor: route of administration determines myocardial and systemic distribution. *Cardiovascular Research* **36**, 78-85 (1997).

39. Montesano R, Pepper M, and Orci L. Paracrine induction of angiogenesis in vitro by Swiss 3T3 fibroblasts. *Journal of Cell Science* **105**, 1013-1024 (1993).

40. Melero-Martin J, Obaldia M, Kang S, Khan Z, Yuan L, Oettgen P, and Bischoff J. Engineering robust and functional vascular networks in vivo with human adult and cord blood derived progenitor cells. *Circulation Research* **103**, 194-202 (2008).

41. Senger D, Water L, Brown L, Nagy J, Yeo K, Yeo T, Berse B, Jackman R, Dvorak A, and Dvorak H. Vascular permeability factor (VPF, VEGF) in tumor biology. *Cancer and Metastasis Reviews* **12**, 303-324 (1993).

42. Blau H, and Banfi A. The well-tempered vessel. *Nature Medicine* **7**, 532-534 (2001).

43. McDonald D, and Baluk P. Significance of blood vessel leakiness in cancer. *Cancer Research* **62**, 5381-5385 (2002).

44. Hendrix M, Seftor E, Meltzer P, Gardner L, Hess A, Kirschmann D, Schatteman G, and Seftor R. Expression and functional significance of VE-cadherin in aggressive human melanoma cells: role in vasculogenic mimicry. *Proceedings of the National Acadamy of Sciences USA* **98**, 8018-8023 (2001).

45. Sund M, Xie L, and Kalluri R. The contribution of vascular basement membranes and extracellular matrix to the mechanics of tumor angiogenesis. *APMIS* **112**, 450-462 (2004).

46. Sennino B, Falon B, McCauley D, Le T, McCauley T, Kurz J, Haskell A, Epstein D, and McDonald D. Sequential loss of tumor vessel pericytes and endothelial cells after inhibition of platelet-derived growth factor B by selective aptamer AX102. *Cancer Research* **67**, 7358-7367 (2007).

47. Baluk P, Morikawa S, Haskell A, Mancuso M, and McDonald D. Abnormalities of basement membrane on blood vessels and endothelial sprouts in tumors. *American Journal of Pathology* **163**, 1801-1815 (2003).

48. Kuphal S, Bauer R, and Bosserhoff A. Integrin signaling in malignant melanoma. *Cancer and Metastasis Reviews* **24**, 195-222 (2005).

49. Nor J, Peters M, Christensen J, Sutorik M, Linn S, Khan M, Addison C, Mooney D, and Polverini P. Engineering and characterization of functional

human microvessels in immunodeficient mice. *Laboratory Investigation* **81**, 453-463 (2001).

50. Singh M, Mensah G, and Bakris G. Pathogenesis and clinical physiology of hypertension. *Cardiology Clinics* **28**, 545-559 (2010).

51. Griffith C, Miller C, Sainson R, Calvert J, Jeon N, Hughes C, and George S. Diffusion limits of an in vitro thick prevascularized tissue. *Tissue Engineering* **11**, 257-266 (2005).

52. Ingber D, and Folkman J. Mechanochemical switching between growth and differentiation during fibroblast growth factor-stimulated angiogenesis in vitro: role of extracellular matrix. *The Journal of Cell Biology* **109**, 317-330 (1989).

53. Ingber D. Mechanical signaling and the cellular response to the extracellular matrix in angiogenesis and cardiovascular physiology. *Circulation Research* **91**, 877-887 (2002).

54. Koike N, Fukumura D, Gralla O, Au P, Schechner J, and Jain R. Tissue engineering: of long-lasting blood vessels. *Nature* **428**, 138-139 (2004).

55. Crone C. The permeability of capillaries in various organs as determined by use of the 'indicator diffusion' method. *Acta Physiologica Scandinavica* **58**, 292-305 (1962).

56. Veith F, Moss C, Sprayregen S, and Montefusco C. Preoperative saphenous venography in arterial reconstructive surgery of the lower extremity. *Surgery* **85**, 253-256 (1979).

57. Simons J, Goodney P, Nolan B, Cronenwett J, Messina L, and Schanzer A. Failure to achieve clinical improvement despite graft patency in patients undergoing infrainguinal lower extremity bypass for critical limb ischemia. *Journal of Vascular Surgery* **51**, 1419-1424 (2010).

58. Edwards W, Holdefer W, and Mohtashemi M. The importance of proper caliber of lumen in femoral-popliteal artery reconstruction. *Surgery, gynecology & obstetrics* **122**, 37-40 (1966).

59. Mohamed Q, Ross A, and Chu C. Diabetic retinopathy (treatment). *Clinical Evidence* (2011).

60. Ugalde V, and Rosen B. Ischemic peripheral neuropathy. *Physical Medicine and Rehabilitation Clinics of North America* **12**, 365-380 (2001).

61. Kimoto K, and Kubota T. Anti-VEGF agents for ocular angiogenesis and vascular permeability. *Journal of Opthalmology* (2012).

62. Roy R, Roy B, and Sengupta S. Emerging technologies for enabling proangiogenic therapy. *Nanotechnology* **22**, 1-9 (2011).

CHAPTER 2

An In-Depth Review of the Role of the Extracellular Matrix in Angiogenesis

2.1 Introduction

During angiogenesis, the ECM dynamically evolves, changing and adapting to cellular processes that are taking place within its structure. As ECs differentiate into tubular structures containing lumens and associated pericytes, significant matrix remodeling occurs. Proteinases carve out areas to allow for invasion of the nascent tubular structures into the surrounding stroma, creating new vasculature in response to hypoxia. A new basement membrane is laid down, and supporting interstitial matrix is layered beneath the newly formed structures. This chapter will discuss angiogenesis as it relates to the surrounding ECM, the various proteinases that are able to modulate key steps of this process, and finally, the link between ECM mechanical properties and cellular remodeling during angiogenesis.

Vasculogenesis and angiogenesis are two distinctly different processes by which blood vessels form (Figure 2.1). In embryonic development, angioblastic cells assemble into a primary capillary plexus to create nascent vasculature *de novo* via vasculogenesis. By contrast, angiogenesis refers to the formation of capillaries via branching from existing vasculature after initial embryonic

development. This requires a complex series of events starting with basement membrane degradation of the existing vasculature, followed by endothelial cell activation, migration, and proliferation, organization into immature vessel sprouts with leading tip cells, maturation and vessel stabilization via mural cell association, and finally, basement membrane deposition and pruning of the new vessels in response to the physiologic demands of the tissue.[5] Each step in this process requires interaction between cells and their surrounding ECM.

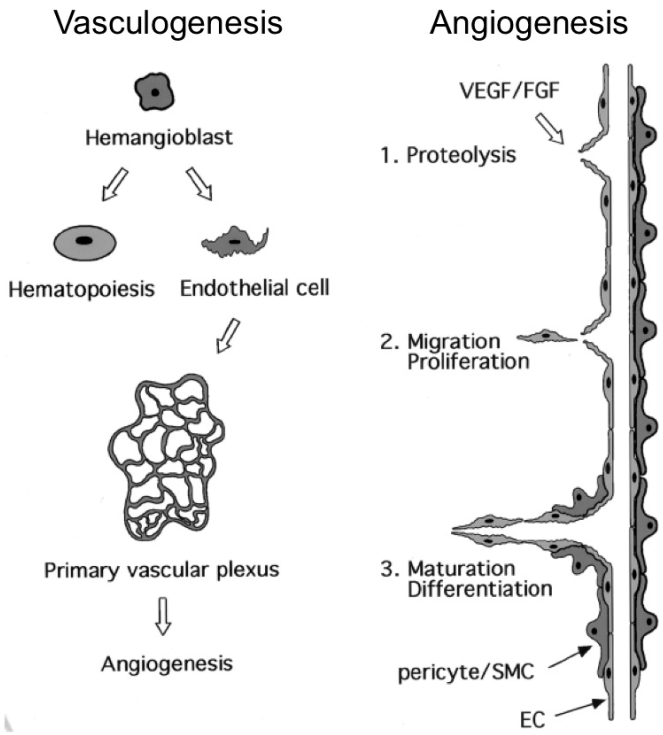

Figure 2.1: Schematic depiction of the two different processes by which new blood vessels form in the body. Vasculogenesis typically occurs in development, with angiogenesis occurring throughout life. This chapter focuses on how the ECM is remodeled during the latter process. (Figure reproduced from [1] with permission from Elsevier.)

A balance between pro- and anti-angiogenic proteins, known as the 'angiogenic switch', is crucial to the control of angiogenesis, with soluble factors and insoluble factors regulating this switch. When the scale is tipped in favor of

molecules that inhibit angiogenesis, the switch is ‘off’ until the levels of activating (pro-angiogenic) molecules are increased and able to overcome the inhibiting molecules. In healthy adults, the switch is typically maintained in the ‘off’ position, unless a pathological state which requires the formation of new vasculature occurs, such as cancer, wound healing, or ischemic disease. (In cancer, tumor growth beyond a threshold is achieved in part by recruiting host vasculature; however, because a detailed discussion of tumor angiogenesis is beyond the scope of this chapter, readers should instead refer to other reviews on the topic.[6]) Many signals can tip the switch in favor of angiogenesis, such as hypoxia, low environmental pH, mechanical stresses, tumor growth, or the presence of immune or inflammatory cells. Soluble growth factors, such as vascular endothelial growth factor (VEGF), platelet-derived growth factor (PDGF), basic fibroblast growth factor (FGF), and hepatocyte growth factor (HGF), are potent pro-angiogenic factors. Stabilizing immature vessels requires molecules such as angiopoietins-1 and -2, TGF-β, and sphyngosine-1 phosphate (S1-P), which are also considered pro-angiogenic. On the other side of the balance, suppressive signals from angiogenesis inhibitors include α-interferon, platelet factor-4, and thrombospondin-1, as well as other cryptic protein fragments.[7, 8] Matrix metalloproteinases (MMPs) and their endogenous inhibitors can also be considered in the context of the angiogenic switch, as they function as both pro- and anti-angiogenic molecules and are essential in each step of capillary formation and remodeling.[9]

2.2 Changes in the ECM Accompany Each Stage of Angiogenesis

During the initial stages of angiogenesis, contact between ECs and the ECM is a key controller of angiogenic signaling. ECs must adhere to the ECM in order to properly migrate, a necessary requirement for initiating angiogenic sprouting.[10] The ECM immobilizes angiogenic cytokines, and thus coordinates signals transduced to ECs via both growth factor receptors and integrin cell adhesion receptors.[10-12] Integrins, in turn, can regulate EC proliferation, survival, and the formation of functional vessel lumens.[12-15] If the ECs fail to adhere to the ECM, proliferation ceases and angiogenesis thus also stops.[11, 16-19]

At the earliest stages of angiogenesis, the basement membrane, consisting primarily of laminin-1 and type IV collagen, gets degraded to expose the ECs to the surrounding interstitial matrix.[20] In a quiescent state, the basement membrane helps insulate the ECs from this interstitial matrix and inhibits EC invasion and migration.[11] Following its degradation, a gradient of ECM components and the cytokines attached to them provide a set of cues to direct EC motility. In wound healing, for example, the interstitial matrix consists primarily of fibrin and type I collagen, and supports subsequent EC migration and sprouting.[21] VEGF plays a particularly critical role at this stage, as it is known to induce $\alpha_1\beta_1$ and $\alpha_2\beta_1$ integrin expression, both of which bind type I collagen. Type I collagen also helps to transform the leading ECs into a tip cell phenotype.[22] One mechanism known to disrupt angiogenesis for therapeutic

or alternative purposes is to disrupt the formation of the collagen triple helix via alteration of the prolines. This results in a cessation of collagen recognition and binding by the ECs, effectively halting angiogenic invasion and tubule formation.[23]

Once a nascent tubule escapes the basement membrane and begins to invade the interstitial matrix, extension of the capillary sprout begins. Type I collagen induces nascent cord formation and a migratory EC phenotype in part by suppressing cyclic AMP, which causes increased actin polymerization and stress fiber formation within the EC cytoskeleton.[11] This enables the ECs to generate substantial contractile forces and apply tension to the matrix over relatively large distances, which in turn supports capillary cord formation along the matrix fibers. Other cell types do not migrate and produce cords when implanted in fibrin or collagen gels in the same way.[24] Disruption of vascular endothelial cadherin (VE-cadherin) intercellular junctions via signaling mechanisms induced by collagen I binding also help to induce initial sprouting of ECs from a base vessel.[20] Disrupted of their quiescent cell-cell contacts, ECs begin to migrate and develop into nascent cords.[23, 25]

The next steps in the angiogenic process include the formation of hollow lumens, followed by maturation of the nascent vessels. As previously mentioned, integrin-mediated interactions between ECs and collagen, fibrin, and fibronectin provide key instructive signals.[26-28] $\alpha_2\beta_1$ and $\alpha_1\beta_1$ are known collagen receptors, while $\alpha_V\beta_3$ and $\alpha_5\beta_1$ are known fibronectin receptors that also permit EC interactions with fibrin. Lumen formation is dependent on the formation of

these integrin-dependent intracellular vacuoles that are initially formed by the process of pinocytosis, in which small vesicles form to create pockets within the cell. These vacuoles fuse together by exocytosis between adjacent ECs and start to direct an apical-basal organization and polarization.[29, 30] This polarization requires membrane type-MMP (MT-MMP) to interact with the ECM at the exterior of the newly formed lumens. The roles of these MT-MMPs will be discussed in greater detail later in this chapter.

The final step in the angiogenic process, tube stabilization, coincides with the production of laminin to form a new basement membrane along the basal surface of the nascent tubules. Integrins $\alpha_6\beta_1$ and $\alpha_3\beta_1$, which bind ECs to specific laminin isoforms, are known indicators of capillary maturation.[31, 32] The expression of these integrins suppresses several signaling pathways, and triggers EC quiescence.[33, 34] The laminin-rich basement membrane also provides an interface with which both ECs and stabilizing pericytes can interact.[11]

2.3 Proteinases Involved in Angiogenesis

The ECM must be broken down and reformed for many processes throughout life, including embryonic development, various morphogenic processes, cellular reproduction, and tissue remodeling. The matrix itself serves as a platform for cell growth and support, but is also capable of controlling cellular attachment, proliferation, migration, and differentiation of cells via cell-ECM interactions. Many cytokines and growth factors can also be sequestered

in the matrix and stored for later use. Several different types of angiogenic proteinases modulate the ECM in varying ways to influence angiogenesis. Some proteases indirectly promote EC proliferation, while others degrade the ECM to allow for tunneling ECs to invade and form tubules. Others control growth factor release from the matrix, altering cues that can direct or inhibit the angiogenic process. A final group of proteinases also controls cell adhesion to the matrix, inducing polarity within the blood vessels. These adhesions may direct cells to migrate, proliferate, or remain quiescent, based on the levels of varying integrins expressed, and the contents of the matrix to which they bind. MMPs are the main degradative enzymes responsible for modulating the ECM in a tissue. They are always contributing to the evolving matrix as it changes in different ways to support and encourage various cellular processes. In addition to both membrane-bound and soluble MMPs, ADAMs are another important group of proteins that influence ECM remodeling. A final grouping of players is the tissue inhibitors of metalloproteinases (TIMPs), which can control angiogenesis and subsequent matrix remodeling by maintaining vascular quiescence and halting angiogenic cues to maintain the angiogenic switch in the “off” position.

A. Soluble Matrix Metalloproteinases

Secreted matrix metalloproteinases are a family of zinc-containing endopeptidases that are able to degrade various ECM components. They are produced as pro-enzymes that are proteolytically processed to become activated. A sulfhydryl group in the pro-domain of all MMPs, known as a “cysteine switch,”

is able to work in sync with the zinc ion of the catalytic site to maintain cell quiescence.[35] By disrupting this cysteine-zinc binding, the MMP takes the first step toward activation.[36]

In general, the naming scheme follows a simple numerical order, starting with the first to be discovered, MMP-1, which acts on collagens. It was originally discovered when collagen gels were degraded by tadpole fin explants. The rest of the MMPs are divided into subgroups based on domain structure and substrate specificities: matrilysins (MMP-7 and MMP-26), collagenases (MMP-1, MMP-8, MMP-13, and MMP-18), stromelysins (MMP-3, MMP-10, and MMP-11), gelatinases (MMP-2 and MMP-9), enamelysins (MMP-20) and epilysins (MMP-28), and others that don't fit into one of these subgroups (MMP-19, MMP-21, MMP-22, MMP-23, and MMP-27).[37-39] MMPs can also be classified based on the basic domain groups that are included in their structures. All MMPs have three common structural domains: the "pre" or signal sequence, the pro-peptide domain, and the catalytically active domain (Figure 2.2). MMPs-7 and -26 contain only these 3 domains, have a broad range of substrate specificity, and are able to degrade many ECM proteins.[40-42] Addition of a hemopexin domain connected to the core region via a proline-rich hinge region at the catalytic domain allows for enhanced substrate specificity over those containing only the three basic regions. This hinge region is also responsible for binding the family of specific MMP inhibitors (TIMPs). Some examples of hemopexin-domain containing MMPs are collagenases, which degrade the native helix of fibrillar collagens such as types I, II, and III, as well as stromelysin-1 and -2, enamelysin,

metalloelastase, and MMPs-19, -22, and -27, which again don't fit into a specific structural class of MMPs.[37] These stromelysins, with their hemopexin domains, still have a rather broad substrate specificity, degrading several groups of ECM proteins, including proteoglycans, fibronectin, and laminin.[36] Another similar grouping is the gelatinases (MMPs-2 and -9) containing three head-to-tail cysteine-rich fibronectin type II-like repeats within the catalytic domain.[40, 43] These MMPs also degrade types IV, V, VII, and X native collagens, as well as denatured collagen (gelatin), fibronectin, and laminin.[43] When the cysteine-rich repeats are instead furin-susceptible sites, stromelysin-3 and epilysin are classified as a grouping. Finally, there are two outlying MMPs, MMP-21, which does not have a hinge region at all, and instead contains a vitronectin-like region within the propeptide region, and MMP-23, which also lacks the hemopexin

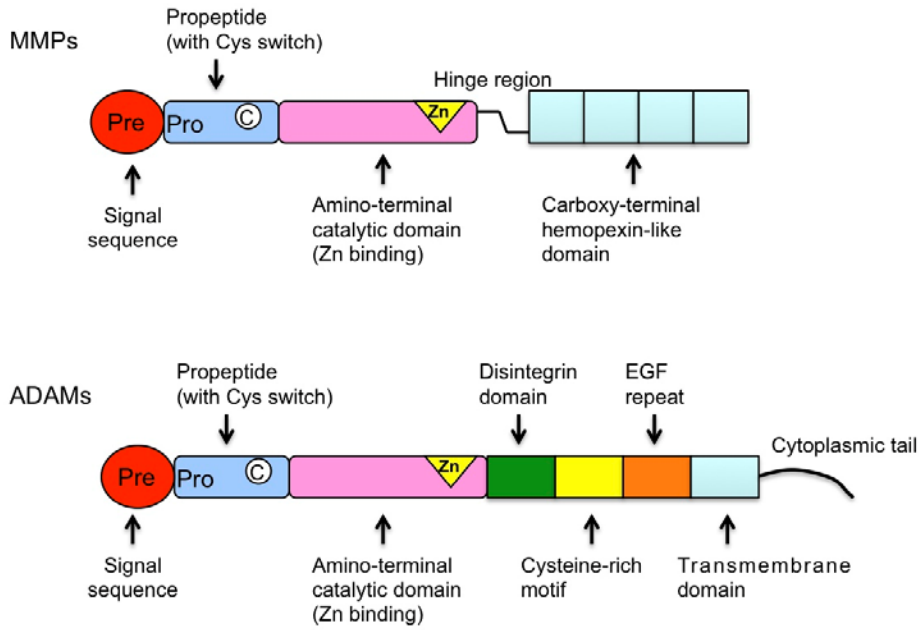

Figure 2.2: Schematic representation of the structures of MMPs and ADAMs. Both protease families contained conserved features, a "pre" or signal sequence, a propeptide domain (pro) (with either a cysteine switch or a furin-susceptible site), and a catalytic, Zn-binding domain. Additional sequences in some MMPs include a hinge region (H) and hemopexin domain, and other features not shown here. ADAMs contain a disintegrin domain, a cysteine-rich motif, an EGF repeat, a transmembrane domain, and a cytoplasmic tail.

domain, containing a cysteine and proline-rich region followed by an immunoglobulin-imitating region.[44]

Soluble MMPs can have both pro- and anti-angiogenic roles. Their pro-angiogenic capacity is perhaps more obvious, given their ability to degrade ECM components and jumpstart the path toward angiogenesis. Many growth factors and cytokines are known to upregulate EC basement membrane degradation, as well as EC proliferation, migration, and differentiation into a pro-angiogenic phenotype. Examples of these molecules are VEGF, bFGF, and several interleukins, which increase the amounts of inactive[45] and active[46] MMP-2 and MMP-9.[47] However, because certain ECM cleavage products have anti-angiogenic properties, MMPs may also be considered anti-angiogenic as well.[48]

A.1. Pro-Angiogenic Roles of Soluble MMPs

During basement membrane degradation, a subgroup of ECs, known as "tip cells", initiate sprouting. These cells possess high proteolytic activity, enabling them to successfully break down the matrix and tunnel through the interstitial ECM and hypoxic tissue.[49] Upon signaling to initiate sprouting, the tip cells must first proteolyze the capillary basement membrane, which is primarily comprised of laminin, collagen IV, heparin-sulfate proteoglycans, and entactin.[50] Multiple MMPs can degrade these ECM components: MMP-2, MMP-3, MMP-7, MMP-9, MMP-10, MMP-12, and MT1-MMP.[37] As mentioned previously, two important growth factors in the initiation of the angiogenic

cascade, VEGF and bFGF, produce vesicles containing pro-MMP-2 and pro-MMP-9, as well as MT1-MMP. Upregulation of these MMPs is thus associated with increased basement membrane invasion abilities of ECs.[51]

After the basement membrane has been broken down, ECs induce MMP expression from interstitial cells by secreting extracellular matrix metalloproteinase inducer (EMMPRIN).[52] The majority of MMP production may be from these surrounding interstitial and inflammatory cells present in the matrix, rather than the ECs forming the actual new capillary sprouts. Interstitial flow from the vasculature to the lymphatics, which is enhanced following degradation of the basement membrane barrier, combined with this increased MMP production, creates chemotactic gradients that further encourage EC invasion into the ECM. This is perhaps achieved by the interaction of various ECM breakdown products with the surface of the ECs.[53] Despite significant differences in pathologic and physiologic microenvironments, only small changes in soluble MMP expression are observed.[54] For example, switching from a physiologic ECM containing mostly collagen I to a provisional ECM comprised of fibrin, fibronectin, and vitronectin typically found during wound healing or prolonged ischemic diseases, results in only slight modulation of the MMP expression profile.[55]

Recent work suggests that there may be no single proteolytic mechanism utilized by ECs to degrade the ECM. Instead several MMPs are likely used in complement, and the specific combination and ratio of MMPs expressed and utilized depends on the identity of the matrix as well as the identity of stromal cell

types that interact with the ECs. For example, when adipose-derived stem cells or fibroblasts were included as interstitial cells to induce capillary sprouting in a fibrin matrix, the plasminogen activator-plasmin axis was the preferred proteolytic mechanism utilized for capillary invasion into the matrix and tubule lengthening, while MMPs appeared to play a distinct role regulating capillary diameter and stabilization only. In contrast, when mesenchymal stem cells from bone marrow were used in place of the adipose-derived cells, MT-MMPs were the sole proteases for ECM invasion and sprouting.[56]

Further work illustrating knockdown of either of the gelatinases, MMP-2 and MMP-9, suggests that these two proteinases may work in concert to remodel the ECM during angiogenic processes. When one of the two is targeted for gene knockdown, sprouting is still able to occur. MMP-9 is unable to degrade type I collagen alone, so thus it does not serve to encourage tunneling and sprouting of ECs during angiogenesis via matrix proteolysis directly. Instead, its pro-angiogenic capacity may lie in its ability to release bound VEGF (secreted by stromal cells) from the matrix to induce sprouting. It is also capable of activating TGF-β, resulting in promotion of tissue remodeling.[57, 58] During *in vivo* wound healing and hind limb ischemia studies, the peak activity levels of these MMPs coincide with granulation tissue formation, fibroblast migration into the tissue, and vascularization of the wound.[59, 60] Several research groups have now fabricated synthetic hydrogels with linkages sensitive to MMP-2 and MMP-9 so that cellular invasion can occur in much the same way as in hydrogels of natural composition (e.g., collagen or fibrin). *In vitro* studies using RGD-functionalized

versions of these MMP-sensitive gels have demonstrated EC adhesion and capillary sprouting by mimicking key elements found in natural matrix proteins.[61, 62] Furthermore, tethering growth factors such as VEGF to the matrix via proteolytically sensitive linkages recapitulates the growth factor sequestration capacity of physiologic ECMs.[63]

A.2. Anti-Angiogenic Roles of Soluble MMPs

As mentioned previously, MMPs can be considered to be both pro- and anti-angiogenic. MMP expression and activity can impede blood vessel formation via one of two possible mechanisms. First, overactive MMPs can compromise ECM stability, which may result in vascular regression. Second, MMP activity can generate matrix fragments with anti-angiogenic capabilities.

With respect to the first possibility, the process of angiogenesis typically culminates with vascular pruning. During this process, vessels that have not been stabilized regress as some of the interstitial collagen is broken down. Specifically, plasmin-mediated activation of MMPs-1, -10, and -13 has been shown to induce vascular regression as each of these MMPs (although predominantly MMP-1) can digest interstitial collagens.[64] This subset of MMPs, in conjunction with MMPs-2, -9, and MT1-MMP, may act together to digest multiple different ECM components based on these enzymes' specificities for different substrates.[64, 65] The first subset breaks down native type I collagen, while the gelatinases more efficiently degrade denatured collagens. A direct

correlation between the levels of active MMPs in maturing capillary beds and the levels of vascular regression has been reported.[66, 67]

With respect to the second possibility, the proteolytic degradation products of MMPs are anti-angiogenic. Proteolytic degradation of collagen IV, one of the primary components of basement membrane, generates anti-angiogenic fragments that include arrestin, canstatin, tumstatin, and metastatin.[38] MMP-9 predominantly produces free tumstatin, as well as smaller amounts of arresten and canstatin. Other MMPs, including MMP-2, -3, and -13, are also able to liberate tumstatin, although not as efficiently as MMP-9.[68] Tumstatin targets the $\alpha_V\beta_3$ integrin, which is not expressed at measurable levels in physiologic angiogenesis, but is seen at much higher levels in tumor angiogenesis. Studies have explored the possibility of using tumstatin to reduce pathologic angiogenesis.[68] Arrestin, another collagen IV breakdown fragment, binds the $\alpha_1\beta_1$ integrin receptor for collagen I, and inhibits EC proliferation, as well as migration and further tube formation *in vitro*. Similarly, collagen XVIII is a component of the interstitial matrix beneath the basement membrane of the vasculature. Collagen XVIII breakdown products are endostatin and neostatins, which are small, varying molecular weight molecules that are the further breakdown products of endostatin. MMPs-3, -7, -9, and -13, as well as MT1-MMP, act on collagen XVIII to produce these fragments. Endostatin affects VEGF signaling, EC proliferation and migration as well, in part by acting on the $\alpha_5\beta_1$ integrin.[69-72] Another unique function of endostatin is its ability to inhibit MT1-MMP and MMP-2 activities.[73]

B. Membrane-Type Matrix Metalloproteinases (MT-MMPs)

The membrane-type MMPs (MT-MMPs) represent another grouping of MMPs, so named because they are bound to the cell's plasma membrane via either a C-terminal transmembrane domain or a glycophosphatidyl inositol (GPI) anchor.[43, 74] Both classifications include a "pre" region, a propeptide region with a furin-susceptible site, a catalytic domain, a hinge region, and a hemopexin domain. After furin activation intracellularly, the proteinase gets processed and sent to the cell membrane, where the catalytic, hinge, and hemopexin domains lie extracellularly. These external regions are held at the cell surface by a transmembrane region attached to a short amino acid tail residing in the cell cytoplasm, or a GPI domain that is fixed in the cell membrane. These MT-MMPs provide spatial control of matrix breakdown directly at the cell membrane surface.[37] MT-MMPs degrade gelatin, fibronectin, and aggrecan, as well as several other ECM substrates.[41, 42]

Once nascent capillaries have formed, a basement membrane, a hallmark of a more mature vessel network, is deposited. Pericytes play a key role in this process. These cells are recruited from the host stroma in part via the secretion of PDGF-β by ECs. PDGF receptor-β signaling then initiates a cascade of events that control pericyte-EC binding, migration to the site, and proliferation. Interestingly, all of these processes are in some manner controlled by MT1-MMP.[75-77] Co-cultures of ECs and stromal cells of various origins in 3-D gels yield stable, pericyte-invested networks of capillaries characterized by the presence of basement membrane subjacent to the ECs along with the

periendothelial location of the stromal cells (Figure 2.3).[2] In the absence of stromal cells, ECs express MT1-MMP, with very little basement membrane production, even at later time points. If stromal cells are included with ECs in culture, MT1-MMP expression is undetectable in the capillary stalks. The ECs in the stalk instead produce basement membrane proteins, and the expression of MT1-MMP is restricted to the tip cells. Similar expression profiles have also been see *in vivo*.[49]

Further examination of the newly deposited basement membrane production yields some other interesting observations. The EC TIE-2 receptor is preferentially expressed in the stalk portion of a maturing capillary sprout, but are notably absent in the tip ECs. This expression is thought to be controlled by the pericytes, which produce Ang-1 to signal to the ECs via the TIE-2 receptor.[49, 78] This Ang-1/TIE-2 interaction is one mechanism by which pericytes and SMCs can regulate MMP activity of ECs. An alternative, and much more direct, means to achieve this control is via TIMP-1 secretion. TIMP-1 inhibits soluble

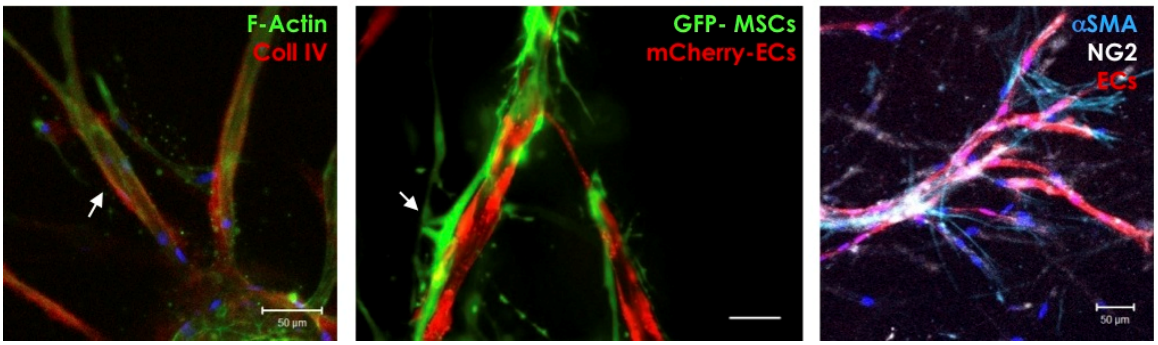

Figure 2.3: Three-dimensional co-cultures of ECs and stromal cells generate stable, pericyte-invested capillary networks *in vitro*. In these experiments, bone marrow-derived mesenchymal stem cells (MSCs) MSCs were distributed throughout a fibrin-based 3-D ECM in the presence of microcarrier beads coated with ECs. (A.) After 7 days, cultures were fixed and IF stained at day 7 for F-actin (green) and collagen IV (red) to visualize basement membrane deposition (white arrows). Scale=50 µm. (B.) MSCs expressing GFP were interspersed with mCherry-transduced ECs. Physical association of the ECs and MSCs were observed (white arrows). Scale=25 µm. (C) Cultures containing mCherry-transduced ECs and MSCs were fixed and IF stained for pericyte markers α-SMA (aqua) and NG2 (white). DAPI-stained nuclei are visible in the blue channel. Scale=50 µm. (Figure reproduced from [2] with permission from Elsevier.)

MMPs, but also appears to stabilize vessels by inducing basement membrane protein production.[79] Other TIMPs also work in conjunction with both cell types to inhibit angiogenic sprouting and stabilize nascent vessels. TIMP-3 is secreted by perivascular cells, and is then presented to the ECs via heparin sulfate proteoglycans in the basement membrane, which suppress MT1-MMP activity and encourage sprouting of the ECs.(Figure 2.4)[3, 80] Furthermore, all EC interactions with associating pericytes via Ang-1 or PDGF serve to inactivate and inhibit MT1-MMP after the basement membrane has been reproduced and to ensure vascular quiescence.

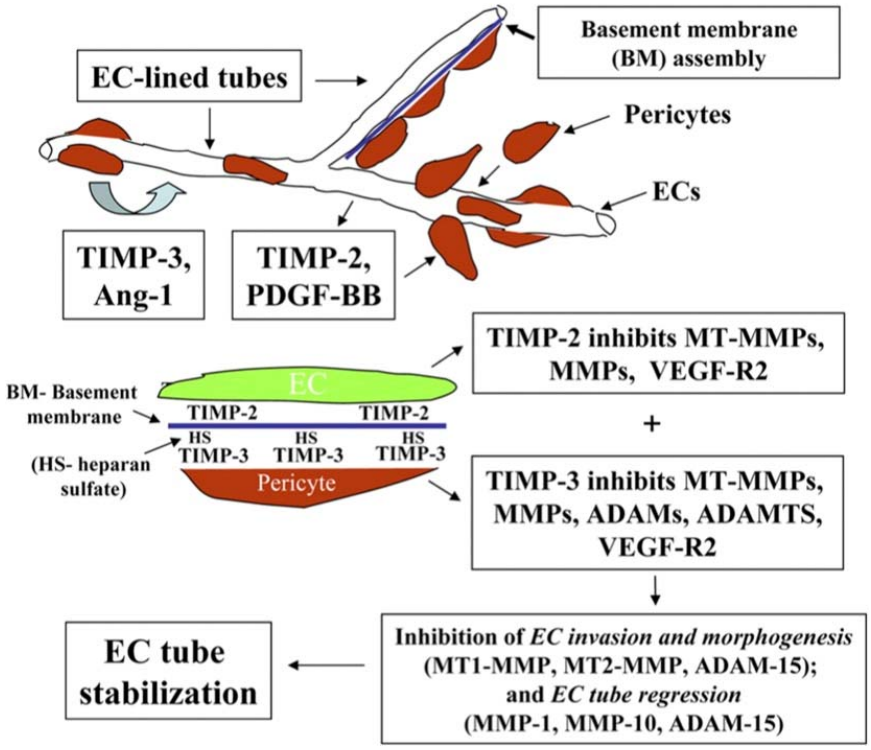

Figure 2.4: Schematic diagram illustrating the contribution of TIMP-2 and -3 to pericyte-induced vascular tube stabilization, as proposed in [3]. TIMP-2 is derived from ECs, whereas TIMP-3 is produced by pericytes. Together, they contribute to vascular stabilization by inhibiting a variety of MMPs, ADAMs, and VEGFR-2. The initiation of tube stabilization requires the blockade of both EC tube formation and EC tube regression, which further leads to the cessation of EC activation and the development of EC quiescence. Pericytes are required for ECs to assemble basement membrane matrices, which may locally capture and present TIMP-3 to ECs through heparin sulfate proteoglycans. (Figure reproduced from [3] with permission from The Rockefeller University Press.)

C. A Disintegrin and Metalloproteinase (ADAM)

ADAMs are a family of secreted and transmembrane proteins that control cell adhesion, as well as proteolytic processing of the ectodomains of cell surface receptors and signaling molecules.[81] Like previously described MMPs, ADAMs have both pre- and propeptide domains, with the pro- domain acting as an intramolecular chaperone that controls protein folding[82] and enzyme latency via a cysteine-switch mechanism.[83, 84] At this point, the structures differ, with ADAMs having a disintegrin-like domain with a loop that is able to interact with neighboring cell integrins.[85] Following this region, a cysteine-rich domain, then an EGF-like domain, followed by a membrane-spanning region and a cytoplasmic tail. The cytoplasmic domain is able to interact with proteins of intracellular signaling importance, as well as to control trafficking of proteins (Figure 2.2). ADAMs are named such due to their original structural homology to the small proteins of hemorrhagic snake venoms that were able to bind platelet integrin $\alpha_{2b}\beta_{3a}$ to block platelet aggregation.[86]

Because ADAMs are an active family of metalloproteinases, they are able to cleave ECM proteins and cause degradation of the bulk ECM in a locale. One example of this is ADAM-9, which is able to cleave laminin and promote invasion.[87] Several studies have shown a connection between ADAM-10 and cleavage of adhesion molecules such as VE-cadherin, where the ADAM is able to disassemble the junctional contacts that control permeability and assist with encouragement of EC migration and tubule sprouting.[11, 88] Other ADAMs that

are known to control ECM degradation and release activators of ECs to a migratory phenotype that will start the angiogenic cascade, are ADAMS-15 and -17.[11] ADAMs are also able to induce shedding of adhesion molecules such as PECAM-1, or their activity may mobilize growth factors, chemokines, or other soluble factors that can influence angiogenic processes.[89]

D. Inhibitors of Matrix Metalloproteinases

Tissue inhibitors of metalloproteinases (TIMPs) are the main enodogenous inhibitors of MMPs. There are four mammalian TIMPs that have been identified and characterized within the literature. They are all known to regulate MMP activity during periods of tissue remodeling, with molecular weights between 20 and 29 kDa.[90] All TIMPs inhibit MMP substrates in a 1:1 stoichiometric ratio,[91] with each TIMP binding the active site cleft in the catalytic domain of an MMP, in the same manner as an ECM substrate would bind the MMP.[44] Each TIMP has disulfide bonds of a three loop N-terminal domain, which is where interaction with the catalytic domains of MMPs occurs, and a complementary three loop C-subdomain.[92]

All TIMPs are secreted proteins, but TIMPs-2, -3, and -4 can all be found near the surface of a cell, in association with different MMPs.[93] All four TIMPs are known to inhibit active forms of all MMPs; however, their inhibition abilities vary widely. The main exception to this rule is that TIMP-1 is a poor inhibitor of MMP-19, MT1-MMP, and MT3-MMP.[94] TIMP-3 easily inhibits many of the ADAMs.[95] Examples of preferential binding are the ability of TIMP-1 to

preferentially bind with pro-MMP-9, and TIMP-2 preferentially binding with pro-MMP-2 to inhibit conversion to active forms of these MMPs.[96, 97]

TIMP-2 has a special functional role in controlling the activation of pro-MMP-2, with MT1-MMP also acting as a modulator. This activation step takes place on the cell surface, thus the need for inclusion of MT1-MMP for activation.[98] According to Strongin et al., the increased activation of MMP-2 in the presence of TIMP-2 is the result of the N-terminal inhibitory domain of TIMP-2 binding to the active site of MT1-MMP, and the C-terminal domain of TIMP-2 interacting with the C-terminal hemopexin domain of pro-MMP-2.[99] An additional unique feature of TIMP-2 is its ability to suppress angiogenesis by reducing EC proliferation cues from bFGF via its C-terminal region. [100]

TIMP-3, as briefly mentioned earlier, can inhibit both MMPs and the ADAM family of proteinases.[44] TIMP-3 is also known to block VEGF to VEGFR-2 binding, which further contributes to the anti-angiogenic capabilities of TIMP-3.[101] A third unique property of TIMP-3 is its restricted diffusion caused by its tight binding to heparin sulfate proteoglycans in the surrounding ECM. Because it does not readily diffuse, it is thought that TIMP-3 instead functions to regulate angiogenesis after the angiogenic switch has been flipped into an “on” position. As MMP degradation of the ECM liberates the matrix-bound TIMP-3, it can then inhibit any subsequent MMP activation at the cell-ECM level.[102] Normally, TIMP-3 functions to form complexes via its C-domain with MMPs-2 and -9, thus effectively slowing pro-angiogenic signaling. [92]

TIMP-4 is found mainly in the human heart, with low levels of the inhibitor found in the kidney, colon, placenta, and testes.[103] Levels are dysregulated in various cardiovascular diseases. This TIMP functions mainly to reduce EC motility, as well as proliferation, and induce apoptosis as well. In *in vivo* models, addition of TIMP-2 results in suppression of angiogenesis, while addition of TIMP-4 is not able to have this same effect.[104] TIMP-4 deficient mice instead showed reduced cardiac function with aging, due to increased apoptosis of cells.[105]

An additional inhibitor of MMPs, while not in the TIMP family, is the GPI-anchored glycoprotein, reversion-inducing cysteine-rich protein with kazal motifs (RECK). It is known to inhibit the release of pro-MMP-9 from the EC surface. It also effectively inhibits MT1-MMP, which will result in inhibition of MMP-2, as previously discussed.[106, 107] In RECK knockout mice, blood vessels cannot reach a mature stage, and mice die *in utero*. Overexpression of RECK in tumor

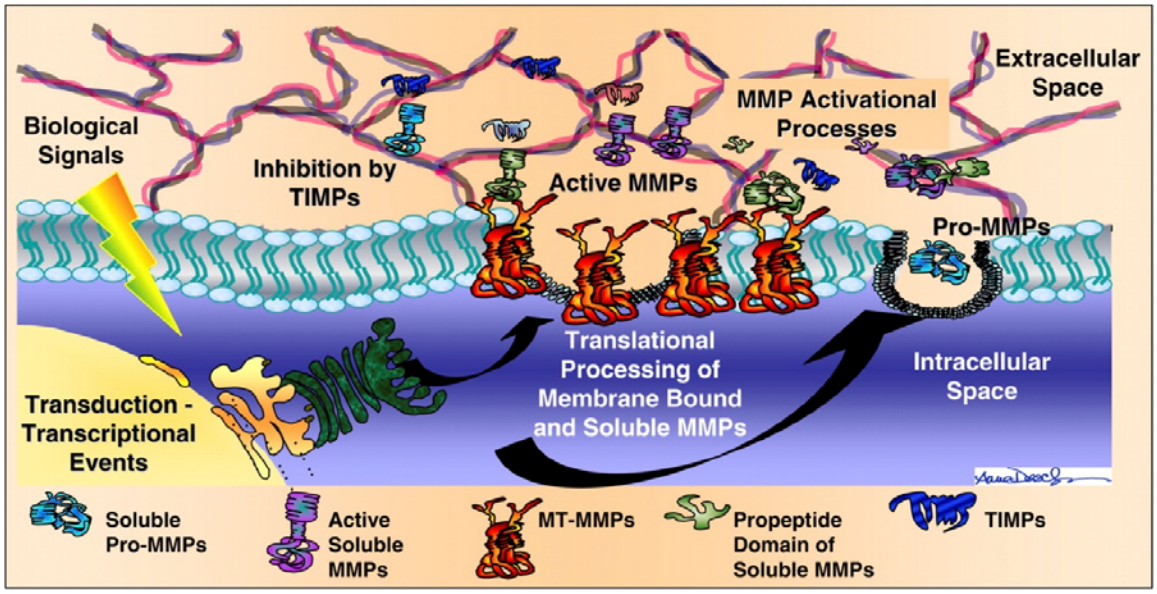

Figure 2.5: A simplified schematic of the current concepts depicting the roles and regulation of MMPs as they pertain to matrix remodeling. Figure reproduced from [4] with permission from The American Physiological Society.)

models results in a reduction of new blood vessel sprouting to sufficiently nourish the tumor.[90] An additional proteinase inhibitor, α_2-macroglobulin, is the primary MMP inhibitor found in blood plasma.[108] Finally, thrombospondin-1, a known inhibitor of angiogenesis, is also known to inhibit pro-MMP-2 and pro-MMP-9 from becoming activated. Thrombospondin-2 is also known to complex with MMP-2 to increase clearance via receptor-mediated endocytosis.[108]

A schematic summarizing many of the effects of soluble and membrane-bound MMPs, as well as the TIMPs, is shown in Figure 2.5.

2.4 Effects of Stromal Cells on the ECM

A. Stromal Cells Influence ECM Synthesis and Degradation

It has been widely established in the literature that the presence of pericytes covering EC tubules results in stabilization of the vessels, a decrease in vascular pruning, and decreased permeability of the nascent vessels.[109] Pericytes are a source of angiopoietin-1, which acts on EC TIE-2 to stabilize these heterogeneous cell-cell junctions.[110] Recent findings have shown that EC-pericyte interactions occur after ECs carve out “vascular guidance tunnels” within the ECM, which provide physical space for the EC-pericyte interactions to take place. Stratman et al. showed that the pericytes are recruited to the ablumenal surface and are able to move along the EC tubules through these pre-formed spaces to regulate tubule maturation and vascular basement membrane assembly.[111, 112] Basement membrane is deposited between ECs and pericytes within these tunnel voids. Further work by this group showed that

PDGF-BB and HB-EGF are necessary for pericytes to accumulate within these tunnels and along EC tubules, and also for proper basement membrane deposition. Without these growth factors directing the behavior of the pericyte-EC interactions, their data suggest that no basement membrane will be laid down.[113] This growth factor-pericyte interplay is known to be regulated by MT1-MMP. Active MT1-MMP directly controls the binding to PDGF receptor-B of pericytes after PDGF- β secretion by ECs. This cascade of events then controls pericyte migration to sites of need along the vasculature, as well as proliferation to induce greater vasculature stabilization and angiogenic quiescence.[75, 77] VEGF, an important initial cue for increased vessel permeability followed by basement membrane degradation and EC sprouting, also affects pericyte coverage. Treatment with VEGF antagonists results in increased pericyte coverage and improved microcirculatory function with lower permeability.[114, 115]

The TIE-2 receptor of ECs on the stalks of sprouting capillaries is a signaling receptor that results in collagen IV expression throughout the stalk but not in the tip cells of capillary sprouts. It is thought to be regulated by Ang-1 in the presence of vascular smooth muscle cells (vSMCs).[49] When vSMCs are absent, the distinction between stalk and tip cells is eliminated, and MT1-MMP is expressed throughout the structure.[49] Pericytes in co-cultures with ECs also express TIMP-1, which inhibits the activity of soluble MMPs and promotes basement membrane deposition by ECs.[79]

As mentioned earlier, pericyte contact with EC tubules reportedly plays a role in basement membrane deposition. Basement membrane proteins such as laminins and collagen IV are produced with the assistance of pericytes. In quiescent vessels, these basement membrane proteins inhibit tube morphogenesis by blocking access to the interstitial collagens that encourage EC migration and invasion. When pericytes are not present to encourage laminin deposition, ECs remain migratory, and vessel stabilization does not occur. Further work has also shown that EC-pericyte interactions induce production of fibronectin, nidogen-1, nidogen-2, and perlecan, as well as the laminins and collagen IV on the ablumenal surfaces of nascent EC tubules, all of which are constituents of basement membrane.[111] Additional work in this area showed that ECs produced the elevated levels of fibronectin found during these EC-pericyte interactions, while nidogen-1 was produced by the pericytes. These two proteins are both known to be binding molecules for the basement membrane specifically.[11, 116] Furthermore, fibronectin binds collagen IV and perlecan, and nidogen-1 binds collagen IV and laminin. Thus, fibronectin and nidogen-1 appear to be essential for assembly of the full basement membrane.[116] Collagen IV is mainly responsible for basement membrane structural support, and binds predominantly fibronectin and nidogen-1, and self-assembly of fibronectin that is induced by pericytes has a direct effect on collagen IV assembly as well.[111]

Most mature capillary networks within the body have approximately 20-25% of their area covered by pericytes.[117] Despite the fact that pericytes

cover only about one fourth of the total EC tubule area, they appear to control basement membrane production and maintenance along the full length of each tubule (see Figure 4). This may be due to their ability to move along the tube surface.[117] Collectively, these results suggest that heterotypic cell-cell contacts between ECs and pericytes, along with the constant pericyte motility along nascent tubules, are required events for basement membrane deposition and ultimate vessel stabilization.

While conventional wisdom suggests that stromal cells that differentiate into pericytes promote vessel stabilization, basement membrane production, and maturation of the interstitial ECM, there are several cases where stromal cells influence ECM protein degradation and subsequent remodeling. The recruitment of mural cells to the stalks of nascent EC tubules anatomically distinguishes tip cells from stalk cells, and leads to the further production of MMPs by the tip cells to facilitate their ability to break down and invade the matrix ahead of them. In aging adults, pericyte coverage can decrease, causing ultimate ECM breakdown and angiogenic activity increases.[118] Similar activities take place in various ischemic diseases and pathologies such as diabetes.

B. Pericytes Modulate Integrin-Mediated EC-to-ECM Attachment

Integrins mediate EC attachment to the ECM, and cross-talk with several growth factor receptors, and thus are of critical importance in the process of angiogenesis. ECs express a wide range of integrins depending on the location and state of activation of the cells. The repertoire of integrins expressed by

quiescent ECs enables adhesion to components of an intact basement membrane. On the other hand, angiogenic ECs upregulate the expression of a small subset of integrins, most notably the $\alpha_v\beta_3$ heterodimer, which has been reported to be required for angiogenesis.[119] It has been proposed that this integrin is upregulated in angiogenic ECs to permit binding to a wide range of provisional matrix components, including fibrinogen, vitronectin, von Willebrand factor, and fibronectin. Consistent with a requirement for this integrin in angiogenesis, a landmark study showed that $\alpha_v\beta_3$ integrin antagonists promote tumor regression by inducing apoptosis of angiogenic blood vessels.[120] There is some evidence that integrin $\alpha_5\beta_1$ expression is also upregulated at the initiation of angiogenesis, perhaps because it allows the newly migrating ECs that are sprouting from a pre-existing vessel to bind the aforementioned components of the provisional matrix.[121, 122] A complete discussion of integrins and their roles in both normal and pathologic angiogenesis is beyond the scope of this chapter. (For an excellent review, the reader is referred to a paper by Stupack and Cheresh.[123])

However, two facts regarding integrin expression are particularly relevant in the context of this chapter on ECM remodeling. The first is that the integrin expression profiles of ECs undergoing angiogenesis are different than those of quiescent ECs, as noted in the preceding paragraph. This is due to the fact that angiogenic ECs are exposed to an interstitial matrix whose composition is significantly different than a basement membrane, as well. The second is that pericytes appear to also be involved in the regulation of EC integrin expression

patterns. ECs that are in contact with pericytes express $\alpha_5\beta_1$ to attach to the basement membrane. When pericytes are not present, expression of this integrin is down-regulated, and the nascent vessels remain in an unstable immature state (perhaps more appropriately called an angiogenic state versus a quiescent state). Other integrin subunits with high affinities for basement membrane components (i.e. nidogens, laminins, and collagen IV), including the α_3, α_6, and α_1 subunits, are also not expressed by the ECs in appreciable amounts when pericytes are absent. In contrast, α_2 integrin, which recognizes collagen I (a component of the interstitial ECM, but not the basement membrane), is expressed at high levels in ECs cultured alone in 3-D collagen matrices, but is down-regulated in EC-pericyte co-cultures after pericytes have been recruited to initiate vessel maturation.[111] This study by Stratman et al. also showed that a strong induction of α_3, α_5, and α_6 integrin mRNAs in ECs, combined with a dramatic increase in pericyte α_1, α_3, and α_6 integrin mRNAs only when ECs and pericytes were cultured together and coincident with the deposition of basement membrane matrices.[111] Thus, there appears to be a complex and dynamic crosstalk between the ECs and pericytes that governs the integrin expression profiles of both cell types. These dynamic changes in integrin expression profiles permit EC adhesion to the interstitial matrix during the initial sprouting phases of angiogenesis, followed by the subsequent adhesion of both cell types to the EC-deposited basement membrane as the capillaries stabilize and mature.

2.5 Linking ECM Mechanical Properties and Remodeling

The ECM's ability to regulate angiogenesis is complex and multivariate. Not only does it impact capillary morphogenesis via biochemical regulatory mechanisms, including through growth factor sequestration, integrin-mediated adhesion, and protease susceptibility, it also acts as an instructive structural framework to support sprouting and nascent capillary functionality. An additional feature of the ECM that has been proposed as a regulator of angiogenesis is its mechanical resistance to cell-generated tractional forces.[124] Evidence from several studies corroborates the idea that mechanical cues directly impact tubulogenesis.[125-132] Vailhe et al. demonstrated that human umbilical vein ECs seeded on top of 2-D fibrin gels varying in concentration from 0.5 to 8 mg/ml only formed capillary-like structures on the softest of the gels. The authors concluded that the ECs do not form capillary-like structures on the more rigid gels because the cells are unable to generate the necessary contractile forces to remodel the more rigid substrate.[127] Another study conducted by Deroanne et al. showed that ECs seeded on collagen-functionalized polyacrylamide gels of different stiffness change morphologies from a monolayer to a tube-like phenotype as substrate rigidity decreases.[125] In 3-D culture, Urech, et al. investigated angiogenic process extension in 3-D fibrin gels and manipulated their mechanical properties by adding exogenous factor XIII to form additional cross-links.[129] Sieminski, et al. also studied the 3-D formation of capillary-like structures by two different types of ECs in freely-floating vs. mechanically-constrained (attached) collagen gels, and concluded that changing the collagen

concentration modulates the formation of these structures by regulating the amount of traction force exerted by the cells.[126] Further evidence links EC-generated traction forces with branching [130], the formation of capillary-like structures [125, 126, 133], and the transcriptional control of soluble pro-angiogenic molecules.[131] A more detailed discussion of the role of ECM mechanics and EC-generated tractional forces is found elsewhere.

In the scope of this chapter, it is important to recognize that the mechanical properties of the ECM are highly dynamic due to active remodeling induced both by the ECs and stromal cells. A study by Lee, et al. used second harmonic generation and two-photon excited fluorescence to show that ECs induce quantifiable alterations in local collagen matrix density via a process that involves cell-generated forces.[134] Another study by Krishnan, et al. tracked changes to the ECM during the process of angiogenesis using a 3-D culture model.[135] The authors reported an overall softening of the ECM as MMP activity increased during the initial sprouting phase, and then a slow stiffening as the MMP activity held steady and sprouts increased in length during tubulogenesis. Other studies have suggested that matrix stiffness may also indirectly modulate MMP activity in ECs [136-138]; however, the underlying mechanisms linking ECM mechanical properties and protease expression and/or activity remain to be elucidated.

In addition to EC-generated forces regulating angiogenesis, a recent study by Kilarski, et al. reported that external forces generated by myofibroblasts pulling on the ECM during wound contraction mediated the formation of vascular

loops by pulling on preexisting vascular beds.[139] This process, known as intussusceptive microvascular growth [140], demonstrates that stromal cells influence the process of angiogenesis in multiple ways. Not only do they secrete pro- and anti-angiogenic soluble factors, some of which influence the expression and activity of certain MMPs, and act as pericytes to stabilize the nascent vasculature, they also generate local forces that dynamically remodel the ECM and preexisting tissue structures. Understanding the complex interplay between ECs, stromal cells, and the ECM remains an ongoing challenge for the field.

2.6 Conclusions

The ECM continuously remodels in response to multiple instructive cues during the complex process of capillary morphogenesis. From early development of the capillary plexus in vasculogenesis, to the angiogenic sprouting of new vasculature in ischemic tissue in adults, many different proteinases work in concert with ECs and stromal cells to drive matrix breakdown, capillary sprouting, and subsequent maturation. Various soluble MMPs, membrane-bound MMPs, ADAMs, and inhibitors of each of these active players, play important roles to maintain the balance between pro- and anti-angiogenic cues in quiescent vessels, and to tip the scales to induce capillary morphogenesis and blood vessel development when needed. An increasing body of literature strongly suggests that pericytes are not only essential in promoting the stabilization and long-term functionality of capillary networks, but they can also exert their influence on vessel formation in a multitude of ways. As

discussed here, pericytes also dynamically communicate with ECs to influence matrix proteolysis, synthesis, integrin expression profiles, and the mechanical properties of the interstitial matrix, all of which can influence angiogenesis. Further work is needed to dissect the exact roles of these various players on matrix remodeling and angiogenesis.

2.8 References

1. Gerwins, P., E. Skoldenberg, and L. Claesson-Welsh, Function of fibroblast growth factors and vascular endothelial growth factors and their receptors in angiogenesis*. Crit Rev Oncol Hematol*, 2000. **34**(3): p. 185-94.
2. Ghajar, C.M., S. Kachgal, E. Kniazeva, H. Mori, S.V. Costes, S.C. George, and A.J. Putnam, Mesenchymal cells stimulate capillary morphogenesis via distinct proteolytic mechanisms*. Exp Cell Res*, 2010. **316**(5): p. 813-25.
3. Saunders, W., B. Bohnsack, J. Faske, N. Anthis, K. Bayless, K. Hirschi, and G. Davis, Coregulation of vascular tube stabilization by endothelial cell TIMP-2 and pericyte TIMP-3. *Journal of Cell Biology*, 2006. **175**(1): p. 179-191.
4. Spinale, F.G., Myocardial matrix remodeling and the matrix metalloproteinases: influence on cardiac form and function*. Physiol Rev*, 2007. **87**(4): p. 1285-342.

5. Jain, R., Molecular regulation of vessel maturation. *Nature Medicine*, 2003. **9**: p. 685-693.

6. Carmeliet, P. and R. Jain, Angiogenesis in cancer and other diseases. *Nature*, 2000. **407**: p. 249-257.

7. Adams, R. and K. Alitalo, Molecular regulation of angiogenesis and lymphangiogenesis. *Nature Reviews in Molcular and Cellular Biology*, 2007. **8**: p. 464-478.

8. Page-McCaw, A., A. Ewalk, and Z. Werb, Matrix metalloproteinases and the regulation of tissue remodeling. *Nature Reviews in Molcular and Cellular Biology*, 2007. **8**: p. 221-233.

9. Ghajar, C., S. George, and A. Putnam, Matrix metalloproteinase control of capillary morphogenesis. *Critical Reviews in Eukaryotic Gene Expression*, 2008. **18**(3): p. 251-278.

10. Ausprunk, D. and J. Folkman, Migration and proliferation of endothelial cells in preformed and newly formed blood vessels during tumor angiogenesis. *Microvascular Research*, 1977. **14**: p. 53-65.

11. Davis, G. and D. Senger, Endothelial extracellular matrix: biosynthesis, remodeling, and functions during vascular morphogenesis and neovessel stabilization. *Circulation Research*, 2005. **97**: p. 1093-1107.

12. Roovers, K. and R. Assoian, Integrating the MAP kinase signal into the G1 phase cell cycle machinery. *Bioessays*, 2000. **22**: p. 818-826.

13. Seger, R. and E. Krebs, The MAPK signaling cascade. *FASEB Journal*, 1995. **9**: p. 726-735.

14. Vinals, F. and J. Pouyssegur, Confluence of vascular endothelial cells induces cell cycle exit by inhibiting p42/p44 mitogen-activated protein kinase activity. *Molecular Cell Biology*, 1999. **19**: p. 2763-2772.

15. Assoian, R. and M. Schwartz, Coordinate signaling by integrins and receptor tyrosine kinases in the regulation of G1 phase cell-cycle progression. *Current Opinion in Genetics & Development*, 2001. **11**: p. 48-53.

16. Akiyama, S., S. Yamada, W. Chen, and K. Yamada, Analysis of fibronectin receptor function with monoclonal antibodies: roles in cell adhesion, migration, matrix assembly, and cytoskeletal organization. *Journal of Cell Biology*, 1989. **109**: p. 863-875.

17. Meredith, J. and M. Schwartz, Integrins, adhesion and apoptosis. *Trends in Cell Biology*, 1997. **7**: p. 146-150.

18. Giancotti, F. and R. Ruoslahti, Integrin signaling. *Science*, 1999. **285**: p. 1028-1032.

19. Wary, K., F. Mainiero, S. Isakoff, E. Marcantonion, and F. Giancotti, The adaptor protein Shc couples a class of integrins to the control of cell cycle progression. *Cell*, 1996. **87**: p. 733-743.

20. Liu, Y. and D. Senger, Matrix-specific activation of Src and Rho initiates capillary morphogenesis of endothelial cells. *FASEB Journal*, 2004. **18**(457-468).

21. Davis, G., K. Bayless, and A. Mavila, Molecular basis of endothelial cell morphogenesis in three-dimensional extracellular matrices. *Anat Rec*, 2002. **268**: p. 252-275.

22. Vernon, R. and H. Sage, A novel, quantitative model for study of endothelial cell migration and sprout formation within three-dimensional collagen matrices. *Microvascular Research*, 1999. **57**(2): p. 118-133.

23. Ingber, D. and J. Folkman, Inhibition of angiogenesis through modulation of collagen metabolism. *Lab Invest*, 1988. **59**(44-51).

24. Whelan, M. and D. Senger, Collagen I initiates endothelial cell morphogenesis by inducing actin polymerization through suppression of cyclic AMP and protein kinase A. *Journal of Biological Chemistry*, 2003. **278**: p. 327-334.

25. Montesano, R., L. Orci, and P. Vassalli, In vitro rapid organization of endothelial cells into capillary-like networks is promoted by collagen matrices. *Journal of Cell Biology*, 1983. **97**: p. 1648-1652.

26. Senger, D., C. Perruzzi, M. Streit, V. Koteliansky, A.d. Fougerolles, and M. Detmar, The alpha1beta1 and alpha2beta1 integrins provide critical support for vascular endothelial growth factor signaling, endothelial cell migration, and tumor angiogenesis. *Am J Path*, 2002. **160**: p. 195-204.

27. Davis, G. and C. Camarillo, An alpha2beta1 integrin-dependent pinocytic mechanism involving intracellular vacuole formation and coalescence regulates capillary lumen and tube formation in three-dimensional collagen matrix. *Exp Cell Res*, 1996. **224**(39-51).

28. Senger, D., K. Claffey, J. Benes, C. Perruzzi, A. Sergiou, and M. Detmar, Angiogenesis promoted by vascular endothelial growth factor: regulation through alpha1beta1 and alpha2beta1 integrins. *Proc Natl Acad Sci USA*, 1997. **94**: p. 13612-13617.

29. Bayless, J. and G. Davis, The Cdc42 and Rac1 GTPases are required for capillary lumen formation in three-dimensional extracellular matrices. *Journal of Cell Science*, 2002. **115**(1123-1136).

30. Davis, G. and K. Bayless, An integrin and Rho GTPase-dependent pinocytic vacuole mechanism controls capillary lumen formation in collagen and fibrin matrices. *10*, 2003. **27-44**.

31. Yurchenco, P., P. Amenta, and B. Patton, Basement membrane assembly, stability and activities observed through a developmental lens. *Matrix Biol*, 2004. **276**(521-538).

32. Fujiwara, H., Y. Kikkawa, N. Sanzen, and K. Sekiguchi, Purification and characterization of human laminin-8. Laminin-8 stimulates cell adhesion and migration through alpha3beta1 and alpha6beta1 integrins. *Journal of Biological Chemistry*, 2001. **276**(17550-17558).

33. Mettouchi, A., S. Klein, W. Guo, M. Lopez-Lago, E. Lemichez, J. Westwick, and F. Giancotti, Integrin-specific activation of Rac controls progression through the G(1) phase of the cell cycle. *Mol Cell*, 2001. **8**(115-127).

34. Klein, S., A.d. Fougerolles, P. Blaikie, L. Khan, A. Pepe, C. Green, V. Koteliansky, and F. Giancotti, Alpha5 beta1 integrin activates an NF-

kappa B-dependent program of gene expression important for angiogenesis and inflammation. *Mol Cell Biol*, 2002. **22**(5912-5922).

35. Nagase, H. and J. Woessner, Matrix metalloproteinases. *Journal of Biological Chemistry*, 1999. **274**: p. 21491-21494.
36. Stamenkovic, I., Extracellular matrix remodeling: the role of matrix metalloproteinases *Journal of Pathology*, 2003. **200**: p. 448-464.
37. Sternlicht, M. and Z. Werb, How matrix metalloproteinases regulate cell behavior. *Annual Reviews in Cell & Developmental Biology*, 2001. **17**: p. 463-516.
38. Hinsbergh, V.v., M. Englese, and P. Quax, Pericellular proteases in angiogenesis and vasculogenesis. *Arterioscler Thromb Vasc Biol*, 2006. **26**: p. 716-728.
39. Bode, W., C. Fernandez-Catalan, H. Tschesche, F. Grams, H. Nagase, and K. Maskos, Structural properties of matrix metalloproteinases. *Cell Mol Life Sci*, 1999. **55**: p. 639-652.
40. Kleiner, D. and W. Stetler-Stevenson, Structural biochemistry and activation of matrix metalloproteinases. *Current Opinion in Cell Biology*, 1993. **5**: p. 891-897.
41. McCawley, L. and L. Matrisian, Matrix metalloproteinases: They're not just for matrix anymore! *Current Opinion in Cell Biology*, 2001. **13**: p. 534-540.
42. Lynch, C. and L. Matrisian, Matrix metalloproteinases in tumor-hose cell communication. *Differentiation*, 2002. **70**: p. 561-573.

43. Lee, M.-H. and G. Murphy, Matrix metalloproteinases at a glance*. Journal of Cell Science*, 2004. **117**: p. 4015-4016.

44. Visse, R. and H. Nagase, Matrix metalloproteinases and tissue inhibitors or metalloproteinases*. Circulation Research*, 2003. **92**(827-839).

45. Taraboletti, G., S. D'Ascenzo, P. Borsotti, R. Giavazzi, A. Pavan, and V. Dolo, Shedding of the matrix metalloproteinases MMP-2, MMP-9, and MT1-MMP as membrane vesicle-associated components by endothelial cells*. American Journal of Pathology*, 2002. **160**(2): p. 673-680.

46. Li, A., S. Dubey, M. Varney, B. Dave, and R. Singh, IL-8 directly enhanced endothelial cell survival, proliferation, and matrix metalloproteinase production and regulated angiogenesis*. Journal of Immunology*, 2003. **170**: p. 3369-3376.

47. Nguyen, M., J. Arkell, and C. Jackson, Human endothelial gelatinases and angiogenesis*. Int J Biochem Cell Biol*, 2001. **33**: p. 960-970.

48. Nyberg, P., L. Xie, and R. Kalluri, Endogenous inhibitors of angiogenesis*. Cancer Cell*, 2005. **3**(589-601).

49. Yana, I., H. Sagara, S. Takaki, K. Takatsu, K. Nakamura, K. Nakao, M. Katsuki, S. Taniguchi, T. Aoki, H. Sato, S. Weiss, and M. Seiki, Crosstalk between neovessels and mural cells directs the site-specific expression of MT1-MMP to endothelial tip cells*. Journal of Cell Science*, 2007. **120**: p. 1607-1614.

50. Kalluri, R., Basement membranes: structure, assembly and role in tumor angiogenesis*. Nat Rev Cancer*, 2003. **3**: p. 422-433.

51. Jeong, J., H. Cha, D. Yu, M. Seiki, and K. Kim, Induction of membrane-type matrix metalloproteinase-1 stimulates angiogenic activities of bovine aortic endothelial cells. *Angiogenesis*, 1999. **3**: p. 167-174.

52. Tang, Y., P. Kesavan, M. Nakada, and L. Yan, Tumor-stroma interaction: positive feedback regulation of extracellular matrix metalloproteinase inducer (EMMPRIN) expression and matrix metalloproteinase-dependent generation of soluble EMMPRIN. *Molecular Cancer Research*, 2004. **2**: p. 73-80.

53. Helm, C., M. Fleury, A. Zisch, F. Boschetti, and M. Swartz, Synergy between interstitial flow and VEGF directs capillary morphogenesis in vitro through a gradient amplification mechanism. *Proc Natl Acad Sci USA*, 2005. **102**: p. 15779-15784.

54. Carlson, M. and M. Longaker, The fibroblast-populated collagen matrix as a model of wound healing: a review of the evidence. *Wound Repear Regen*, 2004. **12**: p. 134-147.

55. Burbridge, M., F. Coge, J. Galizzi, J. Boutin, D. West, and G. Tucker, The role of the matrix metalloproteinases during in vitro vessel formation. *Angiogenesis*, 2002. **5**: p. 215-226.

56. Kachgal, S. and A. Putnam, Mesenchymal stem cells from adipose and bone marrow promote angiogenesis via distinct cytokine and protease expression mechanisms. *Angiogenesis*, 2011. **14**(1): p. 47-59.

57. Lee, S., S. Jilani, G. Nikolova, D. Carpizo, and M. Iruela-Arispe, Processing of VEGF-A by matrix metalloproteinases regulates

bioavailability and vascular patterning in tumors. *Journal of Cell Biology*, 2005. **169**(681-691).

58. Bergers, G., R. Brekken, G. McMahon, T. Vu, T. Itoh, K. Tamaki, K. Tanzawa, P. Thorpe, S. Itohara, Z. Werb, and D. Hanahan, Matrix metalloproteinase-9 triggers the angiogenic switch during carcinogenesis. *Nature Cell Biology*, 2000. **2**(10): p. 737-744.

59. Moses, M., M. Marikovsky, J. Harper, P. Vogt, E. Eriksson, M. Klagsbrun, and R. Langer, Temporal study of the activity of matrix metalloproteinases and their endogenous inhibitors during wound healing. *Journal of Cellular Biochemistry*, 1996. **60**(3): p. 379-386.

60. Muhs, B., G. Plitas, Y. Delgado, I. Ianus, J. Shaw, M. Adelman, P. Lamparello, P. Shamamian, and P. Gagne, Temporal expression and activation of matrix metalloproteinases-2, -9, and membrane type 1-matrix metalloproteinase following acute hindlimb ischemia. *111*, 2003(8-15).

61. Patterson, J. and J. Hubbell, Enhanced proteolytic degradation of molecularly engineered PEG hydrogels in response to MMP-1 and MMP-2. *Biomaterials*, 2010. **31**: p. 7836-7845.

62. Moon, J., J. Saik, R. Poche, J. Leslie-Barbick, S. Lee, A. Smith, M. Dickinson, and J. West, Biomimetic hydrogels with pro-angiogenic properties. *Biomaterials*, 2010. **31**(3840-3847).

63. Zisch, A., M. Lutolf, M. Ehrbar, G. Raeber, S. Rizzi, N. Davies, H. Schmokel, D. Bezuidenhout, V. Djonov, P. Zilla, and J. Hubbell, Cell-demanded release of VEGF from synthetic, biointeractive cell ingrowth

matrices for vascularized tissue growth. *FASEB Journal*, 2003. **17**(15): p. 2260-2262.

64. Davis, G., K. Allen, R. Salazar, and S. Maxwell, Matrix metalloproteinase-1 and -9 activation by plasmin regulates a novel endothelial cell-mediated mechanism of collagen gel contraction and capillary tube regression in three-dimensional collagen matrices. *Journal of Cell Science*, 2001. **114**(917-930).

65. Zhu, W., X. Guo, S. Villaschi, and R. Nicosia, Regulation of vascular growth and regression by matrix metalloproteinases in the rat aorta model of angiogenesis. *Lab Invest*, 2000. **80**: p. 545-555.

66. Saunders, W., J. Bayless, and G. Davis, MMP-1 activation by serine proteases and MMP-10 induces human capillary tubular network collapse and regression in 3D collagen matrices. *Journal of Cell Science*, 2005. **118**: p. 2325-2340.

67. Davis, G. and W. Saunders, Molecular balance of capillary tube formation versus regression in wound repair: role of matrix metalloproteinases and their inhibitors. *J Investig Dermatol Symp Proc*, 2006. **11**: p. 44-56.

68. Hamano, Y., M. Zeisberg, H. Sugimoto, J. Lively, Y. Maeshima, C. Yang, R. Hynes, Z. Werb, A. Sudhakar, and R. Kalluri, Physiological levels of tumstatin, a fragment of collagen IV alpha3 chain, are generated by MMP-9 proteolysis and suppress angiogenesis via alphaV beta3 integrin. *Cancer Cell*, 2003. **3**(6): p. 589-601.

69. Hangai, M., N. Kitaya, J. Xu, C. Chan, J. Kim, Z. Werb, S. Ryan, and P. Brooks, Matrix Metalloproteinase-9-Dependent Exposure of a Cryptic Migratory Control Site in Collagen is Required before Retinal Angiogenesis. *Am J Path*, 2002. **161**(4): p. 1429-1437.

70. Chang, J., J. Javier, G. Chang, H. Oliveira, and D. Azar, Functional characterization of neostatins, the MMP-derived, enzymatic cleavage products of type XVIII collagen. *FEBS Lett*, 2005. **579**: p. 3601-3606.

71. Heljasvaara, R., P. Nyberg, J. Luostarinen, M. Parikka, P. Heikkila, M. Rehn, T. Sorsa, T. Salo, and T. Pihlajaniemi, Generation of biologically active endostatin fragments from human collagen XVIII by distinct matrix metalloproteases. *Exp Cell Res*, 2005. **307**(2): p. 292-304.

72. O'Reilly, M., T. Boehm, Y. Shing, N. Fukai, G. Vasios, W. Lane, E. Flynn, J. Birkhead, B. Olsen, and J. Folkman, Endostatin: An Endogenous Inhibitor of Angiogenesis and Tumor Growth. *Cell*, 1997. **88**: p. 277-285.

73. Kim, Y., J. Jang, O. Lee, J. Yeon, E. Choi, K. Kim, S. Lee, and Y. Kwon, Endostatin Inhibits Endothelial and Tumor Cellular Invasion by Blocking the Activation and Catalytic Activity of Matrix Metalloproteinase 2. *Cancer Research*, 2000. **60**: p. 5410-5413.

74. Vihinen, P. and V.-M. Kahari, Matrix metalloproteinases in cancer: prognostic markers and therapeutic targets. *Int J Cancer*, 2002. **99**: p. 157-166.

75. Hellstrom, M., H. Gerhardt, M. Kalen, X. Li, U. Eriksson, H. Wolburg, and C. Betsholtz, Lack of Pericytes Leads to Endothelial Hyperplasia and

Abnormal Vascular Morphogenesis. *Journal of Cell Biology*, 2001. **153**(3): p. 543-554.

76. Gerhardt, H. and C. Betsholtz, Endothelial-pericyte interactions in angiogenesis. *Cell and Tissue Research*, 2003. **314**(1): p. 15-23.

77. Lehti, K., E.A.H. Birkedal-Hansen, K. Holmbeck, Y. Miyake, T. Chun, and S. Weiss, An MT1-MMP–PDGF receptor-beta axis regulates mural cell investment of the microvasculature. *Genes & Development*, 2005. **19**: p. 979-991.

78. Suri, C., P. Jones, S. Patan, S. Bartunkova, P. Mainsonpierre, S. Davis, T. Sato, and G. Yancopoulos, Requisite role of angiopoietin-1, a ligand for the TIE2 receptor, during embryonic angiogenesis. *Cell*, 1996. **87**: p. 1171-1180.

79. Kraling, B., D. Wiederschain, T. Boehm, M. Rehn, J. Mulliken, and M. Moses, The role of matrix metalloproteinase activity in the maturation of human capillary endothelial cells in vitro. *Journal of Cell Science*, 1999. **112**(Pt 10): p. 1599-1609.

80. Lafleur, M., P. Forsyth, S. Atkinson, G. Murphy, and D. Edwards, Perivascular cells regulate endothelial membrane type-1 matrix metalloproteinase activity. *Biochem Biophys Res Commun*, 2001. **282**(463-473).

81. Edwards, D., M. Handsley, and C. Pennington, The ADAM metalloproteinases. *Molecular Aspects of Medicine*, 2008. **29**(5): p. 258-289.

82. Roghani, M., J. Becherer, M. Moss, R. Atherton, H. Erdjument-Bromage, J. Arribas, R. Blackburn, G. Weskamp, P. Tempst, and C. Blobel, Metalloproteinase-disintegrin MDC9: intracellular maturation and catalytic activity. *Journal of Biological Chemistry*, 1999. **6**: p. 3531-3540.

83. Howard, L., R. Maciewicz, and C. Blobel, Cloning and characterization of ADAM28: evidence for autocatalytic pro-domain removal and for cell surface localization of mature ADAM28. *Biochem J*, 2000. **348**(Pt 1): p. 21-27.

84. Schlomann, U., D. Wildeboer, A. Webster, O. Antropova, D. Zeuschner, C. Knight, A. Docherty, M. Lambert, L. Skelton, H. Jockusch, and J. Bartsch, The metalloprotease disintegrin ADAM8. Processing by autocatalysis is required for proteolytic activity and cell adhesion. *Journal of Biological Chemistry*, 2002. **50**: p. 48210-48219.

85. White, J., ADAMs: modulators of cell-cell and cell-matrix interactions. *Current Opinion in Cell Biology*, 2003. **15**(5): p. 598-606.

86. Niewiarowski, S., M. McLane, M. Kloczewiak, and G. Stewart, Disintegrins and other naturally occurring antagonists of platelet fibrinogen receptors. *Semin Hematol*, 1994. **31**(4): p. 289-300.

87. Mazzocca, A., R. Coppari, R.D. Franco, J. Cho, T. Libermann, M. Pinzani, and A. Toker, A secreted form of ADAM9 promotes carcinoma invasion through tumor-stromal interactions *Cancer Research*, 2005. **65**(11): p. 4728-4738.

88. Schulz, B., J. Pruessmeyer, T. Maretzky, A. Ludwig, C. Blobel, P. Saftig, and K. Reiss, ADAM10 regulates endothelial permeability and T-cell transmigration by proteolysis of vascular endothelial cadherin. *Circulation Research*, 2008. **102**(10): p. 1192-1201.

89. Kenny, P. and M. Bissell, Targeting TACE-dependent EGFR ligand shedding in breast cancer. *J of Clinical Investigation*, 2007. **117**(2): p. 337-345.

90. Baker, A., D. Edwards, and G. Murphy, Metalloproteinase inhibitors: biological actions and therapeutic opportunities. *Journal of Cell Science*, 2002. **115**: p. 3719-3727.

91. Chrico, R., X. Liu, K. Jung, and H. Kim, Novel functions of TIMPs in cell signaling. *Cancer Metastasis Rev*, 2006. **25**: p. 99-113.

92. Brew, K., D. Dinakarpandian, and H. Nagase, Tissue inhibitors of metalloproteinases: evolution, structure and function. *Biochem Biophys Acta*, 2000. **1477**: p. 267-283.

93. Yu, W., S. Yu, Q. Meng, K. Brew, and J. Woessner, TIMP-3 binds to sulphated glycosaminoglycans of the extracellular matrix. *Journal of Biological Chemistry*, 2000. **275**: p. 31226-31232.

94. Will, H., S. Atkinson, G. Butler, B. Smith, and G. Murphy, The soluble catalytic domain of membrane type 1 matrix metalloproteinase cleaves the propeptide of progelatinase A and initiates autoproteolytic activation. Regulation by TIMP-2 and TIMP-3. *Journal of Biological Chemistry*, 1996. **271**: p. 17119-17123.

95. Amour, A., C. Knight, A. Webster, P. Slocombe, P. Stephens, V. Knauper, A. Docherty, and G. Murphy, The in vitro activity of ADAM-10 is inhibited by TIMP-1 and TIMP-3. *FEBS Lett*, 2000. **473**: p. 275-279.

96. Goldberg, G., B. Marmer, G. Grant, A. Eisen, S. Wilhelm, and C. He, Human 72-kilodalton type IV collagenase forms a complex with a tissue inhibitor of metalloproteinases designated TIMP-2. *Proc Natl Acad Sci USA*, 1989. **86**: p. 8207-8211.

97. Wilhelm, S., I. Collier, B. Marmer, A. Eisen, G. Grant, and G. Goldberg, SV40-transformed human lung fibroblasts secrete a 92-kDa type IV collagenase which is identical to that secreted by normal human macrophages. *Journal of Biological Chemistry*, 1989. **264**(29): p. 17213-17221.

98. Sato, H., T. Takino, Y. Okada, J. Cao, A. Shinagawa, E. Yamamoto, and M. Seiki, A matrix metalloproteinase expressed on the surface of invasive tumor cells. *Nature*, 1994. **370**: p. 61-65.

99. Strongin, A., I. Collier, G. Bannikov, B. Marmer, and G. Grant, Mechanism of cell surface activation of 72-kDa type IV collagenase. Isolation of the activated form of the membrane metalloprotease. *Journal of Biological Chemistry*, 1995. **270**: p. 5331-5338.

100. Fernandez, C., C. Butterfield, G. Jackson, and M. Moses, Structural and functional uncoupling of the enzymatic and angiogenic inhibitory activities of tissue inhibitor metalloproteinase-2 (TIMP-2): loop 6 is a novel

angiogenesis inhibitor. *Journal of Biological Chemistry*, 2003. **278**(40989-40995).

101. Qi, J., Q. Ebrahem, N. Moore, G. Murphy, L. Claesson-Welsh, M. Bond, A. Baker, and B. Anand-Apte, A novel function for tissue inhibitor of metalloproteinases-3 (TIMP3): inhibition of angiogenesis by blockage of VEGF binding to VEGF receptor-2. *Nature Medicine*, 2003. **9**: p. 407-415.
102. Yu, W., S. Yu, Q. Meng, K. Brew, and J. Woessner, TIMP-3 binds to sulfated glycosaminoglycans of the extracellular matrix. *Journal of Biological Chemistry*, 2000. **275**: p. 31226-31232.
103. Greene, J., M. Wang, Y. Liu, L. Raymond, C. Rosen, and Y. Shi, Molecular cloning and characterization of human tissue inhibitor of metalloproteinase 4. *Journal of Biological Chemistry*, 1996. **271**(48): p. 30375-30380.
104. Fernandez, C. and M. Moses, Modulation of angiogenesis by tissue inhibitor of metalloproteinase-4. *Biochem Biophys Res Commun*, 2006. **345**: p. 523-529.
105. Koskivirta, I., Z. Kassiri, O. Rahkonen, R. Kiviranta, G. Oudir, T. McKee, V. Kyto, A. Saraste, E. Jokinen, P. Liu, E. Vuorio, and R. Khokha, Mice with tissue inhibitor of metalloproteinase 4 (Timp4) delection succumb to induced myocardial infarction but not to cardiac pressure overload. *Journal of Biological Chemistry*, 2010. **285**(32): p. 24487-24493.
106. Takahashi, C., Z. Sheng, T. Horan, H. Kitayama, M. Maki, K. Hitomi, Y. Kitaura, S. Takai, R. Sasahara, A. Horimoto, Y. Ikawa, B. Ratzkin, T.

Arakawa, and M. Noda, Regulation of matrix metalloproteinase-9 and inhibition of tumor invasion by the membrane-anchored glycoprotein RECK. *Proc Natl Acad Sci USA*, 1998. **95**(22): p. 13221-13226.

107. Oh, J., R. Takahashi, S. Kondo, A. Mizoguchi, E. Adachi, R. Sasahara, S. Nishimura, Y. Imamura, H. Kitayama, D. Alexander, C. Ide, T. Horan, T. Arakawa, H. Yoshida, S. Nishikawa, Y. Itoh, M. Seiki, S. Itohara, C. Takahashi, and M. Noda, The membrane-anchored MMP inhibitor RECK is a key regulator of extracellular matrix integrity and angiogenesis. *Cell*, 2001. **107**(6): p. 789-800.
108. Egeblad, M. and Z. Werb, New functions for the matrix metalloproteinases in cancer progression. *Nature Reviews Cancer*, 2002. **2**: p. 161-174.
109. Thurston, G., Complementary actions of VEGF and Angiopoietin-1 on blood vessel growth and leakage. *J Anat*, 2002. **200**(6): p. 575-580.
110. Thomas, M. and H. Augustin, The role of the Angiopoietins in vascular morphogenesis. *Angiogenesis*, 2009. **12**: p. 125-137.
111. Stratman, A., K. Malotte, R. Mahan, M. Davis, and G. Davis, Pericyte recruitment during vasculogenic tube assembly stimulates endothelial basement membrane matrix formation. *Blood*, 2009. **114**: p. 5091-5101.
112. Stratman, A., W. Saunders, A. Sacharidou, W. Koh, K. Fisher, D. Zawieja, M. Davis, and G. Davis, Endothelial cell lumen and vascular guidance tunnel formation requires MT1-MMP-dependent proteolysis in 3-dimensional collagen matrices. *Blood*, 2009. **114**: p. 237-247.

113. Stratman, A., A. Schwindt, K. Malotte, and G. Davis, Endothelial-derived PDGF-BB and HB-EGF coordinately regulate pericyte recruitment during vasculogenic tube assembly and stabilization. *Blood*, 2010. **116**: p. 4720-4730.

114. Greenberg, J., D. Shields, S. Barillas, L. Acevedo, E. Murphy, J. Huang, L. Scheppke, C. Stockmann, R. Johnson, N. Angle, and D. Charesh, A role for VEGF as a negative regulator of pericyte function and vessel maturation. *Nature*, 2008. **456**(7223): p. 809-813.

115. Jain, R., Normalization of tumor vasculature: an emerging concept in antiangiogenic therapy. *Science*, 2005. **307**: p. 58-62.

116. Miner, J. and P. Yurchenco, Laminin functions in tissue morphogenesis. *Annual Reviews in Cell & Developmental Biology*, 2004. **20**: p. 255-284.

117. Davis, G., A. Stratman, A. Sacharidou, and W. Koh, Molecular basis for endothelial lumen formation and tubulogenesis during vasculogenesis and angiogenic sprouting. *International Review of Cell and Molecular Biology*, 2011. **288**: p. 101-165.

118. Quaegebeur, A., I. Segura, and P. Carmeliet, Pericytes: blood-brain barrier safeguards against neurodegeneration? *Neuron*, 2010. **68**(3): p. 321-323.

119. Brooks, P.C., R.A. Clark, and D.A. Cheresh, Requirement of vascular integrin alpha v beta 3 for angiogenesis. *Science*, 1994. **264**(5158): p. 569-71.

120. Brooks, P.C., A.M. Montgomery, M. Rosenfeld, R.A. Reisfeld, T. Hu, G. Klier, and D.A. Cheresh, Integrin alpha v beta 3 antagonists promote tumor regression by inducing apoptosis of angiogenic blood vessels. *Cell*, 1994. **79**(7): p. 1157-64.

121. Kim, S., K. Bell, S. Mousa, and J. Varner, Regulation of angiogenesis in vivo by ligation of integrin alpha5-beta1 with the central cell-binding domain of fibronectin. *American Journal of Pathology*, 2000. **156**: p. 1345-1362.

122. Ponce, M., M. Nomizu, and H. Kleinman, An angiogenic laminin site and its antagonist bind through the alphav-beta3 and alpha5-beta1 integrins. *FASEB Journal*, 2001. **15**: p. 1389-1397.

123. Stupack, D.G. and D.A. Cheresh, Integrins and angiogenesis. *Current topics in developmental biology*, 2004. **64**: p. 207-38.

124. Ingber, D. and J. Folkman, How does extracellular matrix control capillary morphogenesis? *Cell*, 1989. **58**: p. 803-805.

125. Deroanne, C.F., C.M. Lapiere, and B.V. Nusgens, In vitro tubulogenesis of endothelial cells by relaxation of the coupling extracellular matrix-cytoskeleton. *Cardiovasc Res*, 2001. **49**(3): p. 647-58.

126. Sieminski, A.L., R.P. Hebbel, and K.J. Gooch, The relative magnitudes of endothelial force generation and matrix stiffness modulate capillary morphogenesis in vitro. *Exp Cell Res*, 2004. **297**(2): p. 574-84.

127. Vailhe, B., M. Lecomte, N. Wiernsperger, and L. Tranqui, The formation of tubular structures by endothelial cells is under the control of fibrinolysis and mechanical factors. *Angiogenesis*, 1998. **2**(4): p. 331-44.

128. Kniazeva, E. and A.J. Putnam, Endothelial cell traction and ECM density influence both capillary morphogenesis and maintenance in 3-D. *Am J Physiol Cell Physiol*, 2009. **297**(1): p. C179-87.

129. Urech, L., A.G. Bittermann, J.A. Hubbell, and H. Hall, Mechanical properties, proteolytic degradability and biological modifications affect angiogenic process extension into native and modified fibrin matrices in vitro. *Biomaterials*, 2005. **26**(12): p. 1369-79.

130. Fischer, R.S., M. Gardel, X. Ma, R.S. Adelstein, and C.M. Waterman, Local cortical tension by myosin II guides 3D endothelial cell branching. *Current biology : CB*, 2009. **19**(3): p. 260-5.

131. Mammoto, A., K.M. Connor, T. Mammoto, C.W. Yung, D. Huh, C.M. Aderman, G. Mostoslavsky, L.E.H. Smith, and D.E. Ingber, A mechanosensitive transcriptional mechanism that controls angiogenesis. *Nature*, 2009. **457**: p. 1103-1108.

132. Califano, J.P. and C.A. Reinhart-King, The effects of substrate elasticity on endothelial cell network formation and traction force generation. *Conf Proc IEEE Eng Med Biol Soc*, 2009. **2009**: p. 3343-5.

133. Kniazeva, E. and A. Putnam, Endothelial cell traction and ECM density influence both capillary morphogenesis and maintenance in 3-D. *Am J Physiol Cell Physiol*, 2009. **297**(1): p. C179-C187.

134. Lee, P.F., A.T. Yeh, and K.J. Bayless, Nonlinear optical microscopy reveals invading endothelial cells anisotropically alter three-dimensional collagen matrices. *Experimental cell research*, 2009. **315**(3): p. 396-410.

135. Krishnan, L., J. Boying, H. Nguyen, H. Song, and J. Weiss, Interaction of angiogenic microvessels with the extracellular matrix. *Am J Physiol Heart Circ Physiol*, 2007. **293**(H3650-H3658).

136. Vailhe, B., X. Ronot, P. Tracqui, Y. Usson, and L. Tranqui, In vitro angiogenesis is modulated by the mechanical properties of fibrin gels and is related to alpha(v)beta3 integrin localization. *In Vitro Cell Dev Biol Anim*, 1997. **33**: p. 763-773.

137. Vernon, R. and E. Sage, Contraction of fibrillar type I collagen by endothelial cells: a study in vitro. *J Cell Biochem*, 1996. **60**: p. 185-197.

138. Ghajar, C.M., K.S. Blevins, C.C. Hughes, S.C. George, and A.J. Putnam, Mesenchymal Stem Cells Enhance Angiogenesis in Mechanically Viable Prevascularized Tissues via Early Matrix Metalloproteinase Upregulation. *Tissue Eng*, 2006. **12**(10): p. 2875-2888.

139. Kilarski, W.W., B. Samolov, L. Petersson, A. Kvanta, and P. Gerwins, Biomechanical regulation of blood vessel growth during tissue vascularization. *Nat. Med.*, 2009. **15**(6): p. 657-64.

140. Benest, A.V. and H.G. Augustin, Tension in the vasculature. *Nat. Med.*, 2009. **15**(6): p. 608-10.

CHAPTER 3

Design and Optimization of an *in vitro* Assay to Assess Permeability in a 3D Co-Culture of Engineered Capillaries

3.1 Introduction

The tissue engineering field has seen only limited success because of a lack of functional vasculature to supply nutrients and oxygen to full thickness tissues.(1-3) To address this challenge, we have developed methods to engineer stable capillary-like structures *in vitro* in 3D fibrin gels, and used this platform as a model system to better understand the design rules which govern the formation of functional vessel networks. By starting with endothelial cells and different types of stromal cells, we were able to produce a network of vessels that are stable in culture, with hollow lumens and network architectures.(4, 5) This model of capillary morphogenesis was then further expanded to explore the functionality of these tissue engineered vessels and ensure that they function as normal healthy vessels with controlled permeability. This was done by developing an *in vitro* assay of inverse permeability, where a tracer was added to a bulk gel, allowed to diffuse freely, and then the amounts of tracer, both inside and outside the capillary lumens, were quantified.

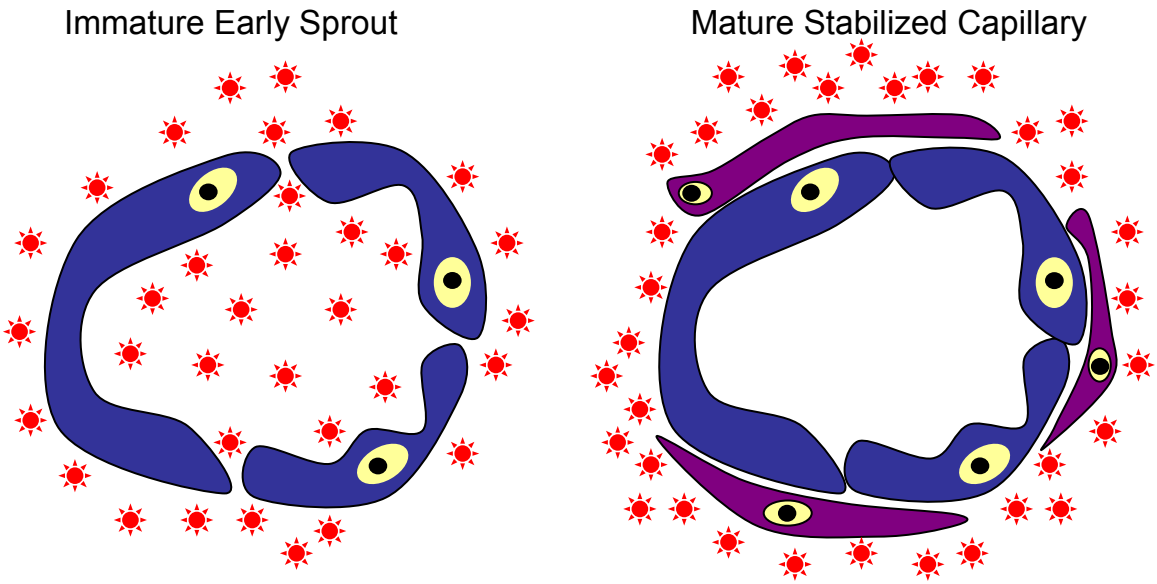

Figure 3.1. Model of inverse permeability used to determine capillary functionality kinetics in a 3D culture. Texas Red-conjugated dextran (70 kDa) is added to the bulk gel for 30 minutes and allowed to freely diffuse. Early capillary sprouts, which lack mature cell-cell junctions between the endothelial cells that form the tubules, will easily allow the tracer to be transported from the tissue space into the interior of the capillary. By contrast, mature capillaries that are stabilized by pericytes and possess more mature cell-cell junctions are capable of excluding the tracer from the lumen.

The premise behind this model is that immature capillaries with incomplete cell-cell junctions are unable to regulate permeability, thus allowing tracer to enter the capillary lumens.(6-10) If the capillaries present are mature, competent cell-cell junctions between endothelial cells, as well as the presence of stabilizing pericytes, will block tracer from entering the hollow lumens of the capillaries (Figure 3.1).

The methodologies required to produce an *in vitro* assay are discussed in detail here. First, the three dimensional fibrin tissue assembly where capillaries were cultured will be discussed. The traditional assay includes a layer of stromal cells on the upper surface of the fibrin constructs to provide cues for sprouting and capillary maturation.(11) For most of the following experiments, the assay has been altered slightly to include the stromal cells distributed throughout the

fibrin matrix. This potentially allows the stromal cells to adopt a pericyte-like phenotype and provide stabilization cues via direct contact with the capillary sprouts.

Next, the steps to achieve successful imaging are discussed, altered, and optimized. The biggest challenge in developing an inverse assay to assess permeability in these 3D cultures was the addition of fluorescent tracer to the bulk gel. The addition of such a large volume of fluorescent material produced high levels of background and caused difficulties in optical imaging techniques. These hurdles were overcome by altering steps in the process, such as staining methods, quantification, and gel construction specifications.

VE-cadherin junctional staining was used as a tool for imaging capillary cell-cell junctions between endothelial cells. As an alternative, hCD31 staining of the endothelial cells was used to define the borders of the capillaries for the permeability assays. Methods to quantify permeability are briefly discussed. Finally, optimization of the imaging methods for quantification was examined. The gel specifications were altered in order to eliminate excessive background signal during imaging. All of these design features and optimizations required to achieve successful model function are discussed in the context of this chapter.

3.2 Methods

Cell Culture

Human umbilical vein endothelial cells (HUVECs) were grown in fully supplemented Endothelial Growth Medium (EGM-2, Lonza, Walkersville, MD). Normal human lung fibroblasts (NHLFs, Lonza) were cultured in Media 199

(Invitrogen, Carlsbad, CA) supplemented with 10% FBS, 1% penicillin/streptomycin (Mediatech, Manassas, VA), and 0.5% gentamicin (Invitrogen) at 37°C and 5% CO_2. NHLFs were used prior to passage ten. ECs were used at passage three. Cells were cultured in monolayers until reaching 80% confluency and serially passaged using 0.05% trypsin-EDTA treatment.

3D Bead Assay & Fibrin Tissue Assembly

Endothelial cells coated onto microcarrier beads were embedded within a 3D fibrin matrix, in which stromal cells were also distributed, to form stable capillary structures. A schematic diagram of the process can be found in Figure 3.2. In more detail, four million HUVECs (p3) were harvested and coated on 10,000 presterilized Cytodex (Sigma-Aldrich, St. Louis, MO) microcarrier beads (131 – 220 μm diameter) in 5 ml of EGM-2 in an inverted T-25 flask over a 4 hour incubation period with mild agitation every 30 minutes. After 4 hours, 5 ml of fresh EGM-2 were added and the total volume was transferred to a fresh T-25 flask for incubation in standard cell culture position overnight. A 2.5 mg/ml bovine fibrinogen (Sigma-Aldrich) solution was made in serum-free EGM-2 and filtered through a 0.22 μm syringe filter. A 500 μl aliquot of the fibrinogen with 5% FBS was mixed with 50 pre-coated beads and polymerized by addition of 10 μl of thrombin (50 U/ml, Sigma- Aldrich) in a single well of a 24-well tissue culture plate. The mixture was incubated at 25°C for 5 minutes, and then at 100% humidity, 37°C and 5% CO_2 for 25 minutes. In the standard assay configuration, 25,000 NHLFs were plated on top of each gel after polymerization, and 1 ml of

fresh, fully supplemented EGM-2 was then added to the top of the gel. For some applications, stromal cells were distributed throughout the gel constructs rather than in a monolayer on top of the constructs. Media were changed every other day.

Thin Gel Fabrication for Confocal Microscopy

In order to produce gels that were thin enough for successful confocal imaging, the standard protocol was slightly modified. Beads were coated and fibrinogen solution was made in the standard manner outlined above. Either a 125 or 150 µl aliquot of the fibrinogen with 5% FBS and 10,000 NHLFs were mixed with 25 pre-coated beads and polymerized by addition of 2.5 or 3 µl of thrombin (50 U/ml, Sigma Aldrich) in a single well of a #1 chambered 8-well coverglass. The mixture was incubated at 25°C for 5 minutes, and then at 100% humidity, 37°C and 5% CO_2 for 25 minutes. 350 µl of fresh EGM-2 were then added to the top of the gel and medium was changed every day.

.

Dextran Tracer Selection & Addition to Fibrin Tissues

A 70 kDa dextran is above the known limit of freely permeable molecules that can diffuse from a capillary lumen to the external tissue under normal conditions.(10, 12) Dextran tagged with Texas Red was added to the bulk gel for 30 minutes after media removal and allowed to freely diffuse. After 30 minutes, a series of three 10 minute washes with PBS pH 7.4 were completed to remove any excess dextran from the sample. Fixation and staining followed. Due to the

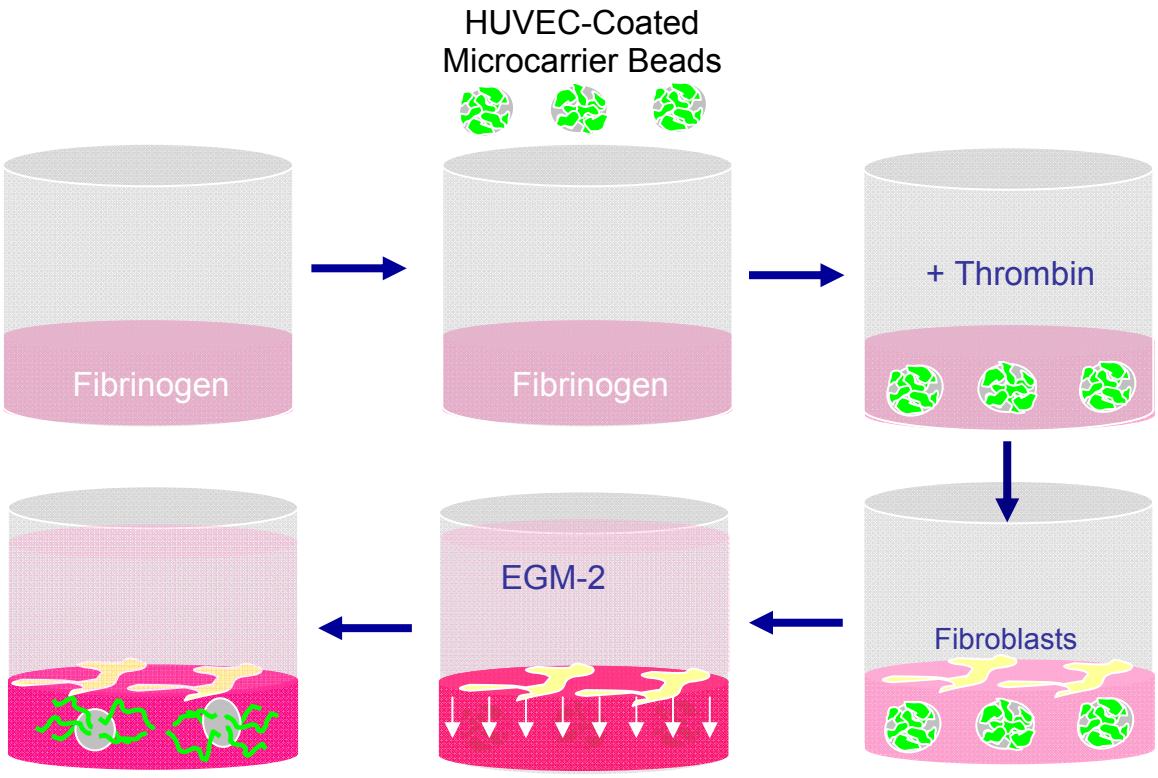

Figure 3.2 Schematic diagram of tissue construct assembly. HUVEC-coated microcarrier beads are suspended in a solution of fibrinogen and thrombin which forms a fibrin clot. A layer of fibroblasts was plated on top of the gel to provide pro-angiogenic cues that induce capillary sprout formation.

free lysines present in the dextran molecules, treatment with 10% formalin fixed the dextran molecules in place.

VE-Cadherin & hCD31 Staining

Constructs were stained for either VE-cadherin or human CD31. After the constructs were allowed to incubate for a specified time period (3, 5, 7, 10, 12, or 14 days), samples were fixed in 10% formalin (Sigma Aldrich) at 4°C for 20 minutes. Formalin was removed with three 5 minute washes in PBS. Cell membranes were permeabilized with 0.25% Triton X-100 in TBS-T for 5 minutes. Non-specific protein binding was eliminated with a 1 hour block in antibody diluting solution (0.1% Triton X-100 in TBS (TBS-T), with 2% bovine serum

albumin) (AbDil), and then washing was repeated 3 times with TBS-T. Human VE-cadherin primary antibody (BV9 clone, Santa Cruz Biotechnology, Santa Cruz, CA) was diluted 1:50 in AbDil and incubated at 4°C overnight. After incubation, excess antibody was removed with 3 washes in TBS-T of 20 minutes each, and then a final overnight wash. Secondary antibody (AlexaFluor 488 goat anti-mouse, Invitrogen) at a 1:100 dilution in Abdil was incubated for 2 hours. Excess antibody was removed with 3 washes in TBS-T of 20 minutes each and then a final overnight wash at 4°C. Cells were also stained with DAPI nuclear stain (Invitrogen) at a 1:10,000 dilution in PBS for 10 minutes and washed for 10 minutes.

For human CD31 staining, the process was similar, with the following exceptions. The permeabilization step was omitted. Human CD-31 primary antibody (Dako, Carpinteria, CA) was diluted 1:50 in AbDil and incubated at 4°C overnight. All subsequent steps were as described above for VE-cadherin staining, with the exception of a secondary antibody concentration of 1:400.

Design of an Image Analysis Program for Quantification

A customized MATLAB algorithm was designed to quantify the amount of dextran that was able to penetrate into the capillaries. All acquired confocal z-stacks were overlayed and compiled into a 3D overlay of the images of each as shown in Figure 3.3, Panel A. A 100-by-100 pixel box was placed in this image to read the background level of green. Each green image from the 3D z-stack is then seen in gray scale (Panel B). The maximum projection of these green

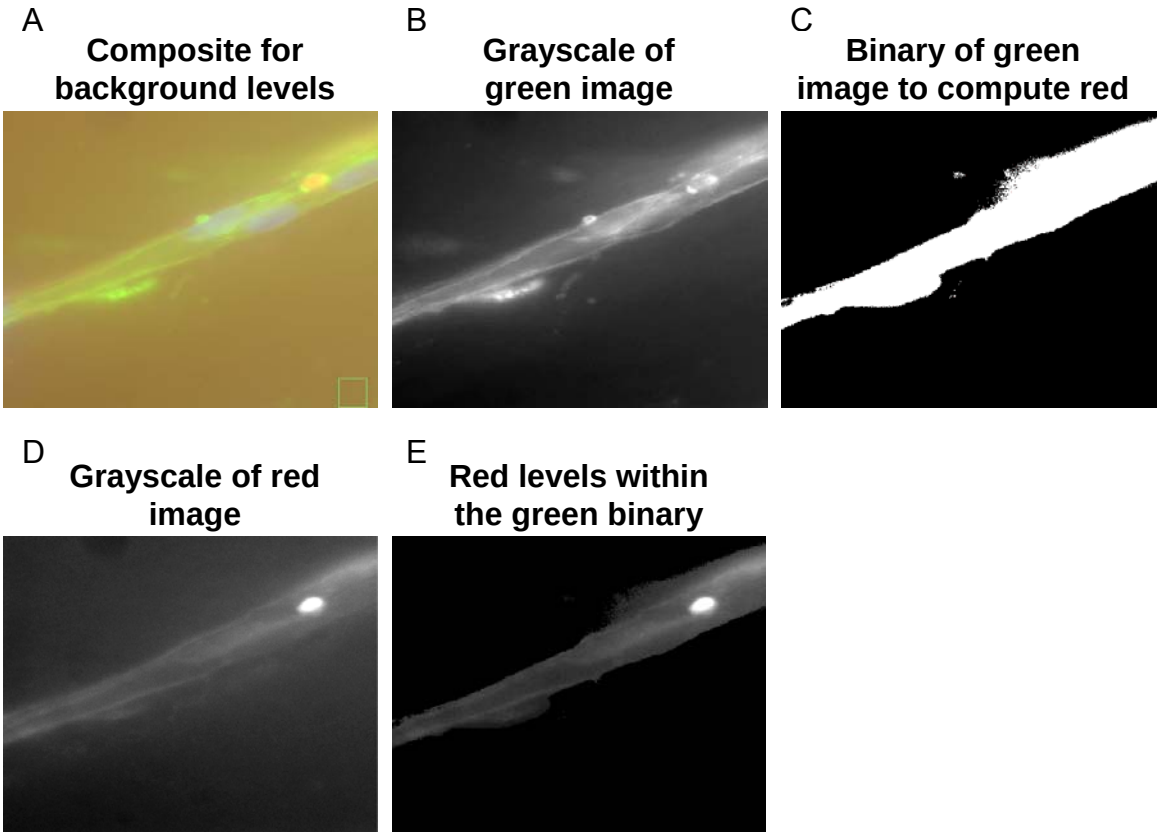

Figure 3.3. Pixel comparison algorithm. In Panel A, the algorithm makes a 3D overlay of the images of each channel. The user defines the location of a background box. In Panel B, each green image from the 3D z-stack is depicted in gray scale. In Panel C, the maximum projection of the green z-stack is converted to a binary image after the background (defined in Panel A) is eliminated. In Panel D, the portion of the red 3D z-stack that corresponds to the same area depicted in the green image is shown in gray scale as a maximum projection. In Panel E, only those pixels from the red image in Panel D that overlap with the green pixels in Panel C are shown. The pixel intensities from the image in Panel E are tallied and output as a ratio of red:green.

images from the z-stack is converted to a binary image. The cutoff for this binary image is the background level which was previously defined in Panel A. The portion of the red 3D z-stack that lies within the green image is seen in Panel D as a gray scale maximum projection image. In Panel E, only pixels from the red image in Panel D that overlap with the image in Panel C are shown. The pixel intensities from the image in Panel E are then tallied and the output as a ratio of red:green.

Statistical Analysis

All statistical analyses were performed using GraphPad Prism (GraphPad Software, La Jolla, California). Data are reported as mean ± standard deviation. One way analysis of variance (ANOVA) was performed with a Newman-Keuls multiple comparison post-hoc test. Statistical significance was assumed when $p < 0.05$.

3.3 Results

A. Reproduction of 3D Angiogenesis Tissue Culture Model

A 3D model of *in vitro* angiogenesis using HUVECs and fibroblasts was reproduced following a previously established protocol.(13) Briefly, HUVECs were seeded on microcarrier beads and embedded in fibrin gels with fibroblasts distributed throughout the gels (See Figure 3.4). At early time points, the HUVECs were coated on the microcarrier bead and

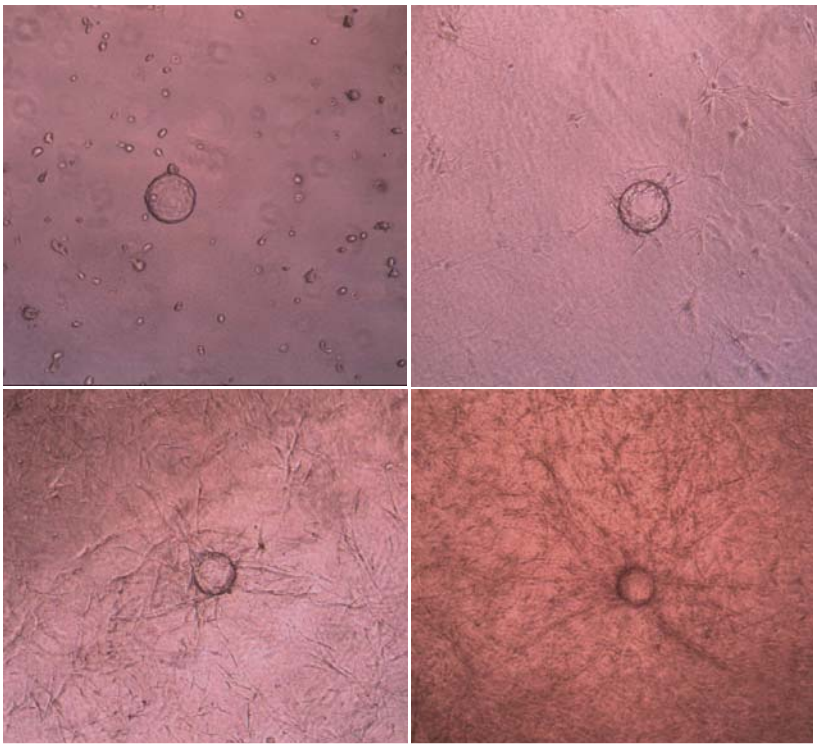

Figure 3.4. Brightfield 4x images of 3D fibrin gels with a single microcarrier bead imaged for days 0, 1, 3, and 7 after seeding. By day 7, a robust capillary network is seen.

fibroblasts were observed as small, round cells within the gel. At later time points, the HUVECs migrated off of the bead into tubular structures and fibroblasts stretched into long, thin cells throughout the gel. Based on prior studies, it was also expected that some fibroblasts are colocalizing with the nascent capillary sprouts and adopting a pericytic phenotype.(14)

B. 2D VE-Cadherin Staining

Vascular endothelial cadherin, also known as Cadherin 5, is an encoded calcium-dependent glycoprotein that links neighboring endothelial cells (ECs). These junctions are known to modulate permeability between aligned ECs, so visualization of these junctions may assist in defining the varying degrees of permeability for each sample and experimental condition. Confluent monolayers of HUVECs were cultured, fixed, and stained using an antibody that binds to VE-cadherin junctions (See Figure 3.5). This method was applied to visualize cell-cell junctions during capillary sprouting and morphogenesis.

C. 3D Imaging of Angiogenesis Model

A 3D model of *in vitro* angiogenesis was reproduced as described in Section 3.2, and capillary sprouts were imaged using 3D confocal microscopy to visualize the cell-cell junctions stained with a VE-cadherin antibody as described above (See Figure 3.6). To characterize the permeability and maturation of these capillary sprouts, fluorescent dextran was added to the culture medium. At early time

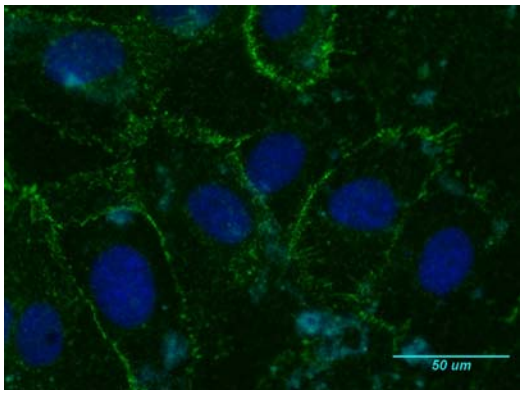

Figure 3.5. VE-Cadherin and DAPI staining of confluent monolayer of HUVECs to illustrate cell-cell junctions formed between cells to modulate permeability.

points (day 5), the concentration of dextran within each capillary sprout was a qualitative indication of the immaturity of the nascent vessels. As the sprouts matured, the junctions between cells became more prominent and started to control permeability into the sprouts, qualitatively reducing the amount of fluorescent dextran that could diffuse from the bulk tissue into the lumens of the capillaries. There were still low levels of dextran detected within the vessels at days 7 and 10, but as the cultures matured further, the dextran was nearly completely excluded from the lumens of the capillaries. However, these images revealed a new challenge, as it was difficult to use a vascular endothelial cadherin antibody to image immature vessels that had yet to form competent cell-cell connections, or vessels where the cell-cell junctions did not fall in a single focal plane as they matured and grew larger.

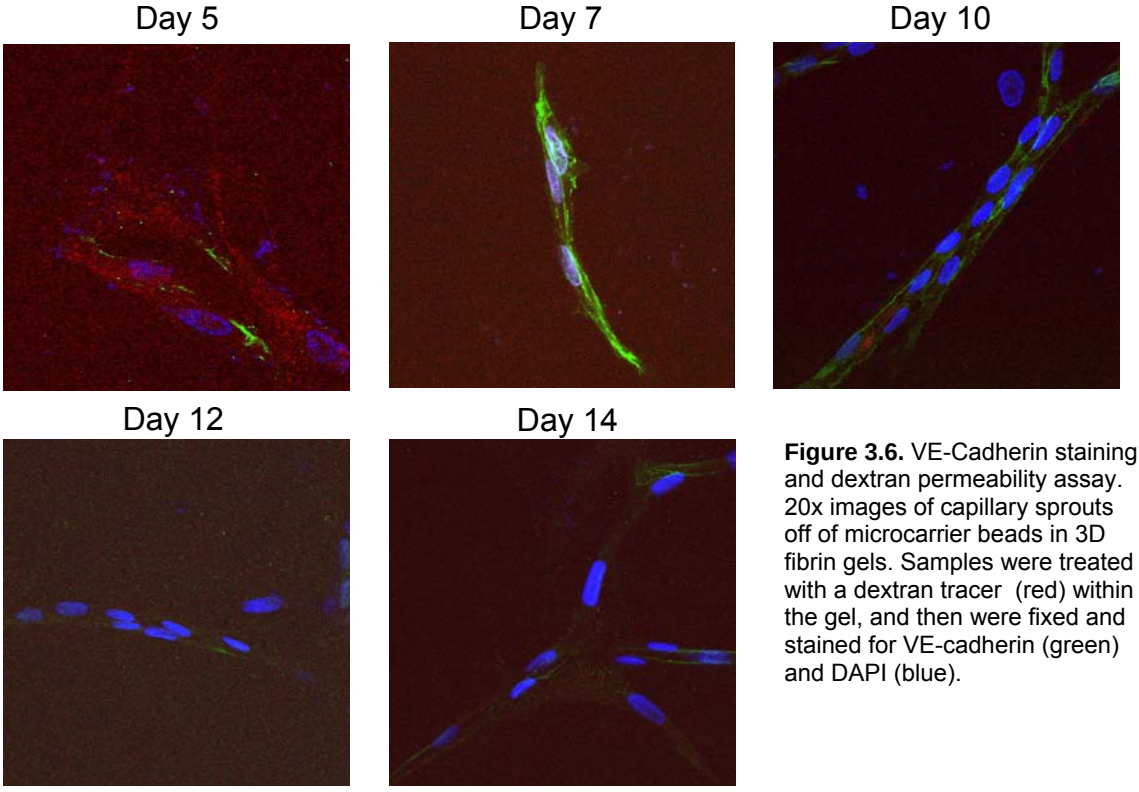

Figure 3.6. VE-Cadherin staining and dextran permeability assay. 20x images of capillary sprouts off of microcarrier beads in 3D fibrin gels. Samples were treated with a dextran tracer (red) within the gel, and then were fixed and stained for VE-cadherin (green) and DAPI (blue).

D. Gel Thickness Optimization for Confocal Microscopy

To facilitate imaging of the capillary structures within the thick 3D cultures, thinner gels were constructed and imaged as maximum projects of 3D vertical z-stacks using confocal microscopy. Gel volumes of 125 and 150 µl were constructed, with resulting gel thicknesses of 1.79 and 2.14 mm, respectively. To visualize the vessels even at an early stage prior to functional cell-cell junction formation, phalloidin was used to stain the actin filaments of all cells. In Figure 3.7, the thicker gels inhibited clear imaging and resulted in hazy images with a high degree of background noise. This noise interfered with proper processing of the images and quantification of the amount of dextran within each capillary. Therefore, gels of 125 µl each were used for all future *in vitro* experiments.

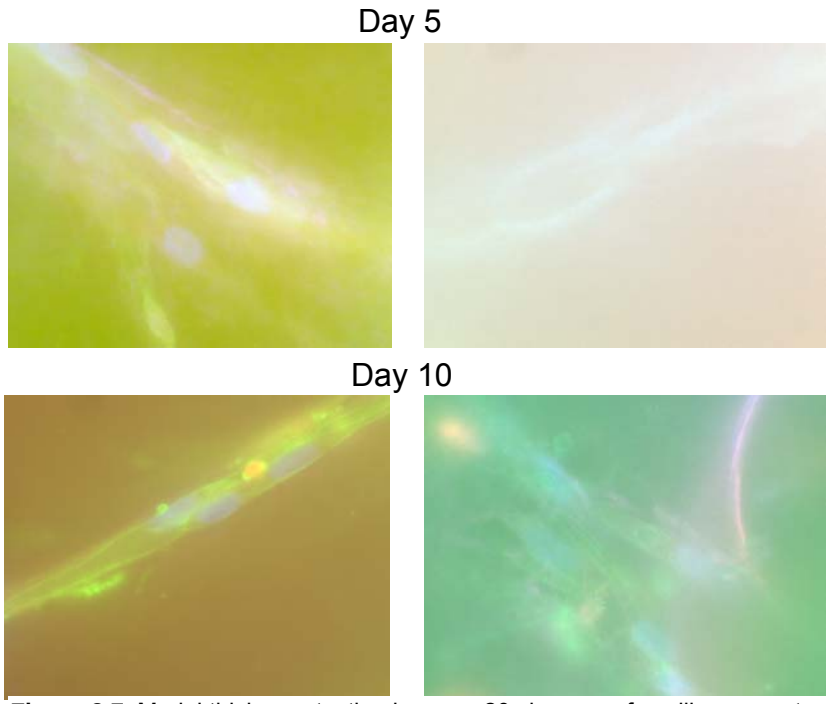

Figure 3.7. Model thickness testing images. 20x images of capillary sprouts off of microcarrier beads in gels of 125 µl (left) and 150 µl (right) at days 5 and 10. Samples were treated with a dextran tracer (red) within the gels, and then were fixed and stained for phalloidin (green) and DAPI (blue).

E. Live Capillary Perfusion Assay in vitro

Prior to constructing the tissues, HUVECs were first infected with GFP to allow for immediate live cell imaging during the assay, rather than requiring fixation and staining to visualize the capillary structures. At each time point, gels were incubated in the fluorescently conjugated dextran tracer solution. The capillary sprouts were found to gradually mature, with less and less dextran transport through the endothelium over time. Prior to day 5 of growth, the tracer easily penetrated through the vessel walls and permeability was high (Figure 3.8). After day 5, dextran accumulated at the periphery of the vessel, with very little transport across the endothelium. This can be clearly seen in Figure 3.9, the quantification of the images from Figure 3.8. Days 3 and 5 produced significantly higher levels of fluorescence within the capillaries than days 7, 10, 12, and 14 ($p < 0.05$). Days 7 and 10 excluded a significant amount of the tracer, and days 12 and 14 resulted in even lower levels of tracer in the capillary lumens. This result shows a clear transition from the initial permeable sprouting phase to a mature, stable, selectively-permeable phase of capillary growth that has shut out the high molecular weight dextran conjugates with a known diameter of 12 nm. Because the dextran was in suspension throughout the gel (not fixed to the fibrin), the challenge with these images was to distinguish where the tracer was concentrating, either at the interior or exterior of each capillary.

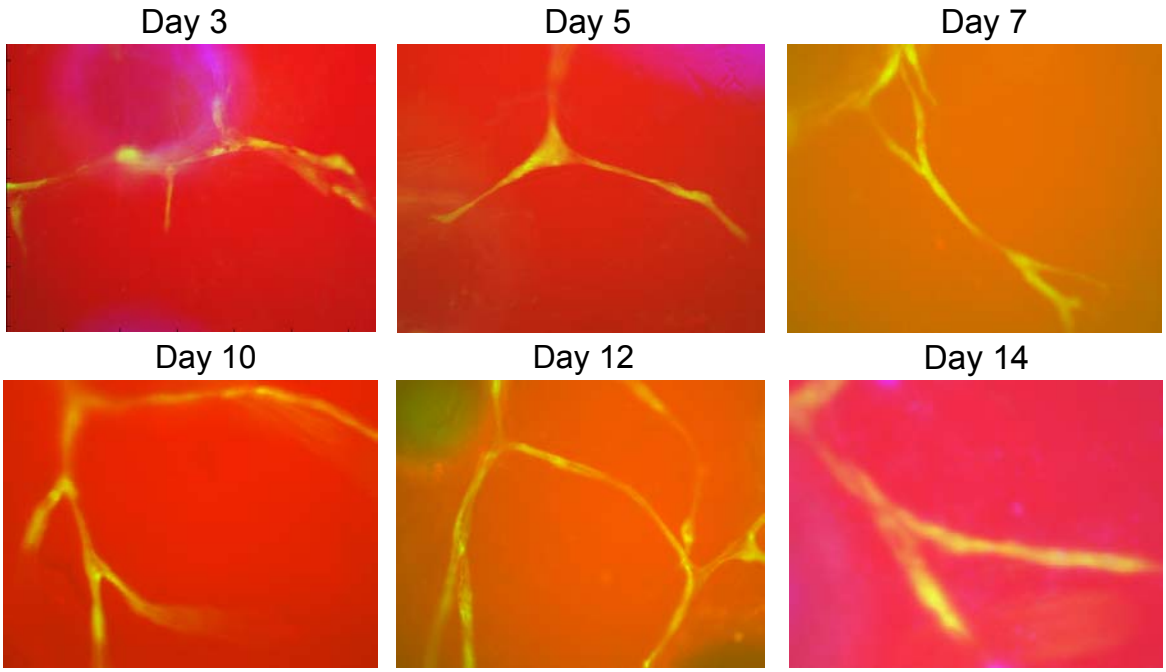

Figure 3.8 Live cell imaging with dextran tracing. 20x images of live GFP-labeled HUVEC capillary sprouts at varying days of growth. During early growth, there are many short, thin sprouts with dextran throughout the structure. At later time points, sprouts are highly branched, thicker, and more stable.

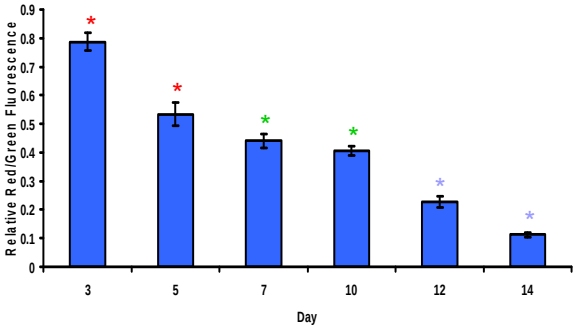

Figure 3.9. Quantification of live-cell imaging with dextran tracing. It can be seen that there are 3 significantly different groupings of fluorescence, with the highest levels of dextran within the vessels at early time points, and much less dextran accumulating within the vessels at later time points, once the vessels have matured.

F. Fixed Capillary Perfusion Assay in vitro

In order to eliminate some of the background noise in the live cell imaging, samples were fixed. This allowed for the free lysines on the dextran molecules to crosslink to the fibrin matrix and remove excess tracer. Samples were stained for human CD31, a known molecular marker of endothelial cells. DAPI, a fluorescent stain that binds to DNA, was used as a nuclear marker. The same trend was seen in these images as was seen in the live cell imaging; however, the tracking

of dextran concentration was much more easily visualized with these fixed samples. The drawback to this type of imaging was the loss of some of the fluorescent dextran, as the molecules are fixed and any tracer that was not cross-linked to the matrix is washed away. In Figure 3.10, at early time points, it can be seen that dextran concentrated within the capillary sprouts (days 3-5), while at later time points (days 12-14), the vessels are more mature and were able to keep the tracer from crossing the endothelium and accumulating in the lumen. For quantification of the images from Figure 3.10, see Figure 3.11.

3.4 Discussion

Capillary functionality is a key component of the developing tissue engineering community. Several groups have effectively used fluorescent tracers of various molecular weights as indicators of capillary permeability. (9) These dextran molecules function as would any molecular components of the blood, which would need to effectively diffuse through the endothelial layer in capillaries.(12) Other groups have previously used microfluidics or transwells with endothelial monolayer cultures to measure transendothelial resistance and permeability; however, these are not effective measures of trans-capillary permeability *in situ*. (15)

As discussed throughout the results section, several hurdles needed to be overcome to successfully develop an assay that is able to detect permeability

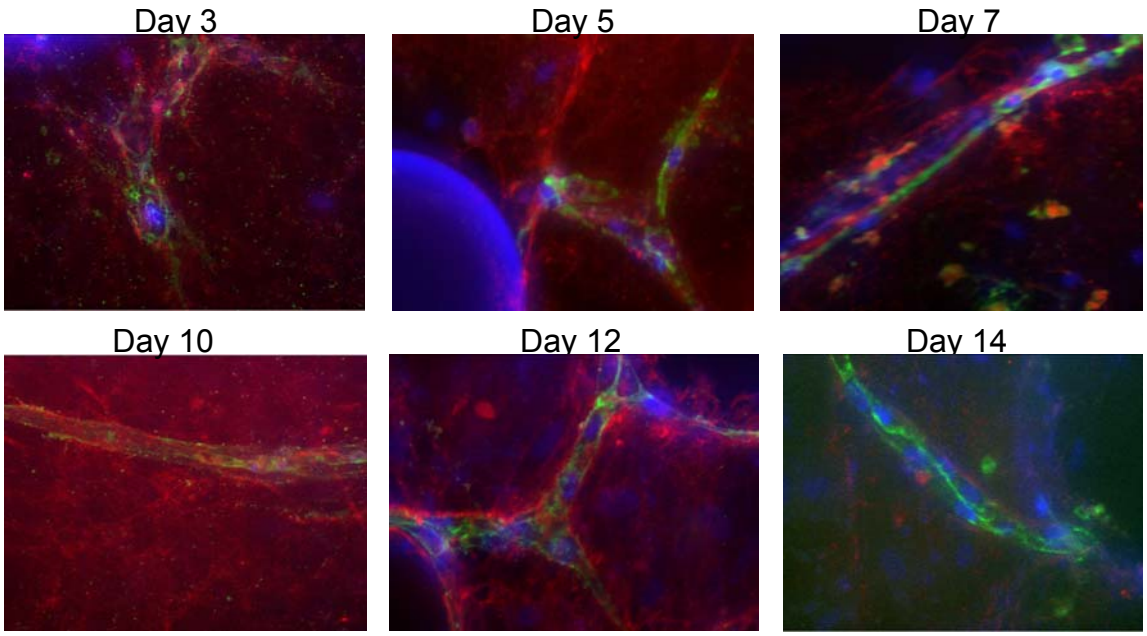

Figure 3.10. Fixed cell imaging with dextran tracing. 20x images of fixed CD-31 labeled HUVEC capillary sprouts (green) at varying days of growth. During early growth, there are many short, thin sprouts with dextran (red) throughout the structure. At later time points, sprouts are highly branched and more stable, with dextran accumulating only at the vessel periphery.

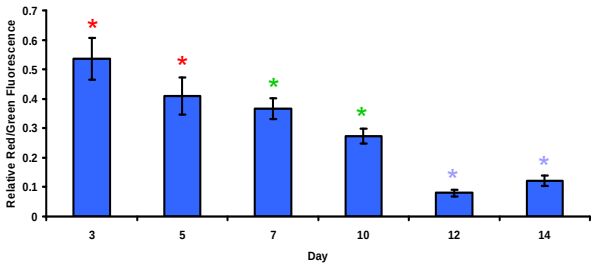

Figure 3.11. Quantification of fixed cell imaging with dextran tracing. It can be seen that there are 3 significantly different groupings of fluorescence, with the highest levels of dextran within the vessels at early time points, and much less dextran accumulating within the vessels at later time points, once the vessels have matured. The trend is the same as in Figure 3.9, with lower absolute values due to the fixation of dextran.

changes in our established 3D *in vitro* model of capillary morphogenesis. First, the cell-cell junctions between endothelial cells were imaged. This was done in an effort to see how these junctional connections control permeability, and to chart the development of these permeability-controlling complexes. However, the challenge with this method was that the appearance of these junctional complexes was a time-dependent process. At early time points, there was a sparse level of expression, thus causing fluorescent imaging and determination of the capillary periphery to be difficult. At later time points, this became an easier

task; however, 3D reconstruction of capillary tubules using confocal microscopy with VE-cadherin fluorescent staining was still difficult, owing to the sparseness of the complexes. Due to the 3D nature of this system, staining could appear in multiple focal planes and was difficult to discern the distinct edges of each capillary. This problem was exacerbated when capillaries did not grow parallel to the bottom of the plate. Because of this, broad-spectrum staining via a known positive marker of the endothelial cells, CD31, was used to mark capillary borders for quantification purposes.

The thickness of the 3D gels was known to have an effect on capillary growth, as was previously determined.(11) Gels were scaled down across all dimensions, in order to eliminate the excessive background noise due to freely diffusing dextran throughout the gels during confocal imaging. Two different gel thicknesses were tested in order to achieve optimal imaging with the thickest possible gels, to most closely mimic previous work and physiological conditions. Thinner gels more closely approximate 2D growth conditions than 3D conditions, so thicker gels were desired.

Both live imaging with GFP-tagged endothelial cells, and imaging after fixation with human CD31 stained endothelial cells was done to ensure that the trend observed was due to the maturation kinetics of the capillaries rather than being an artifact of the staining assay. The same trend was observed with both modalities; thus, the maturation rates of the capillaries were determined to be the varying condition. Fixation of the cultures allowed the dextran to be much less

overpowering in the culture system, and the imaging became much clearer. For all future experiments, fixed cultures were used.

Three distinct phases of capillary maturation were seen in these results, aligning with the previous descriptions of the angiogenic process. Initially, there was a phase where the capillaries were still sprouting and developing into tubules, few cell-cell junctions were observed, and little control over permeability was observed. Next, there was a mid-phase, where cell-cell junctional complexes are beginning to appear, and the capillaries are starting to have some level of functional control. Finally, there was a phase of stabilized, mature capillary functionality, where the sprouts were able to exclude most of the tracer from their lumens.

In summary, the experimental processes discussed in this chapter helped to achieve a robust assay. This assay was then used for comparisons of growth kinetics across several stromal cell types, and was then adapted for use on *in vivo* samples as well.

3.5 References

1. Brey E, Uriel S, Greisler H, and McIntire L. Therapeutic neovascularization: contributions from bioengineering. *Tissue Engineering* **11**, 567-584 (2005).
2. Neumann T, Nicholson B, and Sanders J. Tissue engineering of perfused microvessels. *Microvascular Research* **66**, 59-67 (2003).

3. Melero-Martin J, Obaldia M, Kang S, Khan Z, Yuan L, Oettgen P, and Bischoff J. Engineering robust and functional vascular networks in vivo with human adult and cord blood derived progenitor cells. *Circulation Research* **103**, 194-202 (2008).
4. Ghajar C, Blevins K, Hughes C, George S, and Putnam A. Mesenchymal stem cells enhance angiogenesis in mechanically viable prevascularized tissues via early MMP upregulation. *Tissue Engineering* **12**, 2875-2888 (2006).
5. Kniazeva E, and Putnam A. Endothelial cell traction and ECM density influence both capillary morphogenesis and maintenance in 3-D. *American Journal of Physiology - Cell Physiology* **297**, C179-C187 (2009).
6. Baluk P, Hashizume H, and McDonald D. Cellular abnormalities of blood vessels as targets in cancer. *Current Opinion in Genetics & Development* **15**, 102-111 (2005).
7. Hashizume H, Baluk P, Morikawa S, McLean J, Thurston G, Roberge S, Jain R, and McDonald D. Openings between defective endothelial cells explain tumor vessel leakiness. *Am J Path* **156**, 1363-1380 (2000).
8. Jain R. Molecular regulation of vessel maturation. *Nature Medicine* **9**, 685-693 (2003).
9. Shaterian A, Borboa A, Sawada R, Costantini T, Potenza B, Coimbra R, Baird A, and Eliceiri B. Real-time analysis of the kinetics of angiogenesis and vascular permeability in an animal model of wound healing. *Burns* **35**, 811-817 (2009).

10. Chrobak K, Potter D, and Tien J. Formation of perfused, functional microvascular tubes in vitro. *Microvascular Research* **71**, 185-196 (2006).

11. Griffith C, Miller C, Sainson R, Calvert J, Jeon N, Hughes C, and George S. Diffusion limits of an in vitro thick prevascularized tissue. *Tissue Engineering* **11**, 257-266 (2005).

12. Curry F, Huxley V, and Adamson R. Permeability of single capillaries to intermediate-sized colored solutes. *American Journal of Physiology - Heart and Circulatory Physiology* **245**, H495-505 (1983).

13. Chen X, Aledia A, Ghajar C, Griffith C, Putnam A, Hughes C, and George S. Prevascularization of a fibrin-based tissue construct accelerates the formation of functional anastomosis with host vasculature. *Tissue Engineering Part A* **15**, 1363-1371 (2009).

14. Ghajar C, Kachgal S, Kniazeva E, Mori H, Costes S, George S, and Putnam A. Mesenchymal cells stimulate capillary morphogenesis via distinct proteolytic mechanisms. *Experimental Cell Research* **316**, 813-825 (2010).

15. Sandoval R, Malik A, Naqvi T, Mehta D, and Tiruppathi C. Requirement for Ca+2 signaling in the mechanism of thrombin-induced increase in endothelial permeability. *American Journal of Physiology - Lung Cellular and Molecular Physiology* **280**, L239-L247 (2001).

CHAPTER 4

Functionality Comparisons Across Cell Types in a 3D Co-Culture of Engineered Capillaries

4.1 Introduction

Success within the tissue engineering field continues to be limited due to the inability to form a functional vasculature capable of supplying oxygen and nutrients to sustain tissue growth and metabolism.(1-3) Fabrication of constructs larger than 200 μm in thickness has been mostly unsuccessful, with large, hollow organs or avascular tissues being two exceptions.(4) Tissues thicker than this threshold are unable to overcome the limits of diffusion to properly nourish the tissue. Several possible solutions to overcome this hurdle have been proposed and explored in the literature over the past decade. One promising option involves the delivery of combinations of pro-angiogenic factors with precise spatial and temporal resolution in order to recruit host vasculature.(5) However, this approach can be limited by the fact that the half-lives of these factors are often very short, thereby limiting their bioactivity, and by the fact that even multiple combinations of factors cannot fully recapitulate the complex milieu of pro-angiogenic factors presented to cells *in vivo*. An alternative approach is to

provide the cell types that are required for new vessel formation, so that they can directly deliver the appropriate cocktail of required pro-angiogenic cues as necessary. Amongst the most recent possible solutions to overcome this hurdle is the idea of creating prevascularized tissues, which contain networks of vessels formed *in vitro* that can self-organize and anastamose with the host vasculature *in vivo* shortly after implantation.(6, 7)

Efforts to create prevascularized tissue constructs typically involve co-cultures of ECs and a supporting mesenchymal cell type, which is intended to act as a pericyte coat, within a 3D biomaterial scaffold.(8, 9) Several cell types have been shown to promote capillary morphogenesis and adopt periendothelial locations, including fibroblasts(10), SMCs(11), MSCs(12), and AdSCs.(13, 14) While all of these cell types appear to promote capillary formation, it is unclear if each type yields capillaries whose functional properties are similar to those of healthy, mature capillaries. Previous work from our group shows that different stromal cells promote capillary sprouting in fibrin hydrogels via different proteolytic enzymes(15-17), but the functional consequences (if any) of this difference are unknown.

This study focuses on the functional differences of capillary networks assembled from ECs and these varying mesenchymal cell types as stabilizing pericytes, using permeability as one marker of vessel functionality. A model of inverse permeability was developed, as was described in Chapter 3. Junctional staining and Western blotting were done to further explore the mechanisms of permeability control and pericyte differentiation as well.

4.2 Methods

Ethics Statement

Human umbilical vein ECs (HUVECs) were harvested from fresh umbilical cords following a previously established protocol.(8) The cords were obtained via a process considered exempt by the University of Michigan's institutional review board because the tissue is normally discarded, and no identifying information is provided to the researchers who receive the cords.

Cell Culture

HUVECs were grown in fully supplemented Endothelial Growth Medium (EGM-2, Lonza, Walkersville, MD). Normal human lung fibroblasts (NHLFs, Lonza) were cultured in Media 199 (Invitrogen, Carlsbad, CA) supplemented with 10% FBS, 1% penicillin/streptomycin (Mediatech, Manassas, VA), and 0.5% gentamicin (Invitrogen) at 37°C and 5% CO_2. Mesenchymal stem cells (Lonza) and adipose-derived stem cells (Invitrogen) were cultured in Dulbecco's modified Eagle Medium (DMEM, Sigma-Aldrich, St. Louis, MO) supplemented with 10% FBS, 1% penicillin/streptomycin (Mediatech), 0.5% gentamicin (Invitrogen) at 37°C and 5% CO_2. NHLFs, MSCs, and AdSCs were all used prior to passage ten. Cells were cultured in monolayers until reaching 80% confluency and serially passaged using 0.05% trypsin-EDTA treatment.

Tissue Construct Assembly

Constructs were made as described in detail in Chapter 3. Identical constructs were also made using AdSCs and MSCs. For some applications,

stromal cells were distributed throughout the gel constructs rather than in a monolayer on top of the constructs.

Tissue Construct Assembly for Confocal Microscopy

The modified protocol was followed as described in Chapter 3. In short, small scale gels of 125 µl total volume of a 2.5 mg/ml fibrin solution were constructed in each well of an 8-well chambered #1 coverglass. Gels contained 25 pre-coated endothelial cell-Cytodex beads, and 10,000 stromal cells (either NHLFs, MSCs, or AdSCs) were distributed throughout the matrix.

Permeability Assay

Selectively permeable mature capillaries are known to be impermeable to dextrans over a molecular weight of 65 kDa, so a Texas Red-conjugated dextran ($\lambda_{ex/em}$ of 595/615 nm) with a molecular weight of 70 kDa was chosen (Invitrogen).(23) This dextran molecule also contains free lysines, and is therefore fixable in formalin. All samples were directly incubated at 25°C for 30 minutes with a 5% dextran solution in phosphate buffered saline (PBS), and then excess dextran was removed by 3 washes of 10 minutes each with PBS. In some experiments, histamine (Sigma-Aldrich) was added to capillary cultures prior to dextran addition and culture termination via fixation at a concentration of 100 µM and allowed to incubate for 5 minutes.(22) Assays were continued as previously described above by addition of dextran, fixation, staining, and 3D confocal imaging.

Staining

All VE-cadherin and human CD31 staining was done following the protocols described in Chapter 3.

Western Blotting

After the constructs were allowed to incubate for a specified time period (3, 5, 7, 10, 12, or 14 days), samples were lysed using RIPA lysis buffer (50 mM Tris-HCl pH 7.6, 150 mM NaCl, 1% Triton X-100, 0.5% sodium deoxycholate, 0.1% SDS), homogenized, and two cycles of 30 second sonication and 20 second vortexing were completed. Lysates were cleared via centrifugation at 14,000 x g for 10 minutes at 4°C. Total protein concentration was determined via bicinchoninic acid assay (Thermo Fisher Scientific, Waltham, MA). Samples were boiled, then equal amounts of total protein were loaded for all co-culture conditions into a 10% tris-glycine gel (Invitrogen) and then electrophoretically separated for 3.5 hours. Proteins were then transferred onto a poly(vinylidine fluoride) membrane and probed via mouse anti-human VE-cadherin antibody (Santa Cruz Biotechnology). After washing, secondary horseradish peroxidase-conjugated anti-mouse antibody was incubated on the membrane (Santa Cruz Biotechnology). Protein expression was then visualized via an enhanced chemiluminescence detection system.

Quantification of Total Network Length & Number of Vessel Segments

Prior to bead coating, HUVECs were labeled with cell tracker dye, SP-DiIC$_{18}$(3) (Invitrogen) and tissues were constructed as described above. Low magnification fluorescent images (4x) were taken at days 3, 7, 10, and 14 by tracking the same beads throughout growth via MetaMorph (Molecular Devices, Sunnyvale, CA). Images were then quantified via the Angiogenesis Tube Formation module of MetaMorph to track the total network length and the total number of vessel segments per bead. Upper and lower limits were defined to exclude beads and nodes from the quantification. Five individual beads were imaged per cell type for each of three separate experiments for a total of fifteen images per experimental condition.

Confocal Microscopy

Thin tissue samples were made as described in Chapter 3, incubated for desired time periods, and a dextran assay was done as described earlier. All samples were imaged using an Olympus IX81 spinning disk confocal microscope equipped with a 100-W high pressure mercury lamp (Olympus, Center Valley, PA) and a Hammamatsu camera (Bridgewater, NJ) along a vertical z-stack of the entire diameter of each capillary with 0.5 μm optical slices to visualize the location of dextran within the interior/exterior of each capillary. Each set of images was quantified using the methods described in Chapter 3. Single confocal images were taken for proof of concept dextran localization on a Zeiss LSM 510-Meta laser scanning confocal microscope.

Statistical Analysis

All statistical analyses were performed using GraphPad Prism (GraphPad Software, La Jolla, California). Data are reported as mean ± standard deviation. One way analysis of variance was performed with a Newman-Keuls multiple comparison post-hoc test. Statistical significance was assumed when $p < 0.05$.

4.3 Results

A. Assay Development and Validation

During angiogenesis, new capillary sprouts form following initial budding from a source vessel, and become more elongated, branched, and stabilized by supporting pericytes over time. An important functional hallmark of new capillaries is the reformation of basement membrane and the ability to regulate transport across the vessel wall. In this study, a 3D cell culture model of angiogenesis was combined with a quantitative algorithm to develop a metric of capillary permeability and maturation. At specific time points, fluorescent dextran was added to the culture medium and allowed to incubate for a short period of time, after which the cultures were fixed. The localization of the dextran on the inside or outside of the capillary also provided an indirect determination of the timing of pericyte-EC associations. To better define the edges of capillaries for our quantitative algorithm, HUVECs that sprouted from the microcarrier beads were also stained with hCD31 antibodies.

Within the first few days after the 3D cell culture was initiated, HUVECs coated on the microcarrier beads began to sprout. At relatively early time points (day 5), dextran tracer added to the culture medium permeated throughout the

entire 3D gel, and could even be found within the newly-formed lumens of the nascent vessels (Figure 4.1A), consistent with the idea that these vessels are particularly immature and lack the structural features necessary to regulate permeability. As the sprouts matured, dextran transport across the vessel wall was limited as shown by the reduced amount of fluorescent dextran that diffused from the bulk tissue into the lumens of the capillaries. As the cultures matured further (day 10), the dextran was nearly completely excluded from the lumens of the capillaries (Figure 4.3B), especially as seen in cross-section (Figure 4.1B, inset).

To validate this model system and our quantitative algorithm, cultures were treated with histamine, a known modulator of capillary permeability.(22, 24)

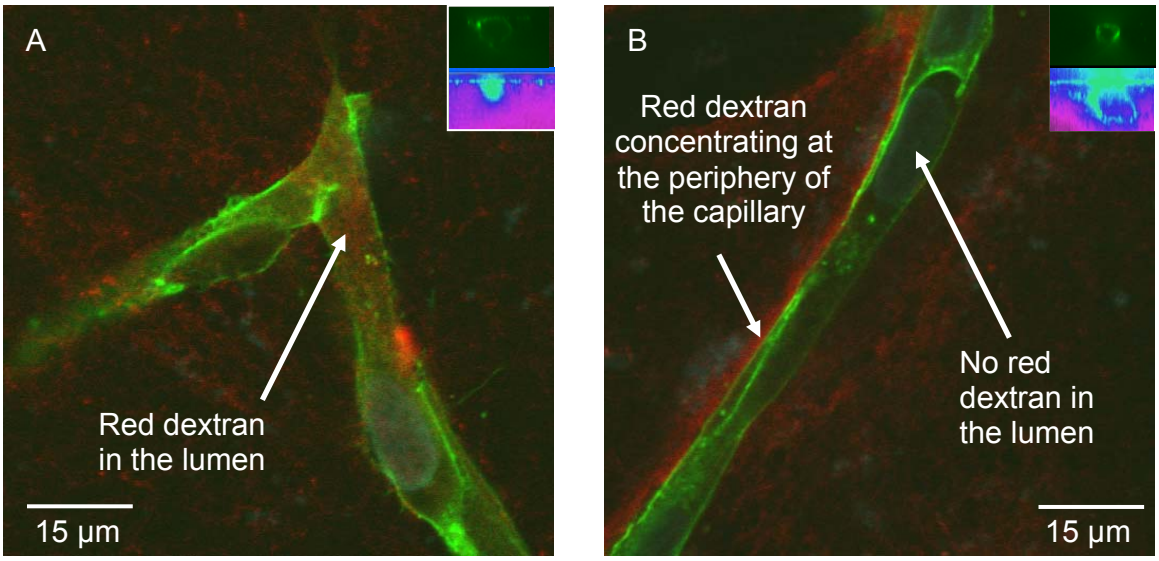

Figure 4.1. Dextran tracer localization via confocal microscopy. 60x confocal microscopy images of days 5 (A) and 10 (B) capillaries after 70 kDa dextran tracer addition (red), fixation with 10% formalin, and human CD31 staining (green) of HUVECs. Inset images: HUVECs (top) and Dextran (bottom) show hollow lumens with or without dextran. A) Red tracer is present within the lumens of the capillaries, demonstrating a low resistance to permeability. B) Red tracer is excluded from the lumens of the capillaries, demonstrating an increased resistance to permeability as the capillaries mature over time.

The output of the quantitative algorithm was a ratio of red (dextran) to green

(CD31) fluorescence for each capillary. After treatment with histamine, cultures showed a marked increase in permeability across all time points (Figure 4.2). At day 3, histamine triggered a 39% increase in permeability over untreated controls, even though the vessels were relatively immature in terms of their structure. By day 14, when the vessels had fully matured, tracer accumulation within the capillaries following histamine treatment was nearly twice that of untreated controls, indicating that the nascent capillaries are indeed capable of regulating their permeability in response to a physiologic stimulus, and that our algorithm is capable of detecting such changes.

B. Control of Permeability Evolves as Capillaries Mature

Next, we used this newly validated approach to characterize the kinetics with which the capillaries formed within our 3D cell culture model as it matures over time. The baseline model system involves the use of stromal fibroblasts (i.e., NHLFs) distributed throughout the 3D gels as the source of stabilizing pericytes. At early time points (days 3 and 5), dextran tracer accumulated within the lumens of capillaries, as shown by the high ratio of red (dextran) to green (the boundary of the capillaries, marked by hCD31 staining) fluorescence (Figure 4.3, solid gray bars). These high levels of permeability gradually decreased with time as the capillaries matured. At intermediate time points (days 7 and 10), the red:green ratio decreased by up to 48% when fibroblasts were used as the stromal cells (Figure 4.3, black bars). By later time points (days 12 and 14), almost all of the

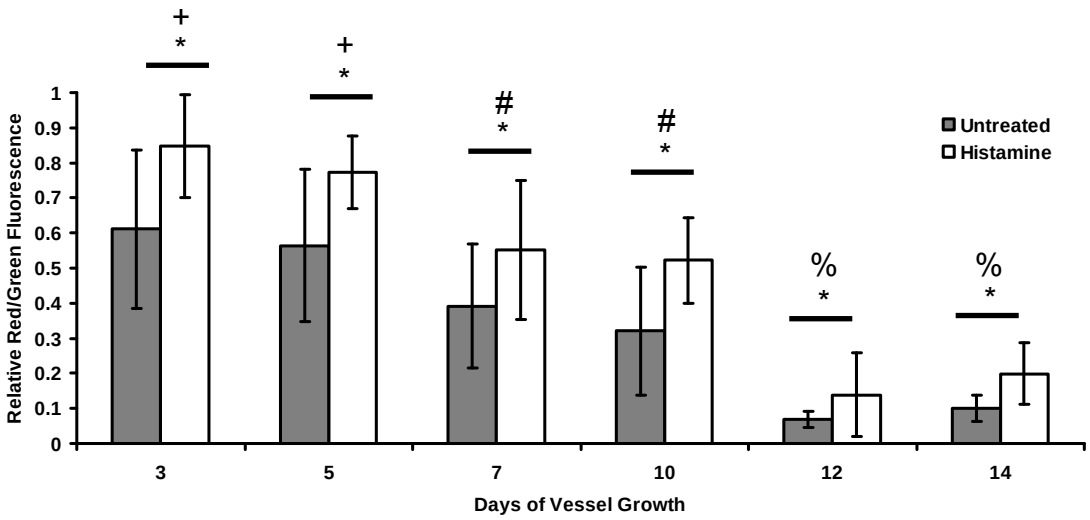

Figure 4.2. Assay validation using histamine to modulate capillary permeability. Histamine treatment quantitatively modulates permeability of the engineered capillary networks, as expected. In this graph, the * symbol indicates statistical significance ($p<0.05$) between the black and white bars (-/+ histamine) at each time point. The +, #, and % symbols indicate statistically significant differences ($p<0.005$) between the data marked by these symbols at certain time points and all other time points marked with different symbols. For example, the values at day 3 and day 5 (for both -/+ histamine) are significantly different from the values at all of the other time points, but not from each other.

dextran was being excluded from the capillary lumens (89% decrease from initial levels).

C. Alteration of Stromal Cell Type Modulates Capillary Permeability

When stromal cell types other than fibroblasts were used to stimulate capillary morphogenesis in this assay, we observed significant differences in the regulation of vessel permeability. Specifically, MSCs and AdSCs produced stable capillaries much more quickly than did the fibroblasts, as shown by a significant reduction in the ratio of red to green fluorescence (Figure 4.3, white and crosshatched bars). At day 3, capillaries composed of HUVEC-MSC co-cultures and HUVEC-AdSC co-cultures showed reductions in red to green fluorescence of 50 and 59%, respectively, compared to the values from HUVEC-fibroblast co-cultures. This indicated that far less of the dextran tracer crossed the capillary

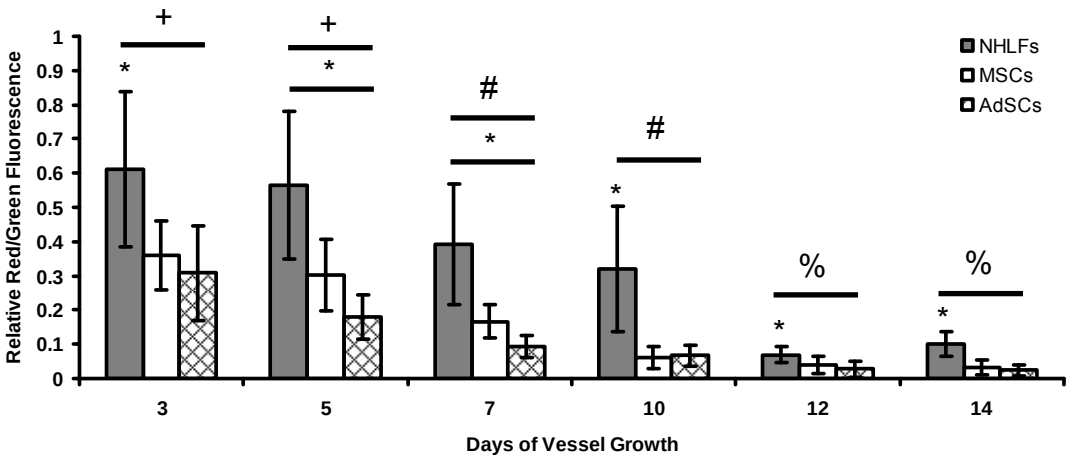

Figure 4.3. Quantification of permeability using a customized algorithm. Quantification generated via the customized MATLAB algorithm to determine the amount of Texas Red-conjugated dextran within the capillary interior at each time point. An isolated * symbol indicates statistical significance ($p<0.05$) between data points (NHLF vs. MSC vs. AdSC) at any one particular time point, whereas a bar beneath the * symbol indicates statistical significance ($p<0.05$) across all 3 experimental groups at each time point. The +, #, and % symbols indicate statistically significant differences ($p<0.005$) between the data marked by these symbols at certain time points and all other time points marked with different symbols.

walls in cultures containing these multipotent stromal cells compared to those containing fibroblasts. At later time points, these capillaries also regulated their permeability much more tightly than their fibroblast counterparts, with highly significant decreases of 68% and 77% in the red:green fluorescence ratios by day 14 for the MSC-mediated capillaries and the AdSC-mediated capillaries, respectively, relative to the fibroblast controls.

To better understand mechanistically how permeability might be differentially controlled by each stromal cell type, the protein levels and organization of VE-cadherin were assessed. Immunofluorescent staining of VE-cadherin revealed that the cell-cell junctions between neighboring endothelial cells of capillary sprouts were more pronounced in EC-AdSC and EC-MSC co-cultures, whereas the EC-NHLF co-cultures showed evidence for more sparse EC-EC junctions (Figure 4.4, Panels A-C). Co-cultures containing stem cells also possessed elevated levels of VE-cadherin protein via Western blotting (Figure

4.4, Panel D). When ECs were omitted from the cultures, the MSCs produced positive levels of VE-cadherin via Western blotting, while the AdSCs and NHLFs were less able to modulate and express vascular markers without ECs in co-culture.

D. Expression of Stromal Cell Markers Modulates in 3D Culture

Western blotting for alpha smooth muscle actin (α-SMA) shows positive staining for all three stromal cell types when cultured in a 2D monolayer culture; however, once placed in 3D, these values change (Figure 4.5). The MSCs express less α-SMA in 3D when co-cultured with ECs, and express no detectable α-SMA when cultured alone in 3D. The AdSCs also attempt to modulate away from this myofibroblastic phenotype when co-cultured with ECs in 3D, while the NHLFs produce positive bands both with and without ECs in co-culture. Calponin, a mature smooth muscle marker, produces no positive bands for any culture conditions after 14 days. Together, these data indicate that the stem cells in co-culture are migrating toward a pericytic phenotype, while fibroblasts are not adopting this shift.

E. Stem Cells Produce Slower Growth Kinetics

Prior work has shown that the presence of stromal cells is required for capillary morphogenesis(25); however, the results presented here indicate that the identity of the stromal cells may also significantly impact the functional properties of the vessel networks. We hypothesized that these observed differences in vessel functionalities may be related to the rates at which the

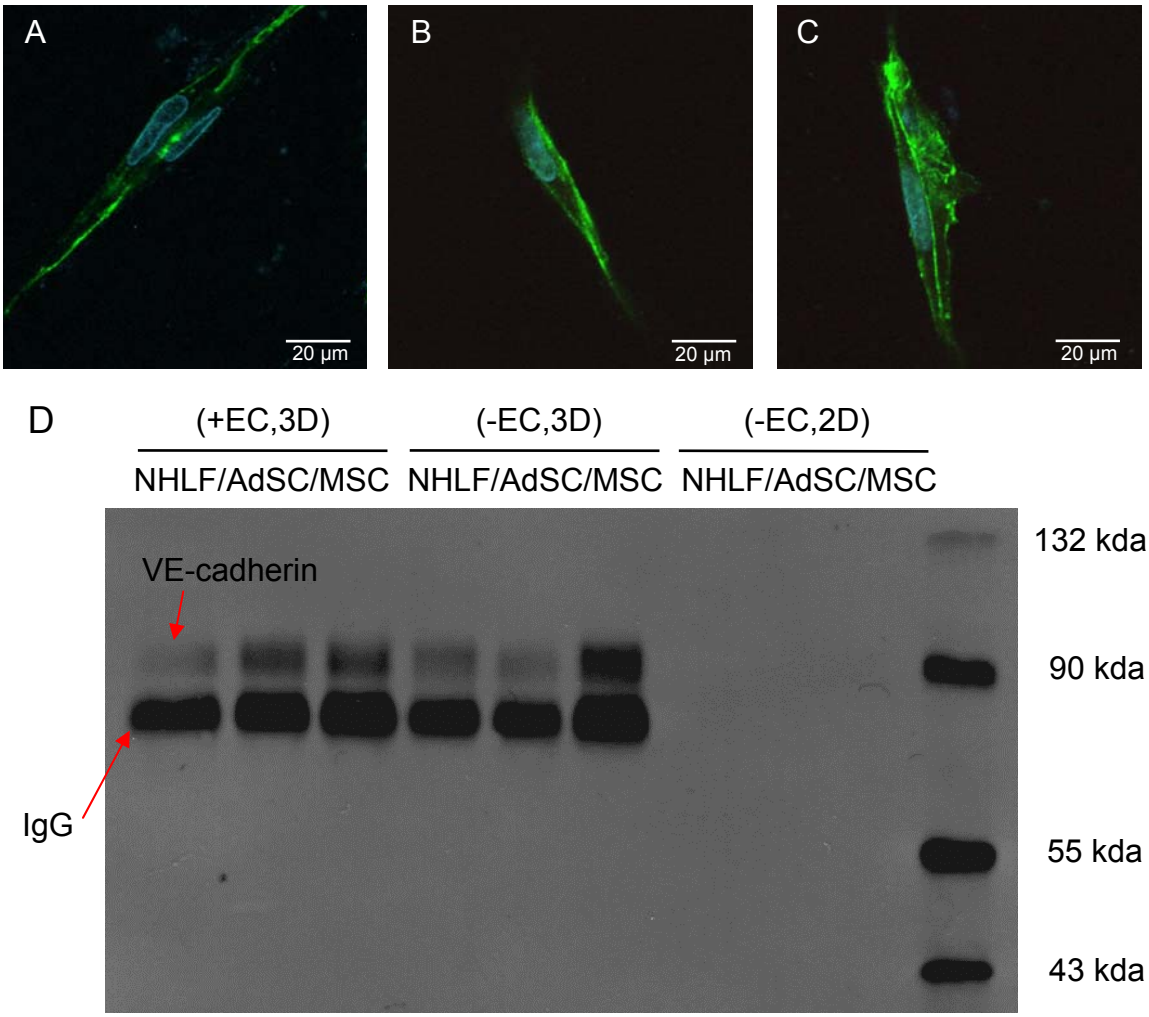

Figure 4.4. VE-cadherin organization and expression vary as a function of stromal cell type. A-C) 20x confocal microscopy images of day 14 capillaries from co-cultures of EC-NHLF (A), EC-AdSC (B), and EC-MSC (C) after staining for VE-cadherin (green) and DAPI (blue). D) Western blot showing expression of VE-cadherin within each of the stromal cell conditions, in 2D and 3D.

vessel networks form. To further explore this possibility, the kinetics of capillary growth were assessed as a function of stromal cell identity (i.e., NHLF vs. MSC vs. AdSC) and their location relative to the capillaries (i.e., as a monolayer a fixed distance away from the HUVECs vs. distributed throughout the 3D gel) (Figure 4.6). When cultured as monolayers a fixed distance above the HUVEC-coated beads, AdSCs and MSCs produced capillary networks that were only 47 and 56% of the total lengths of the capillary networks induced by monolayer fibroblast

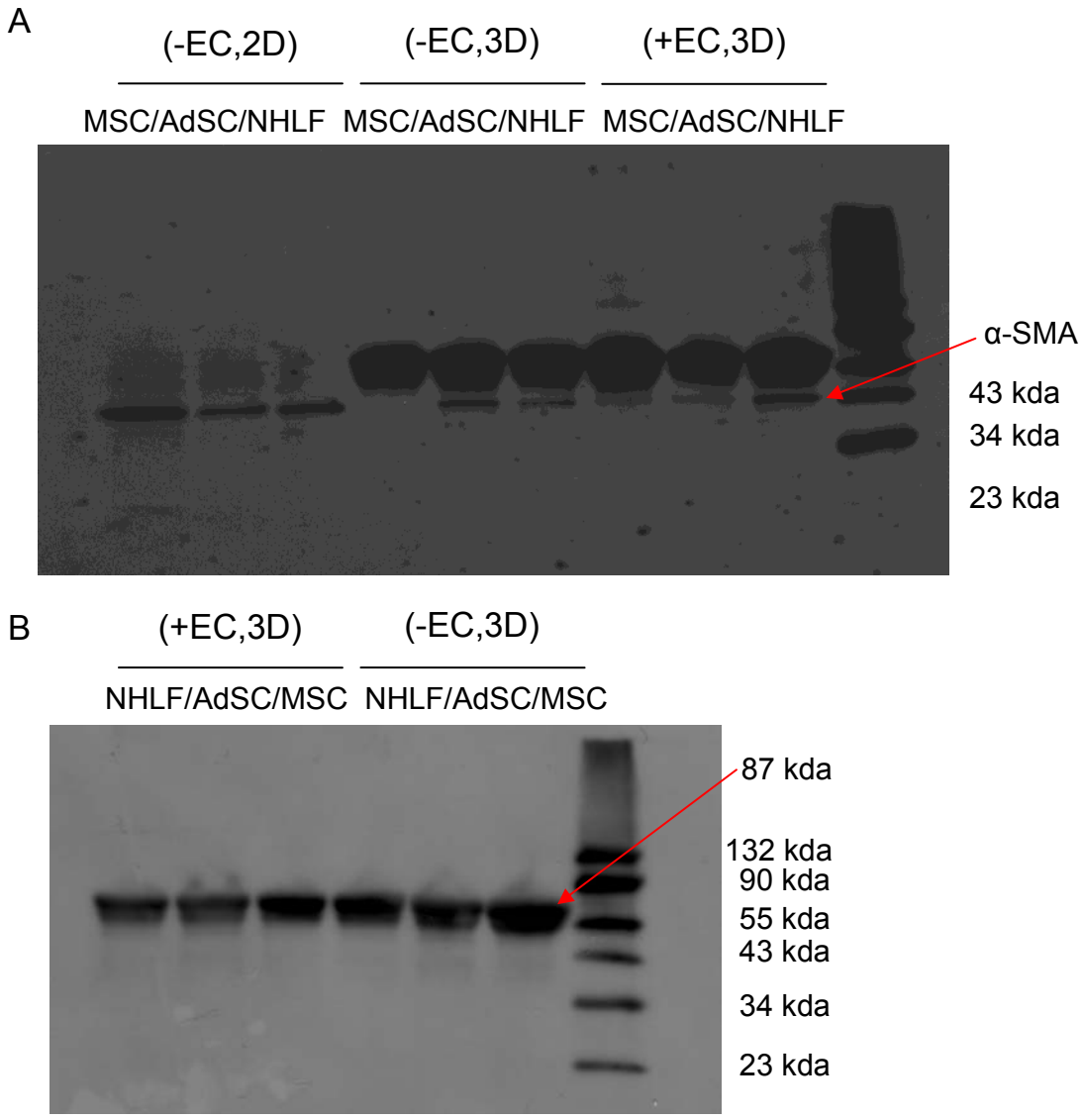

Figure 4.5. α-SMA expression varies as a function of stromal cell type and culture condition, while calponin is not expressed in 2D or 3D cultures. A) Western blot showing expression of α-SMA in 3D with ECs, in 3D without ECs, and in 2D without ECs. B) Western blot showing a lack of expression of calponin within each of the same culture conditions as in (A).

cultures (Figure 4.6D). When stromal cells were distributed throughout the fibrin gels to more closely approximate physiologic conditions, total network lengths increased for all stromal cell types in comparison to constructs in monolayer cultures; however, a similar trend was seen where cultures with stem cells produced networks with much shorter total lengths than those capillaries cultured

with NHLFs as a source of stromal cells. AdSC and MSC capillary cultures produced only 43 and 45% of the total network length of fibroblast cultures after 14 days of growth ($p < 0.005$) (Figure 4.6D).

To further characterize how the identity of the stromal cells affected capillary network growth, the total number of vessel segments per network was also quantified (Figure 4.7E). After 14 days, EC-MSC and EC-AdSC co-cultures produced averages of 207 and 150 segments per dextran bead, while EC-NHLF co-cultures produced fewer segments per network, an average of 111. When these values were used in conjunction with total network lengths, EC-NHLF co-cultures had an average segment length of 463 μm after 14 days of culture, whereas EC-MSC and EC-AdSC co-cultures had average segment lengths of only 110 μm and 148 μm, respectively. Together, these data demonstrate that EC-NHLF co-cultures formed longer, more spindly, and less-branched capillary networks than did co-cultures containing either stem cell type.

4.4 Discussion

Capillaries, composite systems of endothelial cell tubules that are sparsely covered with pericytes and a supporting extracellular matrix, serve many functions within the body, most notably acting as selectively permeable barriers which allow nutrients and oxygen into the surrounding tissues, as well as extracting waste products.(26, 27) Larger vessels must also react to vasoactive stimuli, tightening or expanding when required, in order to maintain a level blood

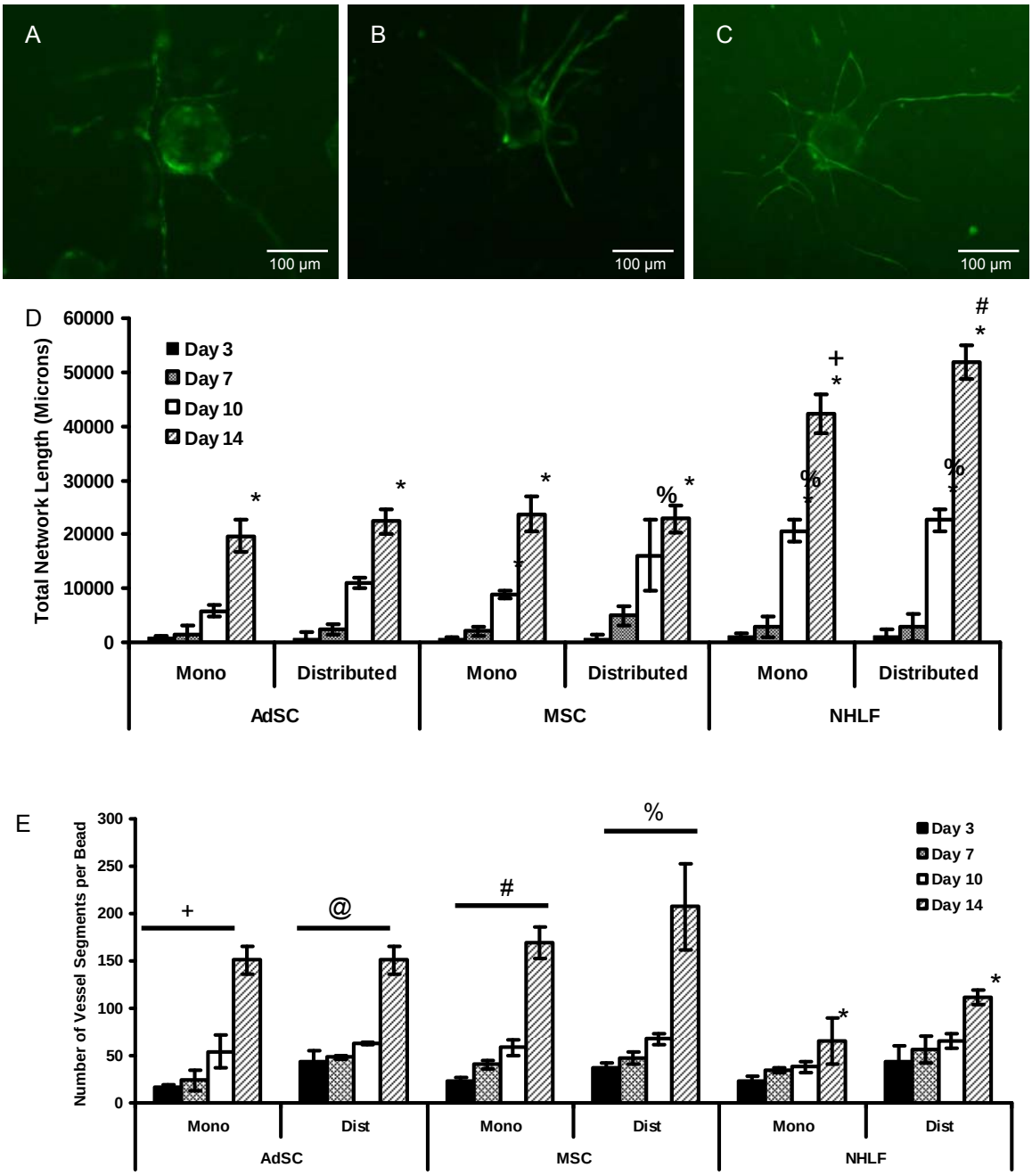

Figure 4.6. Capillary growth kinetics vary by stromal cell type. A-C) Representative 4x images of fluorescently-tagged HUVECs forming capillary networks in co-culture with A) AdSCs, B) MSCs, C) NHLFs. D) Comparison of growth kinetics for several stromal cell types in the bead assay. "Mono" denotes the stromal cells were cultured as a monolayer on top of the fibrin gel, a fixed distance away from the HUVEC-coated beads; "distributed" indicates the stromal cells were distributed throughout the entire 3D gel. E) Comparison of the number of vessel segments per network for each stromal cell type. The * symbol indicates statistical significance ($p<0.05$) between time points within a given culture condition. The +, #, %, and @ symbols indicate statistical significance ($p<0.005$) for a particular culture condition at a given time point versus the other culture conditions. For example, the total lengths of the capillary networks induced by distributed NHLFs are significantly different than those induced by the monolayer NHLFs and those induced by all of the other cell types and distributions (denoted by #).

pressure and to supply oxygenated blood to all organs and tissues, regardless of the external conditions.(28) In order for a vessel to be classified as functional, it must also differentiate to fit into the proper portion of the hierarchical structure.(29) Arteries and arterioles function as a pipeline to deliver oxygen and nutrients to tissues that are further away, while capillaries provide large surface areas for molecular exchange of gases, nutrients, and wastes within the tissue space.(30) Recreating capillary blood vessels remains a limiting hurdle to the successful clinical implementation of engineered tissues.(31)

In the case of implanted tissue constructs, the presence of functional capillary networks has typically been defined by the presence of red blood cells within lumen-containing structures on histological sections; however, observations of leakiness and edema *in vivo* have created a need for a more quantifiable metric of capillary functionality, beyond the mere presence of red blood cells.(6, 28, 31, 32) Furthermore, in diseases such as cancer, phenotypic changes in the pericyte coat and its dissociation from the endothelial cell layer, have been implicated in alterations in vessel permeability.(18, 33, 34) Studies using fluorescent tracers and/or non-invasive imaging methods have enabled vessel perfusion and functionality to be assessed *in vivo*.(21) *In vitro*, established permeability metrics typically measure transendothelial resistance in a Transwell system in which endothelial cells are cultured in a 2D monolayer. (35) However, comparable approaches to assess vessel functionality in 3D are lacking, which in turn creates an inability to determine if a promising approach to either promote or inhibit vessel formation will also alter vessel functionality. Classical assays of

resistance across a monolayer cannot be easily applied to a 3D system where the luminal diameters are less than 20 μm; thus a new approach was required.

To address this limitation, here we have described an *in vitro* method for measuring changes in permeability in the capillary vessels created in a previously established 3D tissue culture model.(8) By quantifying the transport of a fluorescent tracer from the tissue space into the vessel lumens, we have effectively shown that permeability can be inversely measured by the use of 3D confocal microscopy and the design of a customized pixel comparison algorithm. The method detected decreases in capillary permeability over time, and showed that some stromal cell types are better able than others to promote the formation of robust, stable networks after 2 weeks of culture. Higher amounts of fluorescent tracer inside the capillary lumens were detected at early time points, which we attribute to a lack of competent cell-cell junctions between endothelial cells and to the fact that pericytes are not yet stabilizing the capillaries. After the constructs are allowed to mature for longer periods of time, and the stromal cells make direct contact with the capillary sprouts as we have previously shown(15), a direct reduction in the amount of tracer was observed in the capillary lumens.

The quantitative algorithm developed here demonstrated the capability to discern quantifiable differences in permeability induced by histamine, a known modulator of permeability, in both immature and mature capillary sprouts. This result is particularly striking given that the lumenal surfaces of neovessels within our system are not perfused via fluid, which has been shown to influence permeability in other systems.(36) We have also shown here that the use of

different stromal cell types in our capillary culture system produces capillaries of varying phenotypes and maturation levels as determined both visually and quantifiably using our permeability assay. In recent studies, we have also reported that the mechanisms by which endothelial cells proteolytically degrade the surrounding matrix to form new capillary tubules depends on the identity of the stromal cells in HUVEC-stromal cell co-cultures.(15) Whether or not these mechanistic differences account for the functional differences observed here remains to be seen.

We have typically used fibroblasts as the stromal cell type in our *in vitro* models of angiogenesis with the intent of mimicking the wound healing environment.(9) Fibroblasts are recruited into the wound bed from surrounding host tissues in order to facilitate faster healing and regeneration of the vasculature. Fibroblasts function quickly to promote granulation tissue formation via collagen and fibronectin deposition (37), and their ability to drive capillary growth in our model system is consistent with their known roles in wound healing *in vivo*. However, we observed in this work that fibroblasts promote the formation of vessels characterized by a reduced capacity to control permeability, especially at early time points, relative to those promoted by multipotent stromal cells. Fibroblasts also promoted vessels at a significantly faster rate than MSCs and AdSCs in our model, but the resulting vessels were longer, less branched, and possessed fewer cell-cell adherens junctions between ECs than those formed from co-cultures containing stem cells. Also, α-SMA expression, an indicator of a myofibroblastic phenotype, was seen to be downregulated by MSCs in 3D

cultures, unlike NHLFs. These observations suggest that the multipotent MSCs and AdSCs do in fact modulate their functionalities as pericytes to produce capillaries that more closely mimic the physiology of healthy vasculature, with more controlled permeabilities due perhaps to an increase in EC-EC adherens junctions, while the fibroblasts promote a vasculature more reminiscent of pathologic angiogenesis. Therefore, an especially important conclusion with respect to promoting the neovascularization of engineered tissues has emerged: the choice of which cell type to deliver with endothelial cells to create new vasculature may determine in part whether the capillaries are physiologically healthy or not. Explicit studies to address this question *in vivo* are following.

4.5 References

1. Melero-Martin J, Obaldia M, Kang S, Khan Z, Yuan L, Oettgen P, and Bischoff J. Engineering robust and functional vascular networks in vivo with human adult and cord blood derived progenitor cells. *Circulation Research* **103**, 194-202 (2008).
2. Brey E, Uriel S, Greisler H, and McIntire L. Therapeutic neovascularization: contributions from bioengineering. *Tissue Engineering* **11**, 567-584 (2005).
3. Neumann T, Nicholson B, and Sanders J. Tissue engineering of perfused microvessels. *Microvascular Research* **66**, 59-67 (2003).
4. Jain R, Au P, Tam J, Duda D, and Fukumura D. Engineering vascularized tissue. *Nature Biotechnology* **23**, 821-823 (2005).

5. Richardson T, Peters M, Ennett A, and Mooney D. Polymeric system for dual growth factor delivery. *Nature Biotechnology* **19**, 1029-1034 (2001).

6. Langer R, and Vacanti J. Tissue engineering. *Science* **260**, 920-926 (1993).

7. Chen X, Aledia A, Ghajar C, Griffith C, Putnam A, Hughes C, and George S. Prevascularization of a fibrin-based tissue construct accelerates the formation of functional anastomosis with host vasculature. *Tissue Engineering Part A* **15**, 1363-1371 (2009).

8. Ghajar C, Blevins K, Hughes C, George S, and Putnam A. Mesenchymal stem cells enhance angiogenesis in mechanically viable prevascularized tissues via early MMP upregulation. *Tissue Engineering* **12**, 2875-2888 (2006).

9. Ghajar C, Chen X, Harris J, Suresh V, Hughes C, Jeon N, and George S. The effect of matrix density on the regulation of 3-D capillary morphogenesis. *Biophysical Journal* **94**, 1930-1941 (2008).

10. Griffith C, Miller C, Sainson R, Calvert J, Jeon N, Hughes C, and George S. Diffusion limits of an in vitro thick prevascularized tissue. *Tissue Engineering* **11**, 257-266 (2005).

11. Shepherd B, Jay S, Saltzman W, Tellides G, and Pober J. Human aortic smooth muscle cells promote arteriole formation by coengrafted endothelial cells. *Tissue Engineering Part A* **15**, 165-173 (2009).

12. Au P, Tam J, Fukumura D, and Jain R. Bone marrow derived mesenchymal stem cells facilitate engineering of long-lasting functional vasculature. *Blood* **111**, 4551-4558 (2008).

13. Merfeld-Clauss S, Gollahalli N, March K, and Traktuev D. Adipose tissue progenitor cells directly interact with endothelial cells to induce vascular network formation. *Tissue Engineering Part A* **16**, 2953-2966 (2010).

14. Traktuev D, Merfeld-Clauss S, Li J, Kolonin M, Arap W, Pasqualini R, Johnstone B, and March K. A population of multipotent CD34-positive adipose stromal cells share pericyte and mesenchymal surface markers, reside in a periendothelial location, and stabilize endothelial networks. *Circulation Research* **102**, 77-85 (2008).

15. Ghajar C, Kachgal S, Kniazeva E, Mori H, Costes S, George S, and Putnam A. Mesenchymal cells stimulate capillary morphogenesis via distinct proteolytic mechanisms. *Experimental Cell Research* **316**, 813-825 (2010).

16. Ghajar C, George S, and Putnam A. Matrix metalloproteinase control of capillary morphogenesis. *Critical Reviews in Eukaryotic Gene Expression* **18**, 251-278 (2008).

17. Kachgal S, and Putnam A. Mesenchymal stem cells from adipose and bone marrow promote angiogenesis via distinct cytokine and protease expression mechanisms. *Angiogenesis* (2010).

18. Baluk P, Hashizume H, and McDonald D. Cellular abnormalities of blood vessels as targets in cancer. *Current Opinion in Genetics & Development* **15**, 102-111 (2005).

19. Hashizume H, Baluk P, Morikawa S, McLean J, Thurston G, Roberge S, Jain R, and McDonald D. Openings between defective endothelial cells explain tumor vessel leakiness. *Am J Path* **156**, 1363-1380 (2000).

20. Jain R. Molecular regulation of vessel maturation. *Nature Medicine* **9**, 685-693 (2003).

21. Shaterian A, Borboa A, Sawada R, Costantini T, Potenza B, Coimbra R, Baird A, and Eliceiri B. Real-time analysis of the kinetics of angiogenesis and vascular permeability in an animal model of wound healing. *Burns* **35**, 811-817 (2009).

22. Chrobak K, Potter D, and Tien J. Formation of perfused, functional microvascular tubes in vitro. *Microvascular Research* **71**, 185-196 (2006).

23. Curry F, Huxley V, and Adamson R. Permeability of single capillaries to intermediate-sized colored solutes. *American Journal of Physiology - Heart and Circulatory Physiology* **245**, H495-505 (1983).

24. Moy A, Winter M, Kamath A, Blackwell K, Reyes G, Giaever I, Keese C, and Shasby D. Histamine alters endothelial barrier function at cell-cell and cell-matrix sites. *American Journal of Physiology - Lung Cellular and Molecular Physiology* **278**, L888-L898 (1999).

25. Montesano R, Pepper M, and Orci L. Paracrine induction of angiogenesis in vitro by Swiss 3T3 fibroblasts. *Journal of Cell Science* **105**, 1013-1024 (1993).

26. Carmeliet P. Mechanisms of angiogenesis and arteriogenesis. *Nature Medicine* **6**, 389-395 (2000).

27. Blau H, and Banfi A. The well-tempered vessel. *Nature Medicine* **7**, 532-534 (2001).

28. Nor J, Peters M, Christensen J, Sutorik M, Linn S, Khan M, Addison C, Mooney D, and Polverini P. Engineering and characterization of functional human microvessels in immunodeficient mice. *Laboratory Investigation* **81**, 453-463 (2001).

29. Pakwai A, and Jain R. Engineering functional blood vessels in vivo Massachusetts Institute of Technology. [6/10/2010, 2010].

30. Levenberg S, Rouwkema J, Macdonald M, Garfein E, Kohane D, Darland D, Marini R, van Blitterswijk CA, Mulligan R, D'Amore P, and Langer R. Engineering vascularized skeletal muscle tissue. *Nature Biotechnology* **23**, 879-884 (2005).

31. Koike N, Fukumura D, Gralla O, Au P, Schechner J, and Jain R. Tissue engineering: of long-lasting blood vessels. *Nature* **428**, 138-139 (2004).

32. Melero-Martin J, Khan Z, Picard A, Wu X, Paruchuri S, and Bischoff J. In vivo vasculogenic potential of human blood-derived endothelial progenitor cells. *Blood* **109**, 4761-4768 (2007).

33. McDonald D, and Baluk P. Significance of blood vessel leakiness in cancer. *Cancer Research* **62**, 5381-5385 (2002).

34. Morikawa S, Baluk P, Kaidoh T, Haskell A, Jain R, and McDonald D. Abnormalities in pericytes on blood vessels and endothelial sprouts in tumors. *American Journal of Pathology* **160**, 985-1000 (2002).

35. Sandoval R, Malik A, Naqvi T, Mehta D, and Tiruppathi C. Requirement for Ca+2 signaling in the mechanism of thrombin-induced increase in endothelial permeability. *American Journal of Physiology - Lung Cellular and Molecular Physiology* **280**, L239-L247 (2001).

36. Price G, Wong K, Truslow J, Leung A, Acharya C, and Tien J. Effect of mechanical factors on the function of engineered human blood microvessels in microfluidic collagen gels. *Biomaterials* **31189**, 6182-6186 (2010).

37. Midwood K, Williams L, and Schwarzbauer J. Tissue repair and the dynamics of the extracellular matrix. *The International Journal of Biochemistry and Cell Biology* **36**, 1031-1037 (2003).

CHAPTER 5

Stromal Cell Identity Governs the *in vivo* Functionality of Engineered Capillary Networks Formed by Co-Delivery of Endothelial Cells and Stromal Cells

5.1 Introduction

Therapeutic angiogenesis, the process of promoting neovascularization and tissue repair via the delivery of pro-angiogenic molecules, has been explored as a possible means to treat ischemic diseases(1). However, clinical trials relying on bolus injection of individual factors have been disappointing (2), perhaps due to the limited half-life of most protein growth factors, the lack of temporal and spatial control over growth factor release, and the inability of single factors to properly regulate neovascularization (3, 4). Newer strategies involving sustained delivery of pro-angiogenic factors or genes from biodegradable scaffolds to overcome protein stability issues (5-8), as well as delivery of multiple pro-angiogenic factors in a time-dependent fashion to mimic the process of natural vessel development (4, 9), have been shown to induce formation of vascular networks. However even combinations of multiple factors may not fully recapitulate the complex mileiu of pro-angiogenic signals presented to cells *in vivo*.

Cell-based therapies have also been explored to more completely mimic the cascade of signals needed to promote the formation of stable neovasculature. These approaches involve delivering an appropriate cell type(s) that can directly differentiate into capillary structures or provide a physiologic mixture of pro-angiogenic cues to accelerate the recruitment of host vessels. A variety of cell types have been shown to form new capillary networks and/or induce collateral blood vessel development following implantation *in vivo* (10-13). In addition, cells have been implanted using a wide range of scaffold materials and extracellular matrix proteins to improve cell retention and engraftment (14, 15). However, most studies have relied on the presence of red blood cells in lumen-like structures revealed via histology as the sole metric of vessel functionality.

A particular challenge for the tissue engineering community is to induce vascularization of ischemic tissues with blood vessels that are functionally normal. When vascularization is induced too rapidly, as in tumor angiogenesis, ECs do not properly align (16, 17). Blood vessel growth induced by tumor expansion often results in abnormal branching and growth patterns, defective endothelial wall structures, and an abnormal pericyte coat(18). These abnormal characteristics relative to healthy vasculature can lead to capillaries that are leaky and unable to properly control permeability, contributing to edema in the tissue (19, 20). In the case of engineered capillary networks, our lab and many others have had some previous success inducing capillary growth in both 3D *in vitro* cultures (21) and *in vivo* subcutaneous implants(22). The results from such studies have led to the consensus that co-delivery of ECs and a secondary

mesenchymal cell type produces the necessary cues to induce tubular sprouting of ECs, and stromal cell differentiation toward a pericytic phenotype(23).

Despite the consensus of this paradigm, there is virtually no consensus with respect to the choice of cells to co-deliver with ECs. A variety of stromal cell types of mesenchymal origins have been explored, including mesenchymal stem cells from bone marrow(21, 24, 25) or adiopose tissue (26), fibroblasts from human lung (27, 28) and mouse embryos(29), as well as smooth muscle cells (30). For a subset of these cell types, our previous studies using *in vitro* models have shown that stromal cell identity underlies differences in the mechanisms by which capillaries are formed (24, 31), and in the functional properties of the resulting capillaries (32). The goal of this study was to determine if the identity of

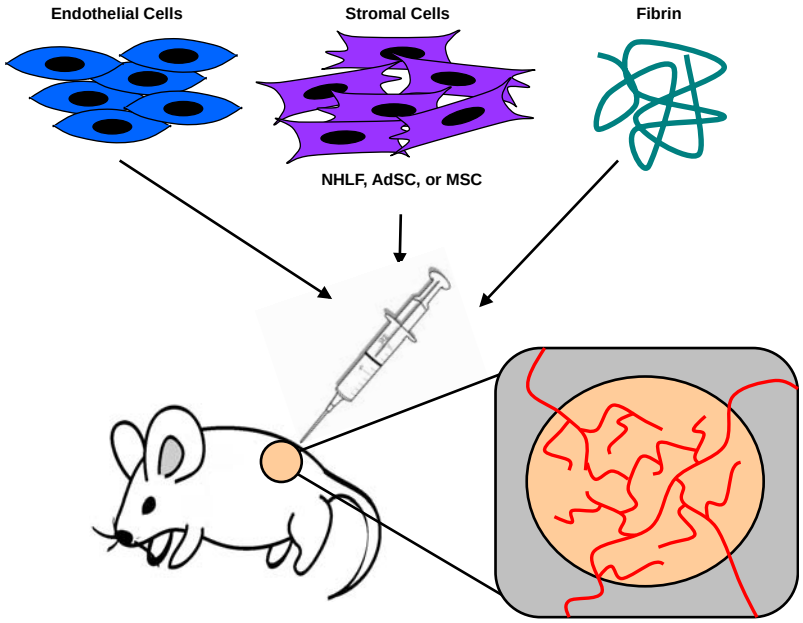

Figure 5.1. Method to engineer vascular networks *in vivo*. In this study, EC alone or in combination with one of three different types of stromal cells (NHLF, AdSC, or MSC) were injected subcutaneously within a fibrin matrix on the dorsal surface of SCID mice. The injected cells form a provisional vascular network that inosculates with the systemic circulation, as has been shown in several previous studies. However, the choice of stromal cells has varied widely across studies, and their impact on the functional qualities of the capillaries produced has not been examined. The goal of this study was to systematically characterize the effects of stromal cell identity on the quantity and functional quality of the resulting neovasculature.

the stromal cells co-delivered with ECs had any similar consequences on the functional properties of engineered capillary networks *in vivo* (Figure 5.1). Our results suggest that the identity of the stromal cells significantly influences the *in vivo* functionality of engineered capillary networks.

5.2 Methods

Cell Culture

Human umbilical vein endothelial cells (HUVECs, hereafter referred to as ECs) were harvested from fresh umbilical cords following a previously established protocol (21), and were grown in fully supplemented Endothelial Growth Medium (EGM-2, Lonza, Walkersville, MD) at 37°C and 5% CO_2. Normal human lung fibroblasts (NHLFs, Lonza) were cultured in Media 199 (Invitrogen, Carlsbad, CA) supplemented with 10% FBS, 1% penicillin/streptomycin (Mediatech, Manassas, VA), and 0.5% gentamicin (Invitrogen). Bone marrow mesenchymal stem cells (MSCs, Lonza) and adipose-derived stem cells (AdSCs, Invitrogen) were cultured in Dulbecco's modified Eagle Medium (DMEM, Sigma-Aldrich, St. Louis, MO) supplemented with 10% FBS, 1% penicillin/streptomycin (Mediatech), 0.5% gentamicin (Invitrogen). NHLFs, MSCs, and AdSCs were all used prior to passage ten. ECs were used at passage 3. Cells were cultured in monolayers until reaching 80% confluency and serially passaged using 0.05% trypsin-EDTA treatment.

Tissue Construct Implantation

Animal procedures were performed in accordance with NIH guidelines for laboratory animal usage following a protocol approved by the University of Michigan's Committee on Use and Care of Animals. Male 7-week old C.B.-17/SCID mice (Taconic Labs, Hudson, NY) were used for all experiments. An anesthetic/analgesic drug cocktail of ketamine (95 mg/kg, Fort Dodge Animal Health, Fort Dodge, IA), xylazine (9.5 mg/kg, Lloyd Laboratories, Shenandoah, IA), and buprenorphine (0.059 mg/kg, Bedford Laboratories, Bedford, OH) was delivered to each mouse via intraperitoneal injection. The dorsal flank of each mouse was then shaved, sterilized with betadine (Thermo Fisher Scientific, Fremont, CA) and wiped down with an alcohol pad prior to implant injection.

A 2.5 mg/ml bovine fibrinogen solution (Sigma-Aldrich, St. Louis, MO) was made in serum-free EGM-2 and filtered through a 0.22 μm syringe filter. Cell mixtures in a 1:1 ratio of EC:stromal cells (either NHLFs, MSCs, or AdSCs) were spun down and resuspended in the previously prepared fibrinogen solution at a final concentration of 10 million cells/mL, totaling 3 million cells per injection sample (300 μl total volume). Immediately prior to injection, 5% fetal bovine serum and 6 μl of thrombin solution (50 U/ml, Sigma-Aldrich) were added to 300 μl of fibrinogen-cell solution. For control samples, 3 million ECs without any stromal cell type were used. Acellular controls containing fibrinogen, FBS, and thrombin were also included. Solutions were immediately injected subcutaneously on the dorsal flank of the mouse, with two implants per animal. Animals were kept stationary for 5 minutes to allow for implant polymerization,

and were then placed in fresh cages for recovery. Five replicates of each sample type were completed (EC-NHLF, EC-MSC, EC-AdSC, EC only, and acellular).

Non-invasive Laser Doppler Perfusion Imaging

At days 3, 7, 10, and 14, mice were anesthetized using the cocktail described above, and then subjected to laser Doppler perfusion imaging (LDPI) (Perimed AB, Sweden). Each mouse was imaged in triplicate. Results are reported as folds increased in relative perfusion units over untreated controls.

Tracer Injection & Implant Removal

Mature capillaries function as selectively permeable membranes and are known to be impermeable to dextrans over a molecular weight of 65 kDa (33). Therefore, a Texas Red-conjugated dextran ($\lambda_{ex/em}$ of 595/615 nm, Invitrogen) was chosen as a functionally-defining tracer. This dextran molecule, containing free lysines, is fixable in 4% PFA. At each retrieval time point, final LDPI was completed, each mouse was placed in a restraint device, and 200 µl of a 5% dextran solution in PBS was then injected via the tail vein. After injection, mice were placed into fresh cages and the tracer was allowed to circulate systemically for 10 minutes. Animals were then euthanized and implants, including the surrounding skin and muscle layers, were surgically excised.

Whole-Mount Live Imaging

Explants were placed onto Petri dishes after removal and immediately imaged using an Olympus IX81 spinning disk confocal microscope (Olympus, Center Valley, PA) with both a Hammamatsu (Bridgewater, NJ) camera for visualization of the fluorescent dextran tracer (Supplementary Figure 1), and a DP2-Twain (Olympus) camera for color brightfield images. Macroscopic images were taken using a Kodak EasyShare Z1015 IS camera (Kodak, Rochester, NY).

Histology & Immunohistochemistry

For histology and immunohistochemical staining, explants were fixed in 4% PFA for 1 hour, 0.4% PFA overnight, then transferred to a PBS pH 7.4 solution, all at 4°C. All samples were forwarded to AML Laboratories (Baltimore, MD) for sectioning. Samples were embedded in paraffin by AML, and then sectioned in 5 μm sections and stained with hematoxylin and eosin (H&E) according to standard protocols. Immunohistochemical staining of hCD31, α-smooth muscle actin, and calponin was performed in our laboratory on unstained serial sections provided by AML. Paraffin sections were rehydrated according to standard protocol(22), then steamed in a vegetable steamer for 25 minutes in antigen retrieval solution (Dako, Carpinteria, CA). Slides were equilibrated in TBS-T, and then all subsequent staining was done using a Dako EnVision System-HRP (DAB) kit (Dako). Primary antibody (human anti-mouse CD31, Dako; human anti-mouse α-smooth muscle actin, Abcam, Cambridge, MA; or human anti-mouse calponin, Abcam) was diluted 1:50 in TBS-T and incubated at

4°C overnight. Slides were then treated with HRP-conjugated anti-mouse secondary antibody provided in the kit. Hematoxylin and eosin counterstaining followed. Negative controls using secondary antibody alone were generated in parallel to ensure that non-specific staining did not occur.

Immunofluorescent Staining

For fluorescent staining, explanted tissue samples were initially incubated in 30% sucrose for 48 hours at 4°C. They were then transferred to a solution containing 1 part OCT embedding compound (Andwin Scientific, Schaumburg, IL) and 2 parts 30% sucrose for another 24 hours. Each sample was then finally embedded in 100% OCT within a disposable plastic mold (Fisher Scientific), and flash frozen on the surface of liquid nitrogen. These frozen samples were then forwarded to AML Laboratories for cryosectioning in 5 μm sections. Frozen sections returned to our laboratory were pre-warmed for 20 minutes at 25°C. Slides were submerged in PBS pH 7.4 for 3 separate 5 minute washes, then blocked using 5% goat serum in PBS to eliminate non-specific protein binding. Primary antibody (anti-rabbit human CD31, Santa Cruz Biotechnologies, Santa Cruz, CA) was diluted 1:50 in 5% goat serum and incubated at 4°C overnight. After incubation, unbound antibody was removed with 3 washes of 5 minutes each with PBS. Secondary antibody (AlexaFluor-488 goat anti-rabbit, Invitrogen) at a 1:100 concentration was incubated for 30 minutes at room temperature. Unbound antibody was removed with 3 washes of 5 minutes each with PBS.

Slides were then covered with VectaShield (Vector Labs, Burlingame, CA) and a #1 glass coverslip.

Design of an image analysis program for quantification

A customized MATLAB algorithm was described previously (32). Briefly, images of the green channel (AlexaFluor 488-hCD31) were used to determine the location of capillaries, either in longitudinal or cross sections on each section. The red channel (Texas Red-dextran) was then overlayed and the percentages of its localization, either within the capillaries, or external to the capillaries, were determined.

Quantification of Average Number of Vessels per Field of View

Using hCD31 stained slides, the number of blood vessels derived from implanted cells were quantified manually. Blood vessels were identified if they exhibited a rim of positive hCD31 stain and a hollow lumen containing erythrocytes. Three sections, with 5 randomly taken images per section at 20x, were used to achieve statistical significance. All values were normalized to represent one mm^2 area.

Statistical Analysis

All statistical analyses were performed using GraphPad Prism (GraphPad Software, La Jolla, California). Data are reported as mean ± standard deviation.

Two-way analysis of variance was performed with a Newman-Keuls multiple comparison post-test. Statistical significance was assumed when $p < 0.05$.

5.3 Results

A. Co-Injection of ECs with Supporting Stromal Cells Restored Perfusion

In this study, ECs alone or in combination with one of three different types of stromal cells (NHLFs, AdSCs, or MSCs) were injected subcutaneously within a fibrin matrix on the dorsal surface of SCID mice as depicted schematically in Figure 5.1. Laser Doppler perfusion imaging (LDPI) was used to non-invasively quantify blood perfusion after subcutaneous injection of one of 5 treatment groups. LDPI was first performed on all mice prior to implantation in order to provide a baseline control value of dorsal vascular perfusion. It was then performed again on days 3, 7, 10, and 14 post-implantation. As shown in Figure 5.2, relative perfusion values increased over the course of the experiment for

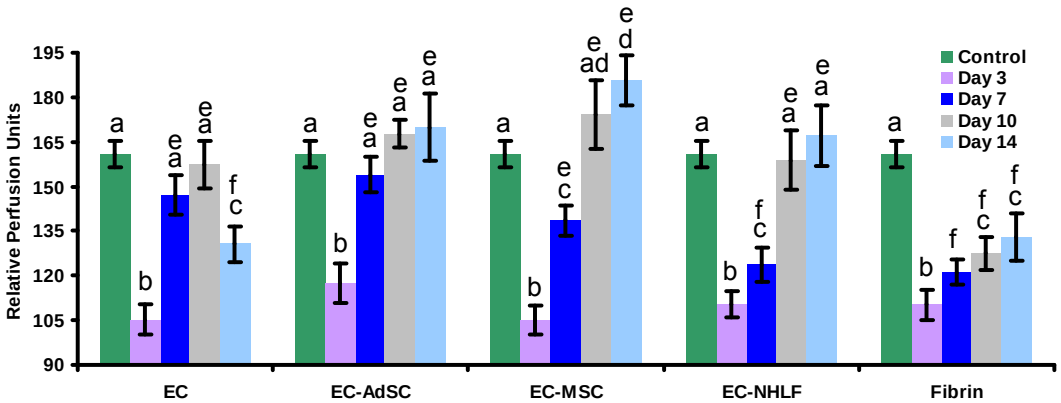

Figure 5.2. Subcutaneous co-injection of EC and supporting stromal cells within fibrin matrices restore perfusion better than delivery of EC alone. Laser Doppler perfusion imaging was used to non-invasively quantify blood perfusion after subcutaneous injection of one of 5 treatment groups (all within fibrin gels): EC, EC-AdSC, EC-MSC, EC-NHLF, or fibrin alone. Co-delivery of EC with AdSC, MSC, or NHLF within a fibrin matrix successfully restored blood flow to pre-injection levels (control). Delivery of EC alone partially restored blood flow by 7 days, but perfusion dropped off as the unstable vasculature was pruned. Acellular fibrin gels failed to restore perfusion to pre-injection levels within 14 days. Statistical comparisons are denoted on the graph by letters. a, b, c, and d denote statistically significant differences ($p < 0.05$) within each experimental group (i.e., a is significantly different than b, c, and d, etc.). e, and f indicate statistically significant differences ($p < 0.05$) across the different experimental groups (i.e., e is significantly different than f).

treatment groups; however, key differences were seen among different conditions. Co-delivery of ECs with AdSCs, MSCs, or NHLFs within a fibrin matrix successfully restored blood flow to pre-injection levels within 7 days. The restored level of perfusion was maintained at 14 days for these multicellular implants. By comparison, delivery of ECs alone partially restored blood flow by 7 days, but perfusion dropped off in the subsequent 7 days. Acellular fibrin gels failed to restore perfusion to pre-injection levels within 14 days.

B. Live Implant Imaging Qualitatively Confirmed Perfusion of the Neovasculature

Immediately after implant removal, whole-mount live imaging was performed, revealing some qualitative, yet striking, differences in the appearance of the explanted tissues (Figure 5.3). At day 7, all of the retrieved implants were red, perhaps indicative of connecting to the host vasculature, although the implant from the EC-NHLF condition was notably the most red (Figure 5.3A). The visible redness suggests erythrocyte leakage into the implant. After 14 days (Figure 5.3B), the bright red color remained present in the EC alone and EC-NHLF conditions; by contrast, the red color diminished in the EC-AdSC and EC-MSC implants. Implants for these latter two conditions were a pale pink/yellow color in macroscopic appearance by day 14, yet retained easily identifiable blood vessels that were bright red in color. At this later time point, the fibrin also appeared somewhat more compacted and perhaps more degraded in the EC alone and EC-NHLF conditions.

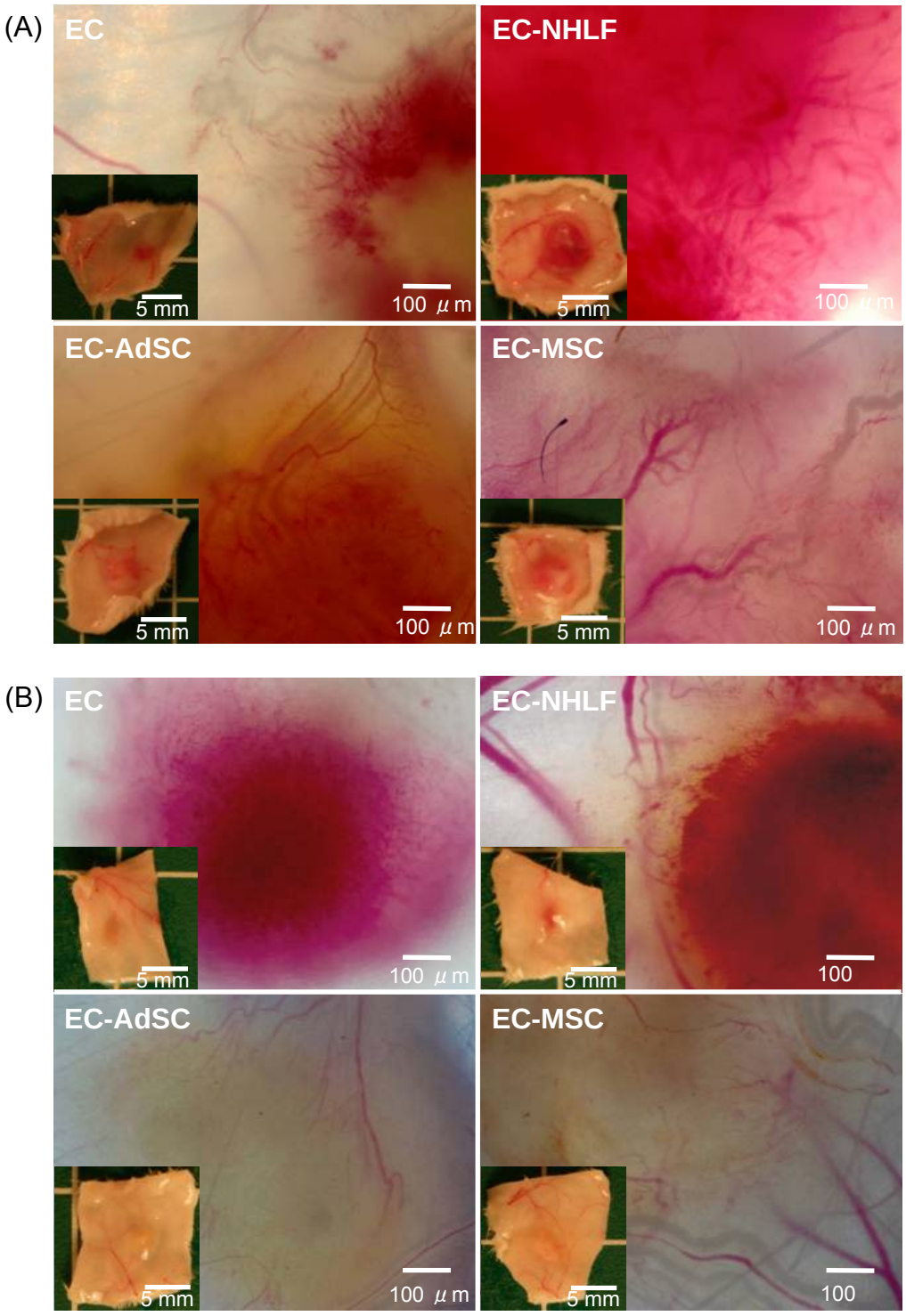

Figure 5.3. Whole-mount live imaging shows perfusion of implant neovessels. Explants of each treatment group imaged as live whole-mounts at (A) day 7 and (B) day 14. Insets are macroscopic photographs. Implants show varying degrees of effective perfusion and edema, dependent on implanted cell types. By day 14, EC only and EC-NHLF groups are visibly more red than the EC-AdSC and EC-MSC groups, suggesting large amounts of free erythrocytes. Thus, while all treatment groups are perfused, the quality of the neovasculature is highly dependent on the identity of the stromal cells.

C. Stromal Cells of Different Origins Produced Vessels with Distinct Morphologies

Images of the H&E-stained day 7 and 14 explants revealed additional qualitative differences in the morphologies of the vessels formed in the various experimental groups (Figure 5.4). Stained sections from the day 7 EC-only implants contained many large vessel-like structures, but these structures lacked a consistent, circumscribed geometry and the implants contained obvious extravascular erythrocytes (Figure 5.4A). Significant vessel regression and matrix degradation was apparent by day 14 (Figure 5.4B). The cells that remained in the fibrin by day 14 were mainly spindle-shaped free ECs, and there was little evidence of organization into capillary structures. EC-NHLF implants also contained many immature, interconnected blood vessels at day 7 (Figure 5.4A), but it was difficult to discern clear vessel boundaries due to the somewhat chaotic and irregular shapes of the vessel-like structures and large amounts of matrix reorganization. After 14 days, there appeared to be a qualitative decrease in the amount of free erythrocytes in the explanted EC-NHLF tissues, but some still remained. By contrast, implants containing the multipotent stromal cells (AdSC or MSC) yielded starkly different results. These samples contained many small capillaries with very well-defined lumens, circumscribed borders, and very few free erythrocytes. These capillaries were distributed throughout the entire implant to produce a vascularized, homogeneous implant containing both large and small blood vessels throughout in order to effectively supply the tissue with oxygenated blood.

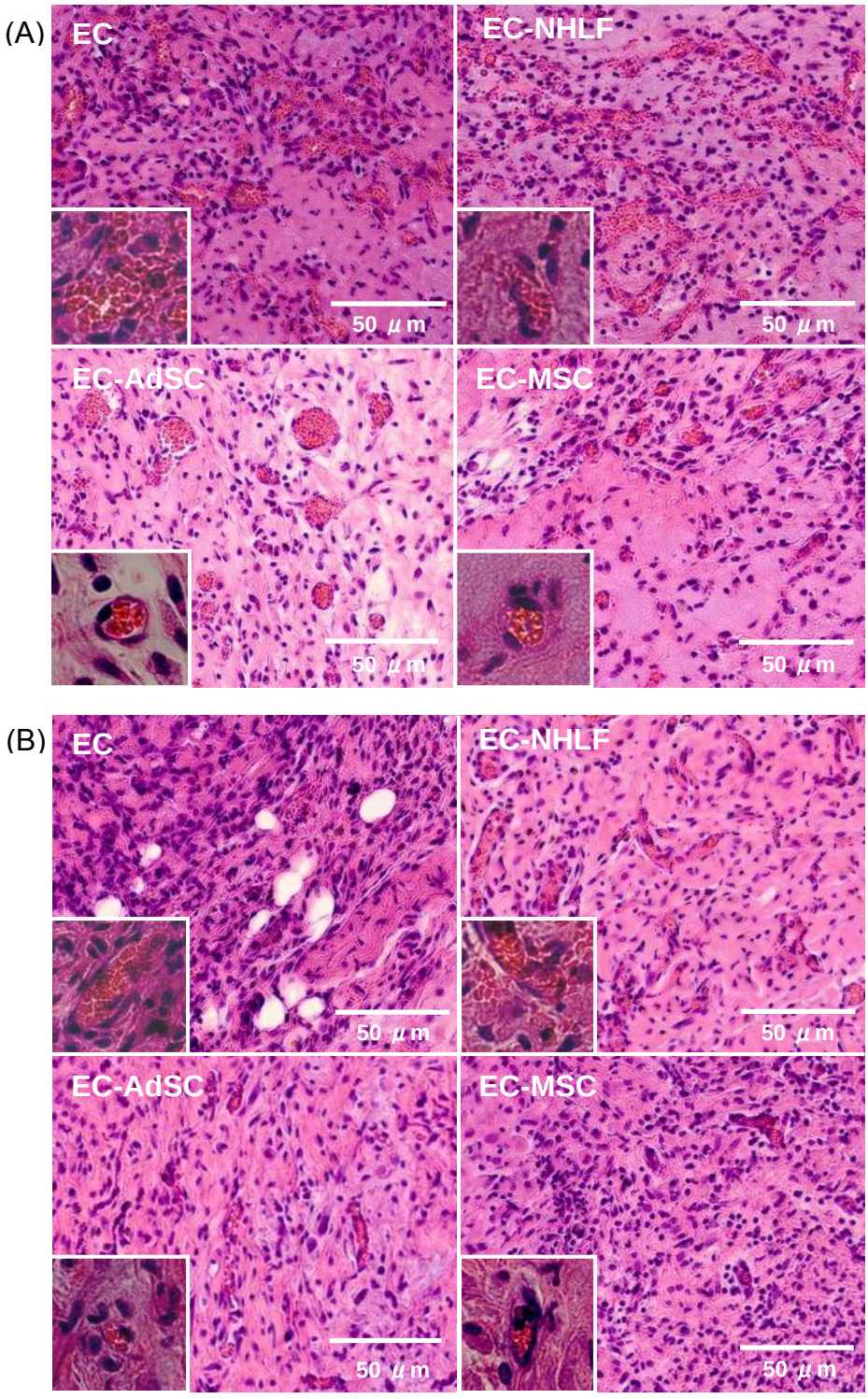

Figure 5.4. Histological staining illustrates varying blood vessel morphologies in implants across treatment groups. Histologically stained sections of implants retrieved at (A) day 7 or (B) day 14 post injection. Nascent vessel morphology varies based on the presence or absence of implanted stromal cells, and the type of stromal cell included. Consistent with the whole mount images (Figure 3), the EC only and EC-NHLF groups show vasculature that is much less defined than the EC-AdSC and EC-MSC groups, particularly at day 7.

Immunohistochemical staining for human CD31 validated the observations from the H&E-stained sections, and confirmed the human origins of the neovasculature (Figure 5.5). In the implants containing ECs only, there was a diffuse brown stain indicating an abundance of human ECs and some lumen-like structures, especially at day 7 (Figure 5.5A). The EC-NHLF implants showed many elongated vessel-like structures. By contrast, the EC-MSC and EC-AdSC implants contained many smaller, tightly-sealed capillaries, consistent with the observations from H&E staining. Quantification of vascular density from these types of images supported these qualitative observations (Figure 5.5C). Specifically, EC only implants contained 46 ± 3 vessels per mm^2 at 7 days, but this value dropped to 9 ± 2 vessels per mm^2 by day 14. EC-NHLF implants contained 47 ± 6 vessels per mm^2 at day 7, which was reduced to 31 ± 2 vessels per mm^2 by day 14. Relative to these two conditions, the EC-AdSC and EC-MSC implants produced fewer numbers of blood vessels. EC-AdSC implants contained 29 ± 7 and 19 ± 4 vessels per mm^2 at days 7 and 14 respectively. EC-MSC implants formed 20 ± 4 and 13 ± 3 vessels per mm^2 at days 7 and 14, respectively. Acellular fibrin implants showed little evidence of vascularization or host network invasion (see Supplementary Figure S5.1). By 14 days post-implantation, the fibrin implants had been resorbed by the host, and normal host dorsal vasculature was observed at the implantation site.

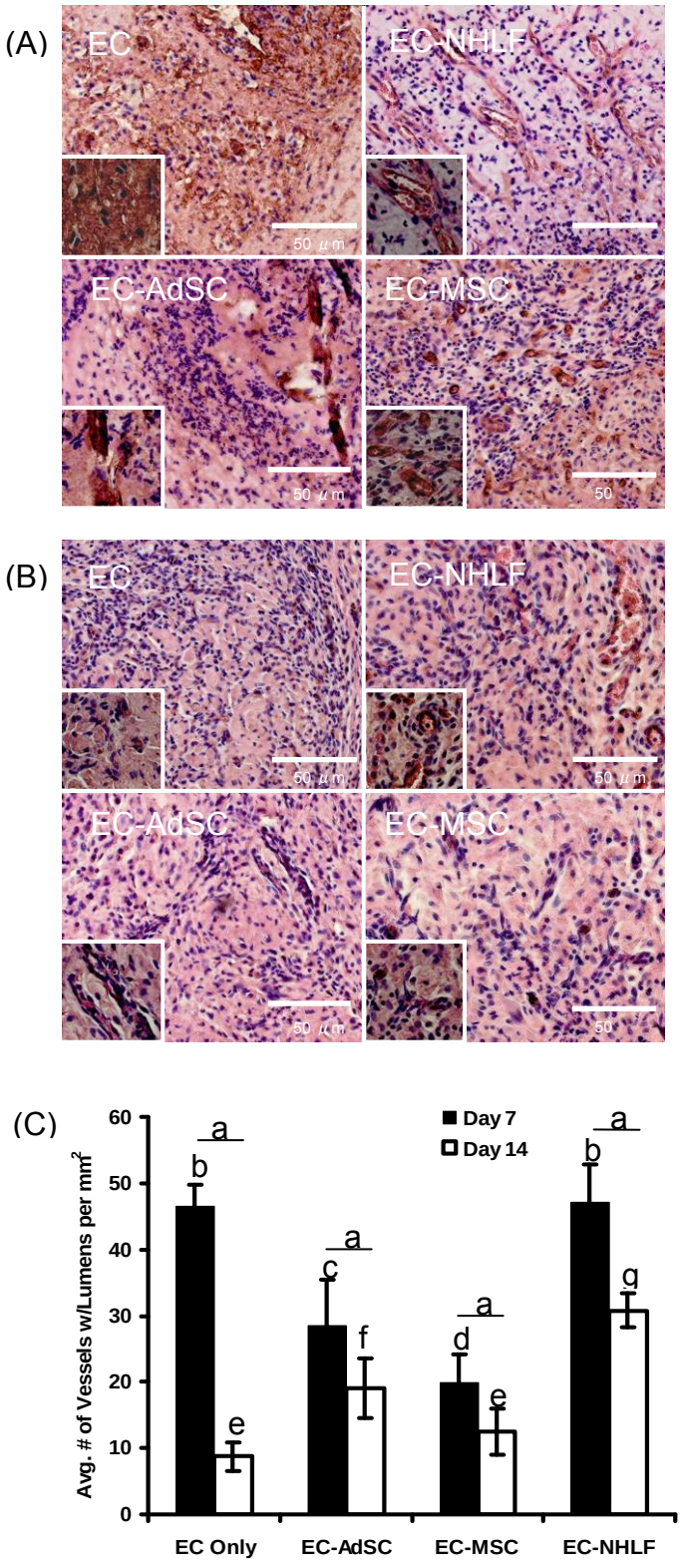

Figure 5.5. Human CD31 staining confirms blood vessel origin. hCD31 staining of implants at either (A) day 7 or (B) day 14 post implantation shows that the nascent vasculature arises due in part to the transplanted human cells (as opposed to due to host vessel infiltration). All samples have been counterstained with H&E. (C) Quantification of images from (A) and (B). In the graph, "a" denotes statistically significant differences ($p < 0.05$) across time points within each experimental group. B, c, d, e, f, and g indicate statistically significant differences ($p < 0.05$) across different experimental groups (i.e. b is statistically different than c, d, e, f, and g, etc.).

D. Stromal Cells with Multilineage Potential Express Markers of Mature Smooth Muscle

One possible explanation for the observed differences in vessel morphology is that the multipotent stromal cells may possess the ability to differentiate into pericytes, or even mature smooth muscle cells, while the fibroblasts cannot. To assess this possibility in our experimental system, we stained histological sections for two different markers – alpha-smooth muscle actin (α-SMA) and calponin (Figure 5.6). α -SMA has been widely used as a pericyte marker(18), while calponin is a marker of mature smooth muscle (34). IHC staining of human α-SMA revealed a broadly positive result for all of the implants containing a co-delivered stromal cell type, particularly at day 7 (Figure 5.6A). By day 14, this positive staining had somewhat decreased across all multicellular implants. In the EC-MSC and EC-AdSC implants, positive α-SMA staining was circumferentially localized around the newly developed blood vessels, while the EC-NHLF implants contained a more diffuse positive staining of cells throughout the matrix. By contrast, calponin staining was only positive at day 14 in the implants containing AdSC or MSC (Figure 7, particularly panel B). These results suggest that, while NHLFs, AdSCs, and MSCs are all capable of promoting the formation of vasculature and expressing α-SMA, only the multipotent AdSCs and MSCs are capable of differentiating into a mature smooth muscle phenotype that is the hallmark of a larger and more mature vasculature.

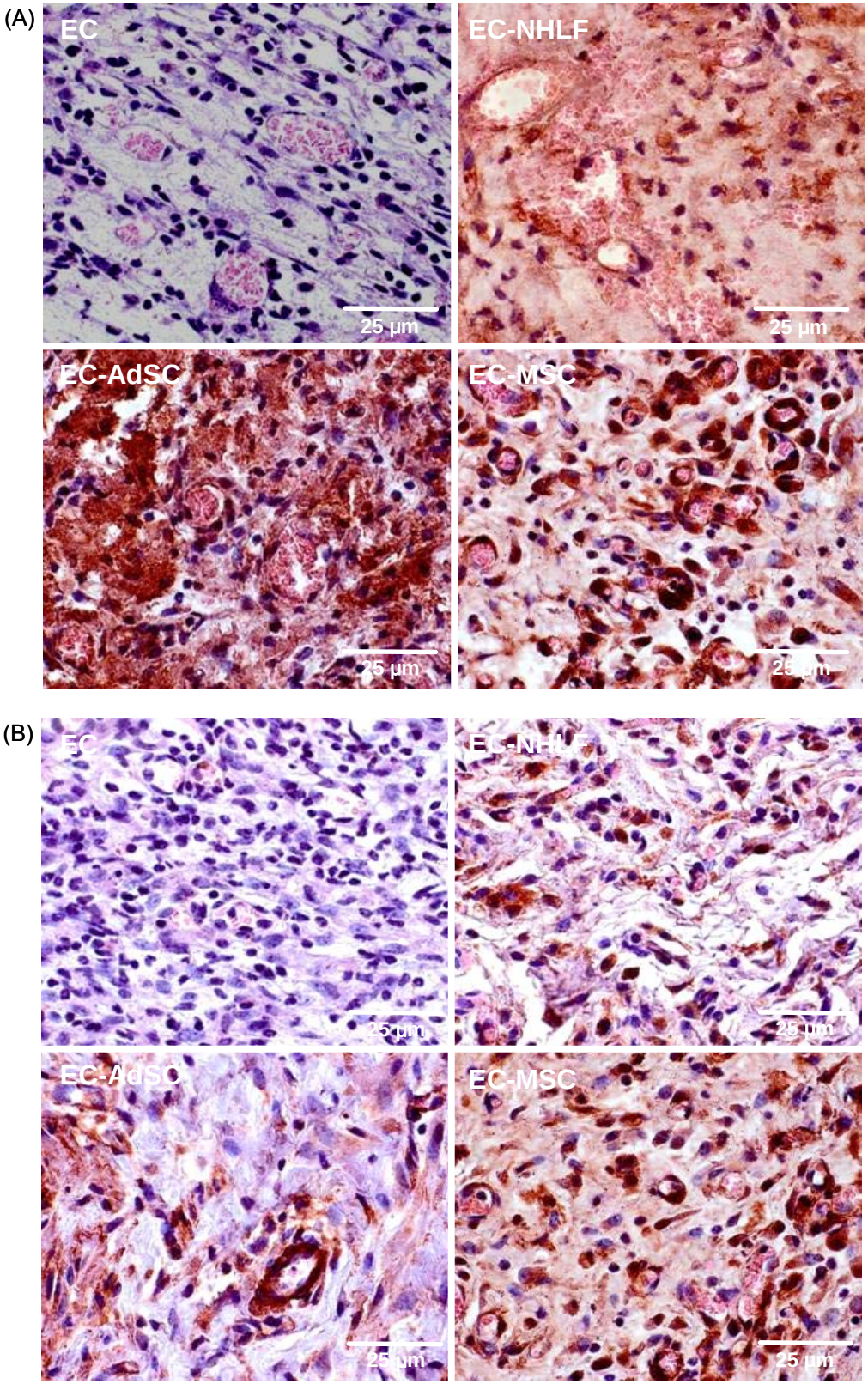

Figure 5.6. α-SMA staining identifies stromal cells within the implant. Human alpha smooth muscle actin staining at (A) 7 days and (B) 14 days post implantation. Broad positive staining is observed in in EC-NHLF, EC-AdSC, and EC-MSC groups at day 7. Expression levels are somewhat modulated by day 14, suggesting a transition from a myofibroblast phenotype to more mature pericytes.

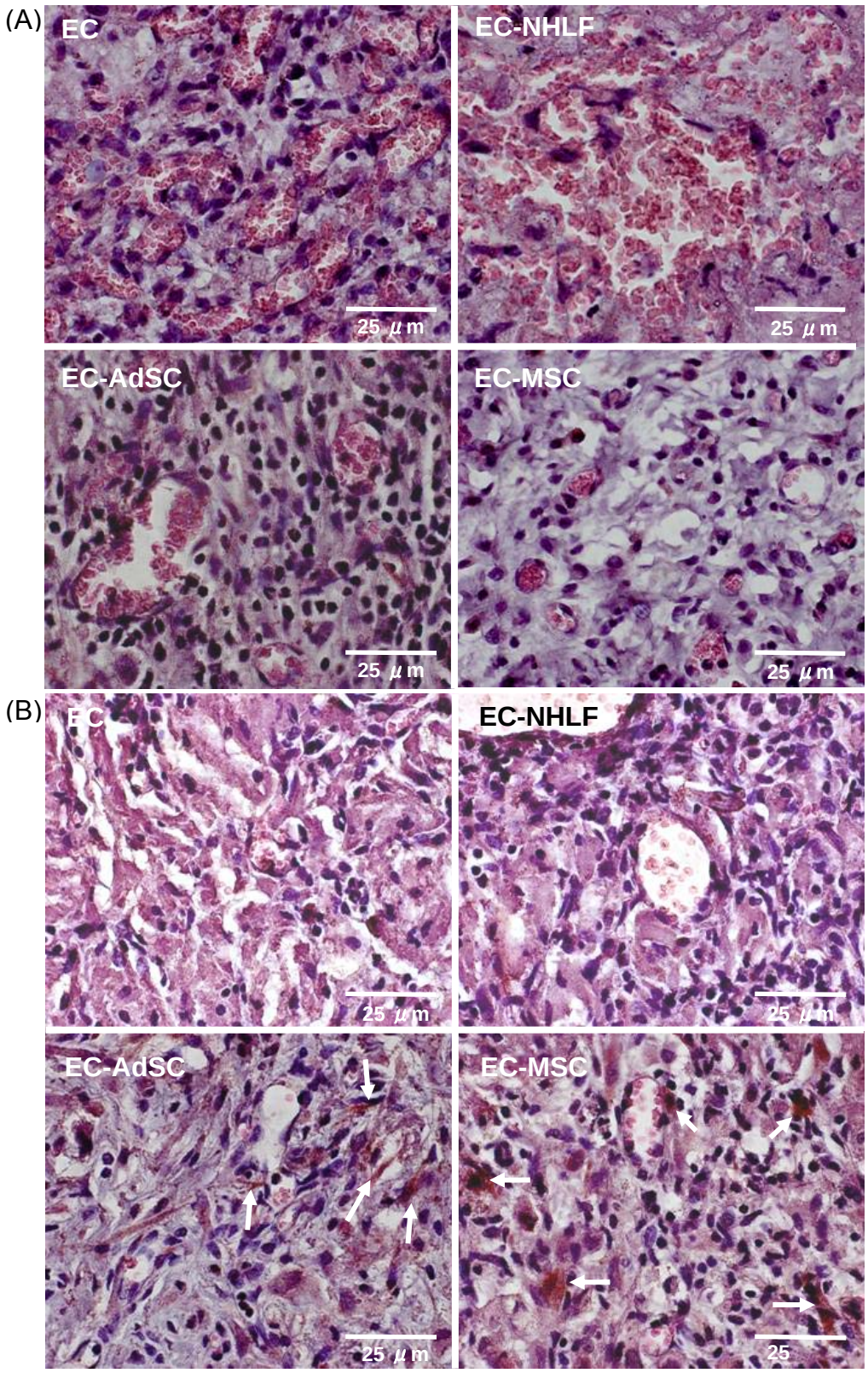

Figure 5.7. Calponin staining identifies mature smooth muscle cells within the implant. Calponin staining at (A) 7 days and (B) 14 days post implantation. No positive staining is observed at day 7 for any of the conditions. By day 14, positive staining (indicated by white arrows) is found in the EC-AdSC and EC-MSC groups, suggesting the co-implanted stromal cells differentiate towards a more mature smooth-muscle-like phenotype over time. The NHLFs do not differentiate in this same manner.

E. Stromal Cell Presence and Identity Alter the Functional Permeability of the Neovessels

The data presented thus far suggest that all 3 stromal cell types – NHLFs, AdSCs, and MSCs – are capable of promoting the formation of vasculature in subcutaneous pockets when co-delivered with ECs. The histological findings hint at possible functional differences in the neovessels that form, but nearly all of the observed differences have been qualitative, subjective, and frankly unsatisfying. Therefore, in the final part of this study, we sought to determine how the inclusion of the stromal cells and their various identities quantitatively affect the functional properties of engineered capillary networks.

Based on some recent *in vitro* findings, we hypothesized that the resistance to permeability of the nascent vessels would strongly depend on stromal cell identity (32). To quantify the relative permeabilities of the vasculature formed *in vivo*, a 70 kDa fluorescent dextran molecule was injected via tail vein in the various experimental animals. (Systemic injection of the functionally-defining tracer can be seen at the host-implant interface in Supplementary Figure S5.2.) Inclusion of either AdSCs or MSCs in the implants resulted in much tighter control of permeability relative to the other conditions (Figure 8). In the EC only and EC-NHLF groups, a significant fraction of the fluorescent dextran was observed outside of the vessel borders (defined by the green CD31 staining), and freely diffused throughout the implant tissue (Figure 5.8A). By comparison, EC-AdSC and EC-MSC groups contained very well-defined vessels in which the Texas Red-dextran was circumscribed by human-CD31+ cells, with significantly less red signal in the surroundings. Importantly, we had also previously

developed and validated an automated, MATLAB-based image-processing algorithm to quantify vessel permeability (32). When we applied this algorithm to quantify the relative fluorescence contained with lumens as described in the Materials and Methods, the resulting data confirmed that co-delivery of ECs with AdSCs or MSCs yields vessels whose control of permeability is superior (Figure 5.8B).

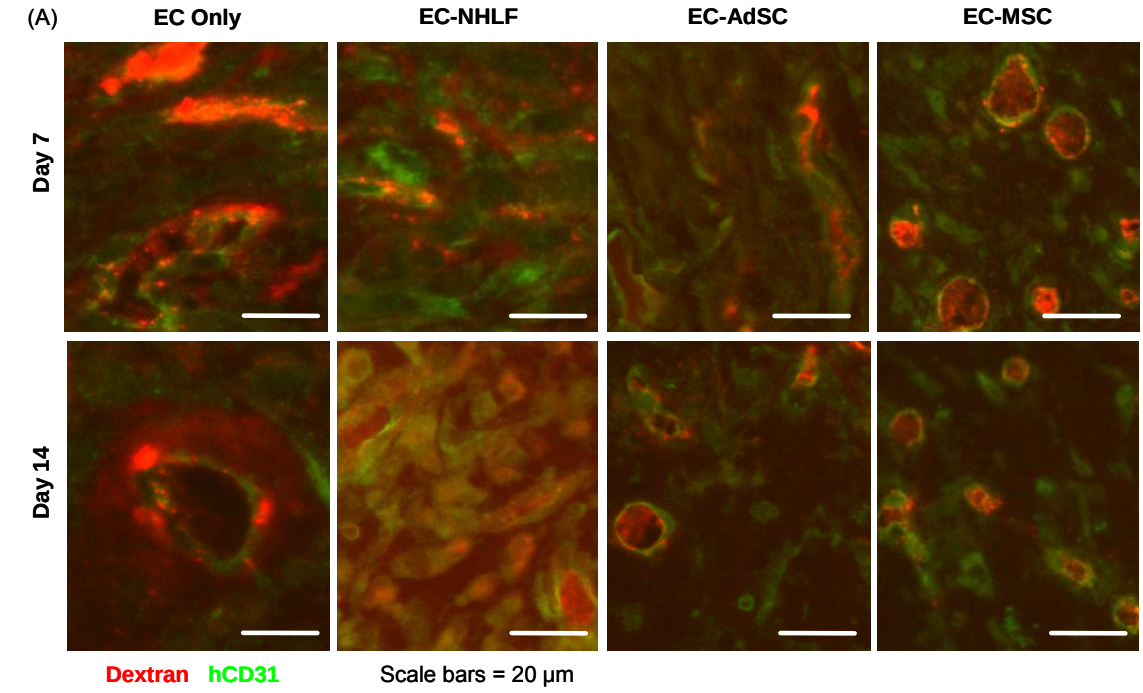

Figure 5.8. Co-injection of EC with AdSC or MSC yields neovasculature with superior functional properties. (A) SCID mice were subjected to tail vein injections of 70 kDa Texas Red-dextran (red) tracer to visualize inosculation and characterize vessel leakiness. Tissues were counter-stained with anti-human CD31 antibodies (green) to verify the human origins of the vessels. In the EC only and EC-NHLF groups, a significant fraction of the Texas Red-dextran is observed outside of the vessel borders (defined by the green CD31 staining). By comparison, EC-AdSC and EC-MSC groups contained very well-defined vessels in which the TRITC-dextran is circumscribed by human-CD31+ cells, with significantly less red signal in the surrounding tissue. (B) Quantitative data confirm that co-delivery of EC with AdSC or MSC yields vessels whose control of permeability is superior. In the graph, "a" indicates statistical significance ($p<0.05$) across time points within a single group. Across groups, each "b" is significantly different from all other "b's", and each "c" is significantly different from all other "c's".

5.4 Discussion

This study examined the quantity and functional quality of engineered capillary networks formed via co-delivery of ECs with one of three types of supporting stromal cells (NHLF, MSC, or AdSC) in a fibrin-based implant. We focused our efforts on these three stromal cell types not only because of our own prior *in vitro* work (24, 31, 32), which has suggested some differences in the mechanisms by which these cells promote vascularization, but also because their use has been gaining traction in the tissue engineering literature in recent years. In the case of fibroblasts, their co-delivery with stem cell-derived cardiomyocytes and ECs has been explored in the context of vascularized cardiac patches (35). A high density of co-transplanted NHLFs in particular in a prevascularized tissue construct was recently shown to accelerate the rate of inosculation between host vessels and the implanted vessels (28). Likewise, AdSCs co-delivered with ECs in collagen-based implants have been shown to enhance vascularization, and to help sustain pancreatic islets or adipocytes (36). There are also a number of studies that have explored the utility of MSCs co-delivered with ECs to build functional vasculature (22, 25).

The results presented here show that all four of the experimental groups (EC alone, EC-NHLF, EC-AdSC, and EC-MSC) yielded new human-derived vessels that inosculated with mouse vasculature and perfused the implant with blood. However, functional differences in the capillary networks were also revealed, depending on the identity of the co-delivered stromal cells. Importantly, the observed differences in vessel function were not apparent in data generated

by manually counting numbers of vessels in H&E or hCD31-stained histological sections, the most common endpoint utilized to assess functional connections between implanted capillary beds and the host vasculature.

Laser Doppler perfusion imaging (LDPI) was also used to assess blood flow, and thus provide an indirect indication of inosculation between the host vessels and the newly developed vasculature within the implant. This method has been widely employed in the tissue engineering literature to assess the success of revascularization therapies (37, 38). The main advantages of this technology are its non-invasive and real-time measuring capabilities. In our study, mice were anesthetized for a short period and experiments performed longitudinally across multiple time points with the same mouse. However, LDPI results may be somewhat misleading, as the data in Figure 5.2 suggest. Specifically, we found that co-delivery of EC with AdSC, MSC, or NHLF within a fibrin matrix successfully restored blood flow to pre-injection levels, with no significant differences between them. Delivery of EC alone partially restored blood flow by 7 days, but perfusion dropped off as the unstable vasculature was pruned. From these data alone, one might conclude that AdSC, MSC, and NHLF are all equal with respect to their ability to promote functional vessels that can perfuse an implant. However, erythrocyte pooling and edema into the implants could not be quantified via LDPI.

Macroscopic images (Figure 5.3) suggested some differences across the different experimental groups. EC-NHLF implants were visibly red to the naked eye, especially at the day 7 time point. EC-MSC and EC-AdSC implants were

significantly lighter in color by comparison. Implants containing only ECs were somewhere in between in gross appearance. H&E staining of the retrieved implants (Figure 5.4) revealed many free erythrocytes within the EC-only and EC-NHLF implants. The presence of multipotent stromal cells, either from bone marrow or adipose, yielded smaller, more well-defined blood vessels throughout the implants. These vessels appeared to be tightly lined with ECs, as identified by the hCD31 staining (Figure 5.5A-B). However, manual quantification of perfused lumen-containing structures on these hCD31-stained sections (Figure 5.5C) seemed to suggest that EC-NHLF co-delivery was superior to EC-MSC or EC-AdSC co-delivery in terms of numbers of vessels. Implants containing ECs alone also appeared to yield greater numbers of vessels initially, but these vessels were unstable in the absence of a co-delivered stromal cell. In fact, it was only when we assessed the permeability of the engineered vessel networks by systemically injecting a fluorescent tracer into the host circulation that the functional superiority of co-delivering ECs with the multipotent stromal cells emerged. As shown in Figure 5.8, a significant fraction of the Texas Red-dextran leaked outside of the vessel borders in the EC only and EC-NHLF groups, especially at the day 7 time point. By comparison, the fluorescent dextran was better retained with the vessels in the EC-AdSC and EC-MSC groups.

One possible explanation for the superior functional properties of the vessels created in the EC-AdSC and EC-MSC groups is the fact that the multipotent AdSCs and MSCs are capable of differentiating into pericytes, and perhaps even functional smooth muscle, while the NHLFs are not. However,

assessing this possibility is difficult due to the limited availability of bona fide pericyte markers. Smooth muscle α-actin is commonly used as a pericyte marker (39, 40), but it is also a marker of myofibroblasts (41). In our results, the EC only condition is negative for α-SMA, but all of the other conditions show some degree of positive staining (Figure 5.6). The EC-NHLF implants show several small, stippled areas of positive staining. By contrast, only the EC-AdSC and EC-MSC implants show positive calponin staining, an indication of possible smooth muscle differentiation, and only after 14 days (Figure 5.7), implying evolvement of a smooth muscle-like phenotype of implanted stromal cells. Together, these two pieces of data suggest that the AdSCs and MSCs may be able to differentiate into functional pericytes, and eventually smooth muscle cells, and thus are much better able to stabilize the new vessel networks and modulate their permeability. By contrast, the terminally differentiated NHLFs (and perhaps fibroblasts more generally) act more as myofibroblasts in a wound-healing environment, rapidly promoting vessel formation in order to heal the wound. Prior results from an *in vitro* comparison of these different stromal cell types show that NHLFs promote capillary morphogenesis at a faster rate (32), consistent with this possible explanation.

In conclusion, the results of this study suggest that the identity of the stromal cells co-delivered with ECs is key to controlling the functional properties of vasculature engineered via cell delivery, and argue that multipotent stromal cells with the ability to differentiate *in situ* are superior to terminally-differentiated fibroblasts. Importantly, this study also underscores the need for more

quantifiable metrics of functionality, rather than relying solely on the manual counting of the numbers of vessels in histological sections.

5.5 References

1. Ferrara N, and Alitalo K. Clinical applications of angiogenic growth factors and their inhibitors. *Nat Med* **5**, 1359-1364 (1999).
2. Davis BH, Schroeder T, Yarmolenko PS, Guilak F, Dewhirst MW, and Taylor DA. An in vitro system to evaluate the effects of ischemia on survival of cells used for cell therapy. *Ann Biomed Eng* **35**, 1414-1424 (2007).
3. Chen RR, Silva EA, Yuen WW, Brock AA, Fischbach C, Lin AS, Guldberg RE, and Mooney DJ. Integrated approach to designing growth factor delivery systems. *Faseb J* (2007).
4. Sun Q, Silva EA, Wang A, Fritton JC, Mooney DJ, Schaffler MB, Grossman PM, and Rajagopalan S. Sustained release of multiple growth factors from injectable polymeric system as a novel therapeutic approach towards angiogenesis. *Pharm Res* **27**, 264-271 (2010).
5. Lee KY, Peters MC, Anderson KW, and Mooney DJ. Controlled growth factor release from synthetic extracellular matrices. *Nature* **408**, 998-1000 (2000).
6. Murphy WL, and Mooney DJ. Controlled delivery of inductive proteins, plasmid DNA and cells from tissue engineering matrices. *J Periodontal Res* **34**, 413-419 (1999).

7. Sun Q, Chen RR, Shen Y, Mooney DJ, Rajagopalan S, and Grossman PM. Sustained vascular endothelial growth factor delivery enhances angiogenesis and perfusion in ischemic hind limb. *Pharm Res* **22**, 1110-1116 (2005).

8. Zisch AH, Lutolf MP, Ehrbar M, Raeber GP, Rizzi SC, Davies N, Schmokel H, Bezuidenhout D, Djonov V, Zilla P, and Hubbell JA. Cell-demanded release of VEGF from synthetic, biointeractive cell ingrowth matrices for vascularized tissue growth. *Faseb J* **17**, 2260-2262 (2003).

9. Richardson TP, Peters MC, Ennett AB, and Mooney DJ. Polymeric system for dual growth factor delivery. *Nat Biotechnol* **19**, 1029-1034 (2001).

10. Iba O, Matsubara H, Nozawa Y, Fujiyama S, Amano K, Mori Y, Kojima H, and Iwasaka T. Angiogenesis by implantation of peripheral blood mononuclear cells and platelets into ischemic limbs. *Circulation* **106**, 2019-2025 (2002).

11. Kinnaird T, Stabile E, Burnett MS, Shou M, Lee CW, Barr S, Fuchs S, and Epstein SE. Local delivery of marrow-derived stromal cells augments collateral perfusion through paracrine mechanisms. *Circulation* **109**, 1543-1549 (2004).

12. Pesce M, Orlandi A, Iachininoto MG, Straino S, Torella AR, Rizzuti V, Pompilio G, Bonanno G, Scambia G, and Capogrossi MC. Myoendothelial differentiation of human umbilical cord blood-derived stem cells in ischemic limb tissues. *Circ Res* **93**, e51-62 (2003).

13. Rehman J, Traktuev D, Li J, Merfeld-Clauss S, Temm-Grove CJ, Bovenkerk JE, Pell CL, Johnstone BH, Considine RV, and March KL. Secretion of angiogenic and antiapoptotic factors by human adipose stromal cells. *Circulation* **109**, 1292-1298 (2004).

14. Nor JE, Christensen J, Mooney DJ, and Polverini PJ. Vascular endothelial growth factor (VEGF)-mediated angiogenesis is associated with enhanced endothelial cell survival and induction of Bcl-2 expression. *Am J Pathol* **154**, 375-384 (1999).

15. Nor JE, Peters MC, Christensen JB, Sutorik MM, Linn S, Khan MK, Addison CL, Mooney DJ, and Polverini PJ. Engineering and characterization of functional human microvessels in immunodeficient mice. *Lab Invest* **81**, 453-463 (2001).

16. Baluk P, Hashizume H, and McDonald D. Cellular abnormalities of blood vessels as targets in cancer. *Current Opinion in Genetics & Development* **15**, 102-111 (2005).

17. Carmeliet P, and Jain R. Angiogenesis in cancer and other diseases. *Nature* **407**, 249-257 (2000).

18. Jain RK, Au P, Tam J, Duda DG, and Fukumura D. Engineering vascularized tissue. *Nat Biotechnol* **23**, 821-823 (2005).

19. Melero-Martin J, Obaldia MD, Kang S, Khan Z, Yuan L, Oettgen P, and Bischoff J. Engineering robust and functional vascular networks in vivo with human adult and cord blood-derived progenitor cells. *Integrative Physiology* **103**, 194-202 (2008).

20. Hashizume H, Baluk P, Morikawa S, McLean J, Thurston G, Roberge S, Jain R, and McDonald D. Openings between defective endothelial cells explain tumor vessel leakiness. *American Journal of Pathology* **156**, 1363-1380 (2000).

21. Ghajar CM, Blevins KS, Hughes CC, George SC, and Putnam AJ. Mesenchymal stem cells enhance angiogenesis in mechanically viable prevascularized tissues via early matrix metalloproteinase upregulation. *Tissue Eng* **12**, 2875-2888 (2006).

22. Kniazeva E, Kachgal S, and Putnam AJ. Effects of extracellular matrix density and mesenchymal stem cells on neovascularization in vivo. *Tissue Eng Part A* **17**, 905-914 (2011).

23. Bergers G, and Song S. The role of pericytes in blood-vessel formation and maintenance. *Neuro-Oncology* **7**, 452-464 (2005).

24. Ghajar CM, Kachgal S, Kniazeva E, Mori H, Costes SV, George SC, and Putnam AJ. Mesenchymal cells stimulate capillary morphogenesis via distinct proteolytic mechanisms. *Exp Cell Res* **316**, 813-825 (2010).

25. Au P, Tam J, Fukumura D, and Jain RK. Bone marrow-derived mesenchymal stem cells facilitate engineering of long-lasting functional vasculature. *Blood* **111**, 4551-4558 (2008).

26. Merfeld-Clauss S, Gollahalli N, March K, and Traktuev D. Adipose tissue progenitor cells directly interact with endothelial cells to induce vascular network formation. *Tissue Engineering Part A* **16**, 2953-2966 (2010).

27. Ghajar CM, Chen X, Harris JW, Suresh V, Hughes CC, Jeon NL, Putnam AJ, and George SC. The effect of matrix density on the regulation of 3-D capillary morphogenesis. *Biophys J* **94**, 1930-1941 (2008).

28. Chen X, Aledia AS, Popson SA, Him L, Hughes CC, and George SC. Rapid anastomosis of endothelial progenitor cell-derived vessels with host vasculature is promoted by a high density of cotransplanted fibroblasts. *Tissue Eng Part A* **16**, 585-594 (2010).

29. Motegi S, Leitner W, Lu M, Tada Y, Sardy M, Wu C, Chavakis T, and Udey M. Pericyte-derived MFG-E8 regulates pathologic angiogenesis. *Arteriosclerosis, thrombosis, and vascular biology* **31**, 2024-2034 (2011).

30. Shepherd BR, Jay SM, Saltzman WM, Tellides G, and Pober JS. Human aortic smooth muscle cells promote arteriole formation by coengrafted endothelial cells. *Tissue Eng Part A* **15**, 165 (2009).

31. Kachgal S, and Putnam AJ. Mesenchymal stem cells from adipose and bone marrow promote angiogenesis via distinct cytokine and protease expression mechanisms. *Angiogenesis* **14**, 47-59 (2011).

32. Grainger SJ, and Putnam AJ. Assessing the permeability of engineered capillary networks in a 3D culture. *PLoS One* **6**, e22086 (2011).

33. Curry FE, Huxley VH, and Adamson RH. Permeability of single capillaries to intermediate-sized colored solutes. *Am J Physiol* **245**, H495-505 (1983).

34. Hughes S, and Chan-Ling T. Characterization of smooth muscle cell and pericyte differentiation in the rat retina in vivo. *Investigative Ophthalmology & Visual Science* **45**, 2795-2806 (2004).

35. Stevens KR, Kreutziger KL, Dupras SK, Korte FS, Regnier M, Muskheli V, Nourse MB, Bendixen K, Reinecke H, and Murry CE. Physiological function and transplantation of scaffold-free and vascularized human cardiac muscle tissue. *Proc Natl Acad Sci U S A* **106**, 16568-16573 (2009).

36. Traktuev DO, Prater DN, Merfeld-Clauss S, Sanjeevaiah AR, Saadatzadeh MR, Murphy M, Johnstone BH, Ingram DA, and March KL. Robust functional vascular network formation in vivo by cooperation of adipose progenitor and endothelial cells. *Circulation Research* **104**, 1410-1420 (2009).

37. Phelps EA, Landazuri N, Thule PM, Taylor WR, and Garcia AJ. Bioartificial matrices for therapeutic vascularization. *Proc Natl Acad Sci U S A* **107**, 3323-3328 (2010).

38. Silva EA, Kim ES, Kong HJ, and Mooney DJ. Material-based deployment enhances efficacy of endothelial progenitor cells. *Proc Natl Acad Sci U S A* **105**, 14347-14352 (2008).

39. Bexell D, Gunnarsson S, Tormin A, Darabi A, Gisselsson D, Roybon L, Scheding S, and Bengzon J. Bone marrow multipotent mesenchymal stroma cells act as pericyte-like migratory vehicles in experimental gliomas. *Molecular Therapy* **17**, 183-190 (2008).

40. Shi S, and Gronthos S. Perivascular niche of postnatal mesenchymal stem cells in human bone marrow and dental pulp. *Journal of Bone and Mineral Research* **18**, 696-704 (2003).

41. Hinz B. Formation and function of the myofibroblast during tissue repair. *Journal of Investigative Dermatology* **127**, 526-537 (2007).

42. Schechner JS, Nath AK, Zheng L, Kluger MS, Hughes CC, Sierra-Honigmann MR, Lorber MI, Tellides G, Kashgarian M, Bothwell AL, and Pober JS. In vivo formation of complex microvessels lined by human endothelial cells in an immunodeficient mouse. *Proc Natl Acad Sci U S A* **97**, 9191-9196 (2000).

Supplementary Information

Methods:

Transduction of Cells for Live Imaging

HUVECs were transduced with monomeric green fluorescent protein (GFP) using the Phoenix Retrovirus Expression System (Orbigen, San Diego, CA). The pBMN-GFP vector was obtained commercially and cells were transduced as described elsewhere.(22) Viral transductions were performed for a 6 hour period daily for a total of 4 days.

Figures:

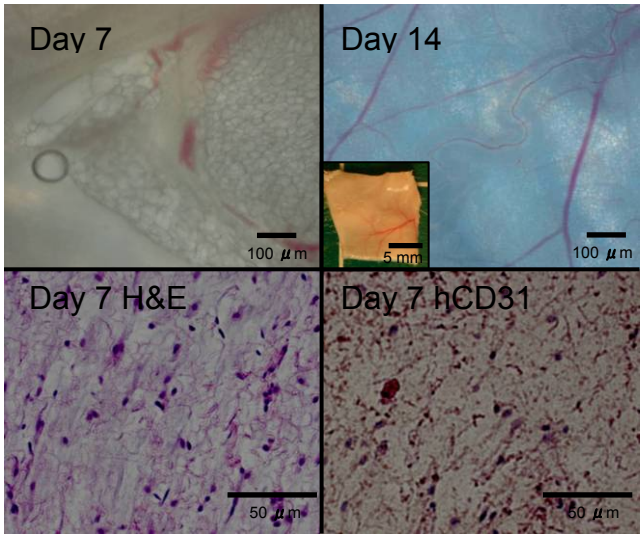

Figure S5.1. Acellular control implants show no evidence of neovascularization. Acellular implants show no evidence of new blood vessel formation either via H&E or anti-hCD31 staining. By day 14, fibrin implants have mostly resorbed.

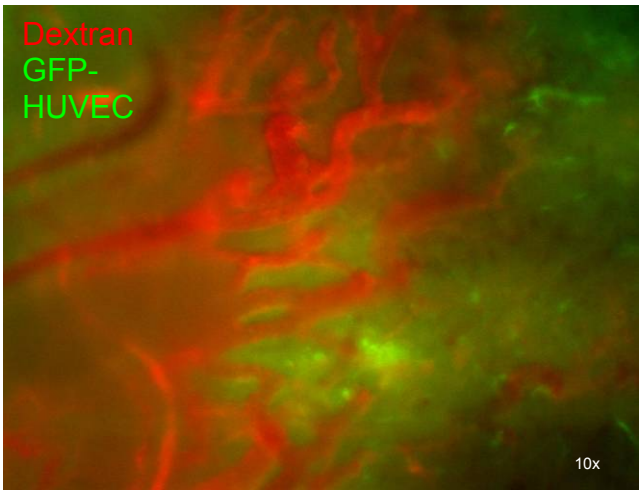

Figure S5.2. Systemic injection allows imaging of host-implant interface. Systemically injected Texas Red-dextran (70kDa) approaches the interface between GFP-hECs in the implant and the host blood vessels that are inosculating with the implant.

CHAPTER 6

Conclusions & Future Directions

6.1 CONCLUSIONS

The main conclusion of this thesis is that stromal cell identity has direct implications on the control of permeability and function of developing capillary networks. This conclusion was reached from several angles. First, three dimensional *in vitro* studies showed that capillaries with different stromal cell components have different morphologies, grow and mature at different rates, and have different ultimate permeability capabilities. Next, some of the mechanistic components of the differentiation of stromal cells into pericytes were examined via western blotting and immunofluorescent staining for proteins such as vascular endothelial cadherin, alpha smooth muscle actin, and calponin. Finally, these results were verified in an *in vivo* model of subcutaneous wound healing. Live imaging of the implants, quantification of blood flow through the implant neovasculature, histology and immunohistochemical staining, and permeability tracer studies allowed for evaluation of the blood vessels produced in implants with each of the different stromal cells studied here. In short, vessels produced from co-implants of MSCs or AdSCs with ECs produced capillaries that were

much more able to control permeability and produce capillaries similar to those of a physiologically healthy nature, over EC alone or EC-fibroblast cultures.

First, an *in vitro* imaging modality and quantification assay were developed, tested, and then translated into an *in* vivo application of subcutaneous wound healing. Early work used an established method of growing capillaries *in vitro* to develop an inverse permeability assay for use in evaluating differences across stromal cell types. Thickness testing showed that thin gels were required in order to allow imaging through bulk gel with a freely diffusible tracer. VE-cadherin staining in 3D allowed for imaging of newly developing cell-cell junctions between endothelial cells. This imaging modality also proved to be difficult in terms of effective definition of developing capillary boundaries. Because of this, HUVECs were tagged with GFP to allow for live cell imaging, or CD31 staining was used to define capillary borders in the assay after fixation. Dextran diffusion throughout the bulk gels posed an initial challenge as described; however, fixation of the cultures to attach the dextran to the fibrin matrices assisted in visualization of the dextran localization in the cultures.

The assay was challenged with a known modulator of permeability on capillaries, histamine. This resulted in across the board increases in permeability, regardless of the number of days in culture or maturation level of the capillary cultures. Regardless of treatment with histamine, three distinct phases of capillary maturation were seen across the two-week cultures. Initially, a phase of sprouting is seen, with few cell-cell junctions between the endothelial cells, and little control over permeability. Much tracer is able to accumulate within the

capillary sprout lumens. Next, a mid-phase is observed, where VE-cadherins junctions are beginning to develop, and permeability levels decrease. Finally, a phase of maturation is observed, with tight control over permeability and well-defined cell-cell junctions.

Once the model was well established, differences in capillary phenotype and permeability control across stromal cell types were compared. In 3D co-culture with ECs, as well as monoculture, MSCs promote higher levels of VE-cadherin expression over the use of NHLFs or AdSCs, implying a mechanism of stabilization is occurring with MSCs, and potentially with AdSCs, to a lesser degree. The stem cells may be capable of modulating their phenotype to induce capillary maturation, while still maintaining a stromal cell phenotype. Also Capillaries with stem cells included in the co-cultures also resulted in much more highly branched constructs than those with fibroblasts. Fibroblasts promoted more of a wound healing environment, with longer, spindly capillaries and less control over permeability than the stem cell co-cultures. We hypothesized that the stem cells are able to differentiate into more of a pericytic phenotype than the fibroblasts, thus resulting in tighter permeability control and effective stabilization of the capillaries.

Next, the model was adapted for an *in* vivo setting. All co-implants showed achievement of normal perfusion levels; however, upon further investigation, phenotypic and functional differences were seen between each of the treatment groups. Live whole-mount and macroscopic imaging revealed large amounts of erythrocyte pooling in the EC-fibroblast co-cultures, even at long time points. A

similar trend was seen in the EC alone group, although these vessels started to regress by 14 days post-implantation due to a lack of stromal cell stabilization. Histology confirmed these results, and also revealed many interconnected, immature blood vessels, as well as the development of granulation tissue in the EC-fibroblast implants. The EC-stem cell implants showed more mature, developed blood vessels, and less erythrocyte pooling than the EC-fibroblast group.

Further exploration into the pericytic differentiation mechanism of each of the stromal cell types yielded interesting results as well. Western blotting for both α-SMA, a myofibroblast and accepted pericytic marker, and calponin, a smooth muscle marker, was done on both 2D and 3D *in vitro* cultures. Positive results for α-SMA were seen across the board in 2D, and in 3D for EC-NHLF co-cultures, but not for cultures containing MSCs and AdSCs. When ECs were included in the co-cultures, MSCs and AdSCs downregulated expression of α-SMA. This result implies a modulation away from a myofibroblastic phenotype in 3D culture for MSCs, and suggests the need for a more definitive marker of capillary pericytes. *In vivo*, positive α-SMA staining was seen for all three stromal cell groups at early time points, but modulated by day 14 in the stem cell groups. In these groups, staining was only present at the periphery of each newly developed blood vessel, implying a pericytic phenotype in the stem cell co-implants. Because the cells are positive for α-SMA in 2D culture, this suggests a myofibroblastic phenotype upon implantation, which is modulated *in vivo* to produce stabilized capillaries.

Along a similar vein, cells are not given the cues *in vitro* to differentiate into smooth muscle cells, resulting in a negative Western blot for calponin, even after long culture times. Staining of calponin within *in vivo* implants produced positive staining only at the longest time points, and only within the stem cell implants, surrounding the larger developing vessels. This result proves that the fibroblasts are not able to differentiate into true smooth muscle cells, as are needed for large vessel development and stabilization in an *in vivo* setting. Collectively, these results imply that the stem cell co-implants are able to produce stabilized, morphologically mature vessels with a hierarchical architecture, unlike the EC-fibroblast implants.

Supporting these phenotypic results, similar permeability trends to those seen *in vitro* were observed across all time points and stromal cell conditions. EC-stem cell co-cultures were able to much more tightly control permeability after two weeks than those containing fibroblasts, effectively keeping tracer within the defined limits of the vasculature. Overall, the results of this thesis have conclusively shown that stromal cell identity is key to controlling permeability and effectively stabilizing developing vasculature.

6.2 FUTURE DIRECTIONS

The results of this work indicate a mechanism for bringing tissue engineered vasculature to the clinic in a timely manner. Effective translation will require further characterization of the resulting blood vessels after injection of cells. Longer time points, further mechanistic characterization, and a platform of

induced ischemia should be tested in an *in* vivo setting prior to moving this work toward clinical applications. Another hurdle on the way to clinical translation is the use of autologous donor cells, rather than readily available, established cell sources. While this work was done with primary cells from human donors, this must be adapted to work in patients with normal immune responses, rather than only in SCID mice. Potential autologous donor cell types, such as endothelial progenitor cells, must be explored in these types of applications. Isolation and subsequent expansion into a useable volume for implantation must be further explored, as these are not trivial tasks. Also, effective isolation and expansion of adult stem cells from a patient must be further optimized if it is to be an option in the clinic. We must work to avoid blind implantation of stem cells in the hope that their healing power may be harnessed, as has been done in the past. Many other patient-to-patient variations in cellular behavior must be ironed out as well, to avoid complications and unanticipated outcomes in human patients. The effects of potentially existing illness on the donor patient cells must be characterized. Work to this point has been done on healthy patient donor cells, but has not yet been explored on cells donated from individuals with ischemic conditions. This may affect the numbers of circulating adult stem cells within the body, or have other implications that we have not anticipated at this point.

Further functional testing of the newly developed vessels must be done as well. The exact locations of pericytes, either in close proximity to, or in direct contact with, developing neovessels must be further explored. Effects of changes in integrin expression during sprout development, and after stabilization, must be

determined. The mechanism by which these stromal cells differentiate into pericytes and smooth muscle cells must ultimately be discovered. This would allow us to directly bypass the vessel development stages and directly treat ischemic diseases by their cause, instead of waiting to deal with the end effects.

We have hinted at the mechanistic results, seeing increased modulation of VE-cadherin and α-SMA expression with the use of stem cells over fibroblasts, and the inclusion of stromal cells over EC alone cultures; however, this is not enough. Further work into the differentiation of pericytes must be explored. If we could pre-direct these cells *in vitro* to decrease the time between implantation and anastamosis, this would produce direct, immediate results in the clinic, rather than waiting for implantation, sprouting, development, and stabilization (and pericytic differentiation) to occur. This could increase response time in the treatment of ischemic diseases, thus avoiding further complications and destabilization of the patient.